

AN ABSTRACT OF THE THESIS OF

Jie Gao for the degree of Doctor of Philosophy in

Electrical and Computer Engineering presented on December 12, 2005.

Title: Channel Estimation and Data Detection for Mobile MIMO OFDM Systems

Abstract approved: _____

Huaping Liu

Designing spectral efficient, high-speed wireless links that offer high quality-of-service and range capability has been a critical research and engineering challenge. In this thesis, we mainly address the complexity and performance issues of channel estimation and data detection in multiple-input multiple-output (MIMO) orthogonal frequency division multiplexing (OFDM) systems over time-varying channels.

We derive the probability density function (pdf) expressions of the condition number (i.e., the maximum-to-minimum-singular-value ratio, MMSVR) of the channel state information matrix of MIMO OFDM systems. It is shown that this ratio is directly related to the noise enhancement in open-loop systems and provides a significant insight on the system capacity.

A decision-directed (DD) maximum *a posteriori* probability (MAP) channel estimation scheme of MIMO systems is derived. Error performance of a zero-forcing receiver with the DD MAP and perfect channel estimates is provided and compared. This scheme has a low complexity and can be applied to time-varying Rayleigh fading channels with an arbitrary spaced-time correlation function.

We propose an iterative channel estimation and data detection scheme for MIMO OFDM systems in the presence of inter-carrier-interference (ICI) due to the nature of time-varying channels. An ICI-based minimum-mean-square error (MMSE) detection scheme is derived. An expectation-maximization (EM) based least square (LS) channel estimator is proposed to minimize the mean-square error (MSE) of the channel estimates and to reduce the complexity of the implementation. With the estimate of the channel and initially detected symbols, ICI is estimated and removed from the received signal. Thus more accurate estimation of the channel and data detection can be obtained in the next iteration.

An EM-based MAP channel estimator is derived by exploiting the frequency/time correlation of the pilot and data sub-carriers. Performance comparison is made between the proposed schemes and the ideal case – time-invariant channels and perfect channel estimation. We optimize the data transmission by exploiting the long term correlation characteristics. The transmitted data is successively detected without an error floor in spatially correlated channels.

The algorithms proposed in this thesis allow low-complexity implementation of channel estimation and data detection for MIMO OFDM systems over time-varying fading channels, while providing good error performance.

©Copyright by Jie Gao

December 12, 2005

All Rights Reserved

Channel Estimation and Data Detection for Mobile MIMO OFDM Systems

by

Jie Gao

A THESIS

submitted to

Oregon State University

in partial fulfillment of
the requirements for the
degree of

Doctor of Philosophy

Presented December 12, 2005
Commencement June 2006

Doctor of Philosophy thesis of Jie Gao presented on December 12, 2005

APPROVED:

Major Professor, representing Electrical and Computer Engineering

Director of the School of Electrical Engineering and Computer Science

Dean of the Graduate School

I understand that my thesis will become part of the permanent collection of Oregon State University libraries. My signature below authorizes release of my thesis to any reader upon request.

Jie Gao, Author

ACKNOWLEDGMENTS

First of all I would like to express my sincere gratitude to my advisor Dr. Huaping Liu for his continuous encouragement, support and guidance throughout my graduate studies. I am very thankful for his patience and always believing in me during the ups and downs of my Ph.D. research. His wide knowledge and logical way of thinking have been of great value for me. His technical advice and constructive comments have provided a good basis for this thesis. I would also like to thank Intel Corp. for providing me the opportunity to work with the great people that I met along the way.

I am deeply indebted to Dr. Bart Eleveld, Dr. Mario E. Magaña, Dr. Thinh Nguyen and Dr. Zhongfeng Wang for their great efforts and significant amount of time to serve on my Ph.D. committee.

My thanks to all the members in my lab for their help and friendship. Special thanks to Orhan C. Ozdural for the collaborative work in Chapter 3, and to Shiwei Zhao, Yu Zhang and Liang Xian for always being available for technical discussions.

Finally, I would like to express my deepest gratitude for the constant support, understanding and unconditional love that I received from my parents and my husband Yutao.

TABLE OF CONTENTS

	<u>Page</u>
1 INTRODUCTION.....	1
1.1 Background and Motivation.....	1
1.2 Objective and Contributions.....	5
1.3 Notation Summary.....	8
2 MIMO OFDM COMMUNICATION SYSTEMS.....	10
2.1 MIMO Channels and Properties.....	10
2.1.1 Information Theory of MIMO.....	12
2.1.2 MIMO Frequency-selective and Time-varying Channels.....	20
2.1.3 Spatially Correlated and Uncorrelated MIMO Channels.....	21
2.2 Simulation Model of MIMO Time-varying Channels.....	22
3 PERFORMANCE MODELLING OF MIMO OFDM SYSTEMS VIA CHANNEL ANALYSIS.....	27
3.1 System Model and Detection Schemes.....	28
3.1.1 System Model.....	28
3.1.2 Detection.....	29
3.2 Analysis of MIMO Channel.....	30
3.2.1 Channel Model.....	30
3.2.2 Analysis of Channel Characteristics.....	31
3.3 Numerical Examples and Discussion.....	35
3.4 Conclusion.....	39
4 DECISION-DIRECTED ESTIMATION OF MIMO TIME-VARYING RAYLEIGH FADING CHANNELS.....	41
4.1 System Model.....	42

TABLE OF CONTENTS (Continued)

	<u>Page</u>
4.2 Channel Estimation and Data Detection	45
4.2.1 Decision-directed Channel Estimation	45
4.2.2 Detection	48
4.3 Numerical Examples and Discussion	49
4.4 Conclusion.....	54
5 CHANNEL ESTIMATION FOR MOBILE MIMO OFDM SYSTEM.....	56
5.1 System Model	59
5.2 EM-Based LS Channel Estimation	63
5.3 Low-complexity MAP Channel Estimation	65
5.3.1 MAP Channel Estimation	67
5.3.2 Low Rank Approximated MAP Channel Estimation	68
5.3.3 EM-based MAP Channel Estimation.....	69
6 DATA DETECTION FOR MOBILE MIMO OFDM SYSTEMS.....	72
6.1 ZF and MMSE Detection	73
6.2 ICI-based MMSE Detection.....	74
6.3 SIC Detection	77
6.4 Numerical Examples and Discussion	80
6.5 Conclusion.....	92
7 CONCLUSIONS.....	94
7.1 Summary	94
7.2 Future Research	96

TABLE OF CONTENTS (Continued)

Page

BIBLIOGRAPHY..... 97

LIST OF FIGURES

Figure	Page
2.1 Blockdiagram of a MIMO OFDM system.	11
2.2 Average capacity of spatially uncorrelated MIMO Rayleigh fading channels versus SNR.	14
2.3 Outage probability of spatially uncorrelated MIMO Rayleigh fading channel versus SNR.	15
2.4 Channel capacity versus SNR.	17
2.5 Relative capacity gain versus SNR.	18
2.6 Spatial multiplexing order of spatially uncorrelated MIMO Rayleigh fading channels versus SNR.	19
2.7 The theoretical and simulated auto-correlation of the modified Jakes model.	23
2.8 The ideal and simulated cross-correlation of real and imaginary parts of the modified Jakes model.	24
2.9 The ideal and simulated cross-correlation of different multipath components of the modified Jakes model.	25
3.1 Analytical and simulated probability density of MMSVR for 2×2 and 2×3 MIMO OFDM configurations.	36
3.2 Analytical and simulated probability density of MMSVR for 3×3 and 3×4 MIMO OFDM configurations.	37
3.3 Throughput comparison of MIMO OFDM systems [70].	38
3.4 Throughput comparison of MIMO OFDM systems [70].	39
4.1 The DD MAP channel predictor for MIMO systems.	49
4.2 BER versus E_b/N_0 with different memory depth L	50
4.3 BER versus E_b/N_0 for different number of transmit and receive antennas.	51
4.4 BER versus E_b/N_0 with different fading rates.	52
4.5 Performance comparison of the proposed scheme and the scheme with the channel treated as block fading.	53

LIST OF FIGURES (Continued)

Figure	Page
6.1 Block diagram of the proposed iterative EM-based LS channel estimation and ICI-based MMSE detection for MIMO OFDM systems.	77
6.2 Block diagram of simplified MAP channel estimation and data detection for MIMO OFDM systems.	79
6.3 BER versus E_s/N_0 with and without ICI cancellation ($(N_t, N_r) = (2, 3)$, $f_dT = 0.113$, and $G = 9$).	81
6.4 The effect of the number of sub-iterations in the EM process ($(N_t, N_r) = (2, 2)$, $f_dT = 0.0452$, after 2 iterations of ICI cancellation).	82
6.5 Comparison of the proposed scheme with a common ZF detection scheme ($(N_t, N_r) = (2, 2)$ and $f_dT = 0.0452$).	83
6.6 The effect of the ratio of pilot spacing to channel coherence bandwidth R ($(N_t, N_r) = (2, 3)$ and $f_dT = 0.113$).	84
6.7 Performance comparison between the proposed scheme and the ideal case ($(N_t, N_r) = (2, 3)$ and $L = 5$).	85
6.8 The effect of antenna configurations ($f_dT = 0.113$ and $R = 0.4375$).	86
6.9 The effect of the number of sub-iterations in the EM process ($N_T = 2$, $N_R = 3$, uncorrelated spatial channels).	87
6.10 Performance comparison of various channel estimation schemes ($N_T = 2$, $N_R = 2$, uncorrelated spatial channels).	88
6.11 Performance comparison of various channel estimation schemes ($N_T = 2$, $N_R = 3$, uncorrelated spatial channels).	89
6.12 The effect of the ratio of pilot spacing to channel coherence bandwidth ($N_T = 2$, $N_R = 3$, uncorrelated spatial channels).	90
6.13 Performance of the proposed scheme with different antenna configurations ($R = 0.4375$, uncorrelated spatial channels).	91
6.14 Performance of the proposed scheme in the presence of high spatial correlation ($N_T = 2$, $N_R = 2$, $f_dT = 0.04$).	92

Channel Estimation and Data Detection for Mobile MIMO OFDM Systems

1. INTRODUCTION

1.1. Background and Motivation

With the rapid growth of wireless communications, there has been an increasing demand for high data rate communications in many applications, such as wireless local area network (WLAN), wireless metropolitan area network (WMAN), and home audio/visual (A/V) network. WLAN provides homes, businesses, and campuses with enhanced opportunities to connect to the Internet outside the limited area covered by wired networks. In the last ten years, Wi-Fi, which includes IEEE wireless standards 802.11, 802.11b, 802.11a and 802.11g, provides wireless services in WLAN. Based on IEEE 802.16 specifications, worldwide inter-operability of microwave access (WiMax) is emerging as a last-mile broadband wireless Internet access solution. It provides wireless services in WMAN and it has the potential to make broadband service available in regions where it is currently not feasible, particularly in rural communities. Home A/V network involves wireless connection of electronic and data devices for the convenient access to information and entertainment. The main challenge of all these wireless applications is to support high data rate of over one hundred megabits per second with limited bandwidth and restricted power consumption.

Multiple-input multiple-output (MIMO) systems use multiple transmit and receive antennas to create multiple spatial channels between the transmitter and

receiver. MIMO systems have been shown to provide high spectral efficiencies [1, 2], which offers the basis for increasing the data rate with limited bandwidth. If perfect channel state information (CSI) is available at the receiver, the average capacity grows linearly with the smaller of the numbers of transmit and receive antennas under certain channel conditions. The major potential advantage of MIMO is that signals at both the transmitter and receiver sides are processed in a way such that either the quality measured by bit error rate (BER) or the data rate of the system can be improved. The performance improvement of MIMO systems can be assessed by diversity gain and spatial multiplexing gain. Diversity gain is achieved by transmitting the same signal over multiple independent fading environments, e.g., time, frequency and space. Space-time coding (STC), space-frequency coding (SFC), and space-time-frequency coding (STFC) are designed to exploit the diversity gain. In [3], Alamouti proposed an orthogonal space-time block coding for systems with two transmit antennas, which requires low-complexity decoding and provides full diversity gain. Space-frequency codes that achieve the maximum diversity gain and optimal coding advantage in frequency-selective MIMO fading channels were proposed in [4, 5]. The upper bound for pairwise word error probability of space-time-frequency codes was derived in [6].

Spatial multiplexing gain is evaluated by the linear increase in capacity without additional power or bandwidth resources. This gain is realized by transmitting independent data streams from individual antennas to maximize data rates. V-BLAST (vertical Bell Labs Layered space-time) proposed in [7, 8] is an effective approach to achieve spatial multiplexing gain. However, the interference between signals simultaneously transmitted from the multiple transmit antennas considerably increases the detection complexity. The optimal detection scheme is maximum likelihood (ML) where the receiver compares all possible combinations of the

transmitted symbols with the observed ones. However, it suffers from significant increase in complexity, which grows exponentially with the number of transmit antennas. It could become prohibitive with many antennas and high-order modulations. Thus, several suboptimal detection schemes have been developed, e.g., zero-forcing (ZF) and minimum-mean-square error (MMSE). Both ZF and MMSE can decouple spatial interference by matrix inversion. ZF detection scheme will result in poor performance due to the large noise enhancement under certain ill-conditioned channels. MMSE scheme enhances the detection accuracy by utilizing the noise and interference statistics.

An open-loop MIMO is a system where the CSI is only required at the receiver, while in the closed-loop MIMO, CSI is also required at the transmitter as well. By exploiting CSI at both the transmitter and receiver, full diversity gain and full spatial multiplexing gain can be achieved by eigen-beamforming. However, feeding back CSI to the transmitter with limited delay and cost is not a trivial task, especially for mobile communications for which the channel exhibits fast-fading [9, 10]. It is shown in [11] and [12] that the relative gain in capacity of closed-loop systems over open-loop systems is significant at low signal-to-noise ratios (SNR), but it converges to zero as SNR increases.

Orthogonal frequency division multiplexing (OFDM), a multi-carrier modulation technique, divides the wideband channel into many narrow parallel sub-channels, thus increasing the symbol duration and reducing the inter-symbol-interference (ISI) due to multipath [13–16]. OFDM has been used in digital video and audio broadcasting, e.g., terrestrial digital video broadcasting (DVB-T), and is a promising technique for future high data rate wireless systems. Demodulation and modulation are efficiently implemented by means of fast Fourier transform (FFT) and inverse fast Fourier transform (IFFT). To mitigate the ISI caused by the chan-

nel multipath spread, each block of IFFT coefficients is preceded by a cyclic prefix (CP) whose length is at least equal to the channel length. The signal is orthogonal under the assumption that the channel is time-invariant. It allows the system to transmit data reliably in a time-dispersive, or frequency-selective, channel without the need for a complex time-domain equalizer [17].

The combination of MIMO and OFDM has been designed to improve the quality of service (QoS) and/or data rate of the system by exploiting the multiplexing gain and/or the diversity gain. Evolving wireless standards, such as the mobile WiMax (IEEE 802.16e) and Wi-Fi (IEEE 802.11n), will employ multiple transmit and receive antennas with OFDM modulation for increased spectral efficiency and improved performance. However, the system performance relies on the knowledge of CSI at the receiver. Perfect channel estimates can be obtained only if the channel is noiseless and time invariant. Inter-carrier-interference (ICI) due to the nature of time-varying and rapid channel variations makes perfect channel estimates impossible in mobile channels [18–20].

CSI can be estimated by using either non-blind pilot assisted approaches that a fraction of the bandwidth is allocated to the known training sequence or blind approaches. The latter can be implemented by exploiting the statistical information or the deterministic information of the transmitted symbol properties (e.g., finite alphabet, constant modulus, etc.). Compared with the pilot assisted scheme, blind channel estimation requires long time of data observation. A very slow convergence rate limits the application of the statistical approach to mobile channels [21] and the huge computation complexity due to the maximization operation restricts the deterministic approach [22, 23]. For pilot assisted channel estimation scheme [24], two pilot insertion patterns were considered: one exploits the frequency-domain correlation by inserting pilot symbols on certain sub-carriers; the other exploits the

time-domain correlation by inserting pilot symbols on all sub-carriers at some time slots. For slow-fading channels, the time-domain approach, owing to the slower correlation decaying rate, requires fewer pilot symbols than the frequency-domain approach. In [25], channel estimation algorithms based on comb-type pilots with improvements through interpolation at data frequencies were studied. Performance bound of a pilot assisted least square (LS) channel estimator over a multipath slowly fading channel was derived in [26]. Recent works [22, 27] have adopted the quasi-static model, assuming that the channel coefficients remain approximately constant over the entire OFDM symbol duration. Under this assumption, there is no ICI. However, this assumption is no longer valid for fast-fading channels, especially when the number of sub-carriers is large. ICI makes channel estimation more challenging in mobile channels. In order to mitigate ICI effects, various detection structures were proposed and compared in [24]. These schemes generally have a high complexity. In [28], an iterative multistage channel estimator, which iteratively cancels ICI by maximizing the signal-to-noise-plus-ICI ratio was derived. A Kalman filter based scheme to estimate the state-transition matrix of time-varying MIMO OFDM channels and a scheme based on minimizing the mean-square error (MSE) of a cost function were developed in [29, 30] and [27, 31], respectively. The discrete Fourier transform (DFT) and discrete cosine transform (DCT) interpolation-based channel estimation schemes were proposed in [32–34] for MIMO OFDM systems.

1.2. Objective and Contributions

In this thesis, we propose low-complexity channel estimation and data detection schemes for MIMO OFDM systems over frequency-selective and fast-fading channels. MIMO OFDM communication systems are described and the statistical

properties of the simulation models for the time-varying Rayleigh fading channels are also discussed in Chapter 2. The advantage of implementing multiple antennas at the transmitter and receiver is shown by reviewing the average and outage capacity of MIMO systems. It is also demonstrated that the CSI at the transmitter does not dramatically increase the average capacity when the SNR is high.

Because of the high sensitivity of MIMO detection scheme with respect to the channel matrix properties, channel modelling is particularly critical to assess the performance of various MIMO configurations. In Chapter 3, we derive the analytical probability density function (pdf) expression of the condition number (i.e., maximum-to-minimum-singular-value ratio, MMSVR) of the CSI matrix. We show that this ratio is directly related to the noise enhancement in open-loop MIMO systems and it provides a significant insight on the overall system capacity. The pdf of this ratio could be used to predict the relative performance of various MIMO configurations with respect to each other without complex system-level simulations. The pdf can also be used to compute the probability of whether certain channels will fail in high-throughput mode. Extensive channel analysis simulations are performed for different MIMO configurations to validate the accuracy of the derived closed-form pdf of the MMSVR.

In order to exploit the potential advantage of MIMO systems, channel information has to be estimated at the receiver. A decision-directed (DD) maximum *a posteriori* probability (MAP) channel estimation scheme for MIMO time-varying fading channels is derived in Chapter 4. With the estimate of the channel matrix for the current symbol interval, a zero-forcing (ZF) receiver is applied to detect the spatially multiplexed data on a symbol-by-symbol basis. Symbol decisions are then fed to the channel predictor for estimation of channel coefficients in future symbol intervals. Simulated error performance of a ZF receiver with the DD MAP

and perfect channel estimates is provided and compared. This scheme has a low complexity and can be applied to time-varying Rayleigh fading channels with an arbitrary spaced-time correlation function. The fading rate has a high impact on system performance, and the proposed scheme is more appropriate for channels with low to medium Doppler shifts. Large block length between adjacent pilot blocks can be deployed with the proposed scheme, which results in minimum overhead for pilot symbols. For wideband transmission, OFDM is combined with MIMO scheme to mitigate the ISI over frequency-selective fading channels.

In fast-fading channels, ICI could be very severe for OFDM systems with a large number of sub-carriers. We propose an iterative channel estimation and data detection scheme for MIMO OFDM systems over frequency-selective and fast-fading channels. After analyzing ICI for each sub-carrier, we derive an ICI-based minimum-mean-square error (MMSE) detection scheme to significantly improve the initial detection accuracy. In order to minimize the mean square error (MSE) of the least square (LS) channel estimate, consecutive rows of Hadamard matrix are designed as pilot sequences for transmit antennas. The complexity of the implementation can be very high due to the frequent inversion of large size matrices. Therefore, in Chapter 5, an expectation maximization (EM) based LS channel estimator is derived to reduce the receiver complexity while maintaining a high system performance.

MAP algorithms generate optimal results. However, for many applications, the computational complexity could be prohibitive due to the need of inversion of large-size matrices. By exploiting the channel statistical information and employing low rank approximation, we derive an EM-based MAP channel estimator of MIMO OFDM systems to achieve excellent performance without the need of any matrix inversion. Channel estimates are initially obtained by EM-based LS algo-

rithm. Then, a successive interference cancellation (SIC) scheme is considered for the data detection. With the estimate of the channel and the detected data, the ICI component is approximated and removed from the received signals. Finally, the detected symbols and the received signals after ICI cancellation are fed back to the derived EM-based MAP estimator to refine the CSI. In Chapter 6, the simulated error performance of the proposed scheme is compared with that of the LS scheme and the ideal case – time-invariant channels and perfect channel estimation. Most recent work is based on the assumption of uncorrelated MIMO spatial channels. However the channel can be correlated due to the small angular spread and/or not large enough antenna spacing. In this thesis, the system performance in spatially correlated channels is also analyzed. Via such analysis, we optimize, by exploiting the long term correlation characteristics, the data transmission to eliminate an error floor.

1.3. Notation Summary

Acronyms and mathematical notations are listed below.

Notation	Description
$(\cdot)^T$	Transpose
$(\cdot)^H$	Hermitian
$(\cdot)^*$	Complex conjugate
$(\cdot)^\dagger$	Pseudo-inverse
$(\cdot)^{1/2}$	Matrix square-root
$(\cdot)^{-1}$	Matrix inversion
$\delta(\cdot)$	Dirac delta
$\text{trace}(\cdot)$	Sum of diagonal elements

$\det(\cdot)$	Matrix determinant
MIMO	Multiple-input multiple-output
OFDM	Orthogonal frequency division multiplexing
i.i.d.	Independent and identically distributed
BTS	Base transceiver station
SU	Subscriber unit
RCG	Relative capacity gain
ZF	Zero-forcing
MMSE	Minimum-mean-square error
ML	Maximum likelihood
MAP	Maximum <i>a posteriori</i> probability
EM	Expectation maximization
ISI	Inter-symbol-interference
ICI	Inter-carrier-interference
CSI	Channel state information
MMSVR	Maximum-to-minimum-singular-value ratio
BER	Bit error rate
SNR	Signal-to-noise ratio
SVD	Singular-value decomposition

2. MIMO OFDM COMMUNICATION SYSTEMS

The blockdiagram of a MIMO OFDM system is shown in Fig. 2.1. At the transmitter side, the source bitstream is mapped to a symbol stream by the digital modulator. Spatial multiplexing is a MIMO technique that independent multiple symbol streams are transmitted at the same frequency band over different spatial channels. Each of the parallel output symbol streams corresponding to a particular transmit antenna follows the same procedure. Pilot symbols are inserted based on the prior-known pilot patterns. The modulation of OFDM could be efficiently implemented by using IFFT. A CP is usually appended to each OFDM symbol to avoid ISI due to the effect of channel multipath spread. Then the symbol stream is parallel-to-serial (P/S) converted for transmission. At the receiver side, the guard interval of each OFDM symbol is removed. The demodulation of OFDM could be implemented by using FFT. Then the CSI can be extracted and estimated by using the received signal and the pilot information. Transmitted symbols are detected based on the processed received signal and the estimated CSI. Finally, the detected symbols are demodulated to restore the transmitted bitstream.

2.1. MIMO Channels and Properties

This section describes the mobile MIMO wireless channels, which are characterized as time-varying. Because there are obstacles and reflectors in the wireless propagation channels, the transmitted signals arrive at the receiver from various directions over multiple paths. The received signal is the summation of these arriving waves with different phase, amplitude, and delay. If the waves of multipath signals undergo phase reversal, reduction of the signal strength at the receiver can occur. This kind of phenomenon is called multipath fading, which is generally modeled

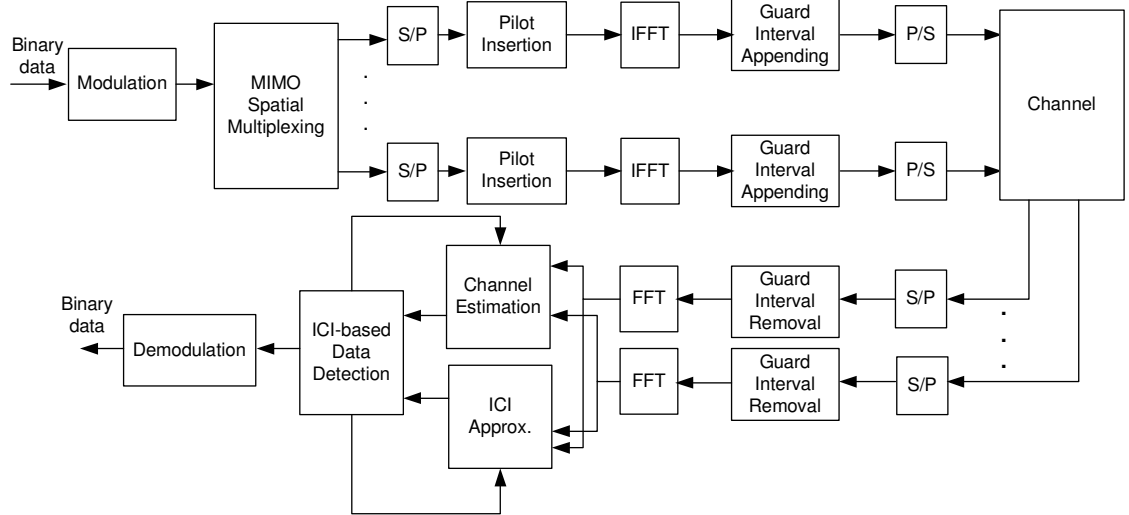


FIGURE 2.1. Blockdiagram of a MIMO OFDM system.

as Rayleigh fading [35, 36]. It is a major obstacle to the reliability of the wireless channels and causes significant degradation in the performance of digital wireless communications systems.

Different arrival time of the multiple reflections of the transmitted signal may result in ISI. This time dispersion of the channel is called multipath delay spread or channel delay spread, which is an important parameter to assess the performance of wireless systems. Common measures of multipath delay spread are the root-mean square (rms) delay spread and maximum multipath delay. For a reliable wireless communication without using an adaptive equalizer or other anti-multipath techniques, the transmitted data rate should be smaller than the coherent bandwidth, which equals approximately the inverse of the channel multipath spread.

2.1.1. Information Theory of MIMO

The system capacity is defined as the maximum transmission rate such that the probability of error could be arbitrary small. Consider a MIMO system with N_T transmit and N_R receive antennas over a frequency-flat fading channel, which can be modeled as

$$\mathbf{y} = \sqrt{\frac{E_s}{N_T}} \mathbf{H} \mathbf{s} + \mathbf{n} \quad (2.1)$$

where E_s is the transmitted symbol energy, \mathbf{y} is the $N_R \times 1$ received signal vector, \mathbf{s} is the $N_T \times 1$ transmitted signal vector, \mathbf{H} is the $N_R \times N_T$ MIMO CSI matrix, \mathbf{n} is the additive white complex Gaussian noise with $E\{\mathbf{n}\mathbf{n}^H\} = N_0 \mathbf{I}_{N_R}$, and $(\cdot)^H$ denotes Hermitian. Let us define ρ as the signal-to-noise ratio (SNR) at any receiver antenna (i.e., $\rho = \frac{E_s}{N_0}$). With equal power (EP) transmission for N_T transmit antennas, the system capacity can be expressed as [1]

$$C_{EP}(\mathbf{H}) = \log_2 \left[\det \left(\mathbf{I}_{N_R} + \frac{\rho}{N_T} \mathbf{H} \mathbf{H}^H \right) \right] \quad (2.2)$$

where $\det(\cdot)$ denotes the determinant operator. The normalization by the number of transmit antenna, N_T , ensures a fixed total transmit power. Eq. (2.2) can be rewritten in an eigenmode form as

$$C_{EP}(\mathbf{H}) = \sum_{i=1}^m \log_2 \left(1 + \frac{\lambda_i \rho}{N_T} \right) \quad (2.3)$$

where m is rank of the MIMO channel matrix and λ_i is the i -th eigenvalue of the Wishart matrix \mathbf{Q} , which is defined as [60]

$$\mathbf{Q} = \begin{cases} \mathbf{H}^H \mathbf{H}, & N_R \geq N_T \\ \mathbf{H} \mathbf{H}^H, & N_T > N_R. \end{cases} \quad (2.4)$$

Thus the capacity of MIMO systems grows linearly with the smaller of the number of transmit and receive antennas rather than logarithmically. Eq. (2.2) and Eq.

(2.3) only describe the instantaneous channel capacity of a fixed or one realization of the wireless channel. The capacity of the random channel can be characterized by two values: the average (or ergodic) capacity and outage capacity.

The average capacity ($C_{EP,A}$) can be obtained by averaging over all realizations of the CSI matrix as

$$C_{EP, A} = E\{C_{EP}(\mathbf{H})\} \quad (2.5)$$

where $E\{\cdot\}$ denotes statistical expectation.

Example: Fig. 2.2 shows the average (or ergodic) capacity of spatially uncorrelated MIMO Rayleigh fading channels versus SNR with different MIMO configurations. (N_T, N_R) denotes a MIMO system with N_T transmit antennas and N_R receive antennas. It is shown in the figure that the average capacity grows linearly with the smaller of the numbers of transmit and receive antennas.

Let us define the fixed transmission rate as T_R . The outage capacity, $C_{EP, O, \varepsilon}$, is defined as the maximum achievable rate with the outage probability of ε .

$$C_{EP, O, \varepsilon} = \{T_R : \text{Prob}\{C_{EP}(\mathbf{H}) < T_R\} < \varepsilon\}. \quad (2.6)$$

Example: Fig. 2.3 shows the outage probability of spatially uncorrelated MIMO Rayleigh fading channels versus SNR with different MIMO configurations. The fixed transmission rate T_R is set to be 4 bits per second per Hz.

Let \mathbf{V} denote the covariance matrix of the transmitted signal \mathbf{s} , the channel capacity can be expressed as

$$C(\mathbf{H}) = \max_{\mathbf{V}} \log_2 [\det(\mathbf{I}_{N_R} + \mathbf{H}\mathbf{V}\mathbf{H}^H)] \quad (2.7)$$

with the power constrain of $\text{trace}(\mathbf{V}) \leq \rho$. If the CSI is unknown at the transmitter and the transmitted signal has Gaussian distribution, the equal power with

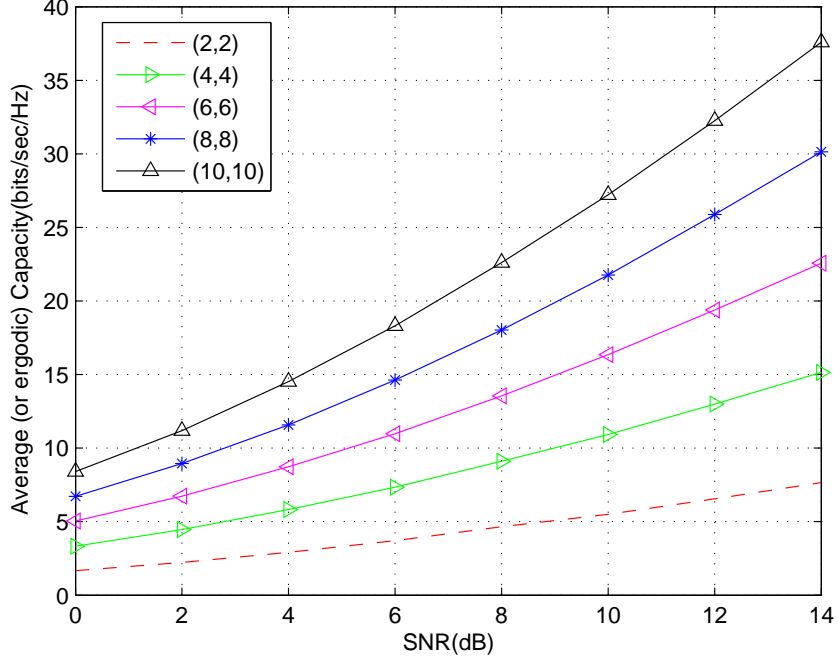


FIGURE 2.2. Average capacity of spatially uncorrelated MIMO Rayleigh fading channels versus SNR.

uncorrelated sources is the optimal solution. If the CSI is fed back to the transmitter, the optimal covariance matrix can be obtained by the water-filling (WF) algorithm. And more power is dynamically allocated to the good condition channels while keeping the same total transmission power. The channel capacity of one specific MIMO system is defined as

$$C \equiv \sum_{i=1}^{N_T} \log_2 \left[1 + \frac{P_i \lambda_i}{\sigma^2} \right] \quad (2.8)$$

where σ^2 is the noise variance at the receive antenna and λ_i is the eigenvalue of the Wishart matrix defined in Eq. (2.4). In order to obtain the optimal power allocation, let us define

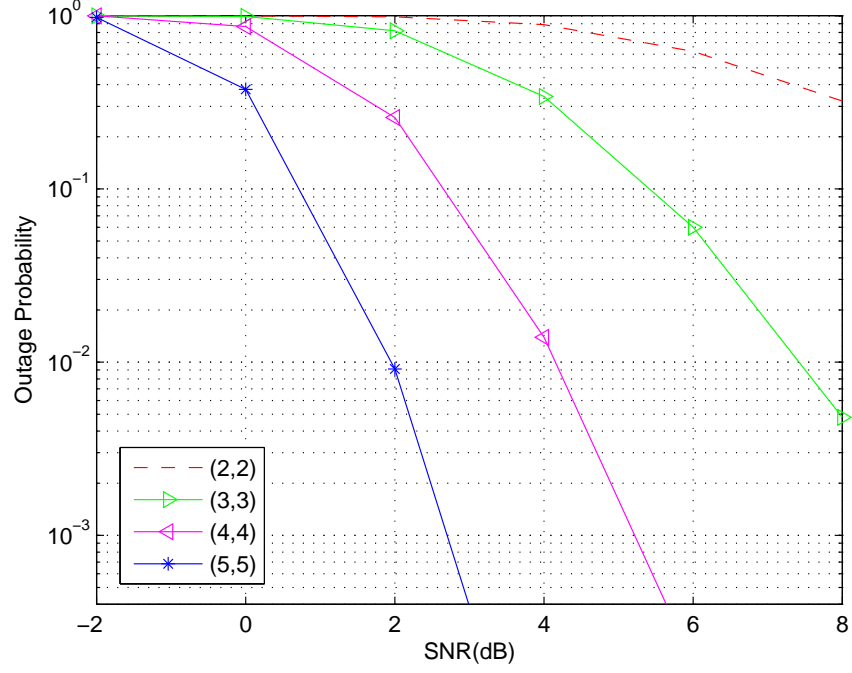


FIGURE 2.3. Outage probability of spatially uncorrelated MIMO Rayleigh fading channel versus SNR.

$$C_O \equiv \sum_{i=1}^{N_T} \log_2 \left[1 + \frac{P_i \lambda_i}{\sigma^2} \right] + \nu \left(P - \sum_{i=1}^{N_T} P_i \right) \quad (2.9)$$

where ν is the Lagrange multiplier. After setting the partial derivative of C_O with respect to P_i to zero (i.e., $\frac{\delta C_O}{\delta P_i} = 0$), we obtain

$$\frac{\delta C_O}{\delta P_i} = \frac{1}{\log_2} \frac{\lambda_i / \sigma^2}{1 + P_i \lambda_i / \sigma^2} - \nu = 0. \quad (2.10)$$

By defining $\mu = \frac{1}{\nu \log_2}$, the optimal power allocated to the i -th transmit antenna is expressed as

$$P_i = \left(\mu - \frac{\sigma^2}{\lambda_i} \right)^+ \quad (2.11)$$

where μ is determined by the power constraint such that

$$\sum_{i=1}^{N_T} P_i = P. \quad (2.12)$$

The channel capacity with water-filling can be expressed as [2]

$$\begin{aligned} C_{WF} &= \sum_{i=1}^{N_T} \log_2 \left(1 + \frac{P_i \lambda_i}{\sigma^2} \right) \\ &= \sum_{i=1}^{N_T} \log_2 \left[1 + \left(\frac{\lambda_i \mu}{\sigma^2} - 1 \right)^+ \right] \end{aligned} \quad (2.13)$$

where $(x)^+$ is defined as

$$(x)^+ = \begin{cases} x, & x > 0 \\ 0, & x \leq 0. \end{cases} \quad (2.14)$$

Since μ is a nonlinear function of the eigenvalues, the optimal capacity can be analyzed numerically for the random channel.

Example: Analyze the optimal power allocation numerically based on the water-filling principle for a (3, 3) MIMO channel, whose CSI matrix is expressed as

$$\mathbf{H} = \begin{bmatrix} 0.1092 - 0.3028i & -0.6553 + 0.0836i & -0.7821 + 0.4241i \\ 0.1451 + 0.6475i & -0.1169 - 0.5050i & -0.1749 - 0.2595i \\ 0.3263 + 0.5736i & 0.3248 + 0.5213i & 0.3793 + 0.3307i \end{bmatrix}. \quad (2.15)$$

The eigenvalues of the corresponding Wishart matrix, $\lambda_i (i = 1, 2, 3)$, are calculated as $\{2.2508, 0.9010, 0.0527\}$. Let us assume that the total transmit power is normalized to 1 and the SNR is 10dB. Thus the noise variance is $\sigma^2 = 0.1$ and ρ can be calculated as

$$\rho = 10^{SNR/10} = 10. \quad (2.16)$$

Step 1: Assume that non-zero power is allocated to all the channels including the worst channel with smallest eigenvalue. The μ defined in Eq. (2.11) can be calculated as

$$\mu = \frac{P + \sigma^2(\frac{1}{\lambda_1} + \frac{1}{\lambda_2} + \frac{1}{\lambda_3})}{3} = 1.0182. \tag{2.17}$$

However, since $\frac{\sigma^2}{\lambda_3} = 1.8992$ and $\mu < \frac{\sigma^2}{\lambda_3}$, the assumption is not valid.

Step 2: Since the above assumption is not valid, no power is allocated to channel 3. A new assumption is made such that non-zero power is allocated only to channel 1 and channel 2, and μ is recalculated as

$$\mu = \frac{P + \sigma^2(\frac{1}{\lambda_1} + \frac{1}{\lambda_2})}{2} = 0.5777. \tag{2.18}$$

Since $\frac{\sigma^2}{\lambda_2} = 0.1110$ and $\mu > \frac{\sigma^2}{\lambda_2}$, this assumption is valid.

Step 3: The optimal power can be calculated as $P_i = \mu - \frac{\sigma^2}{\lambda_i}$. Thus, we obtain $P_1 = 0.5333$, $P_2 = 0.4667$, and $P_3 = 0$.

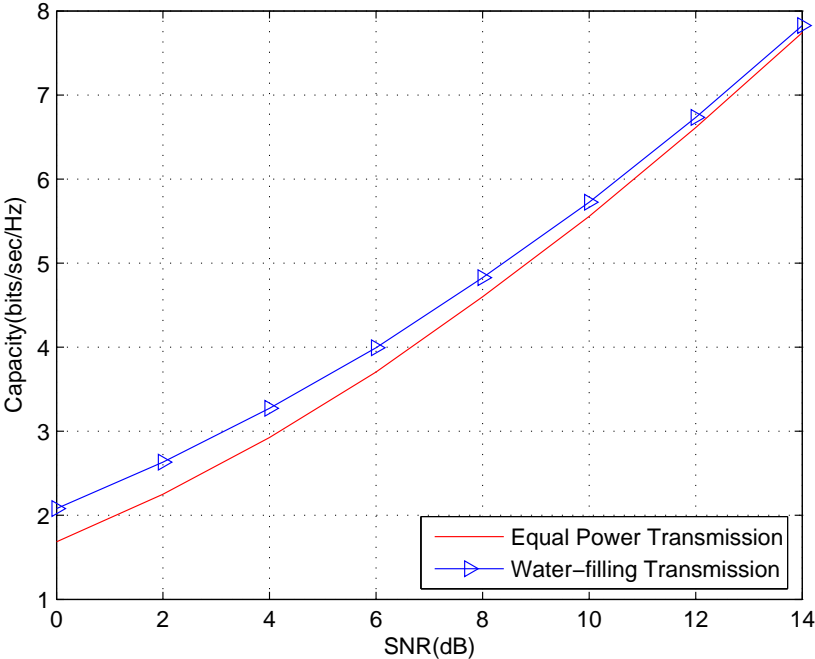


FIGURE 2.4. Channel capacity versus SNR.

The relative capacity gain (RCG) is defined as

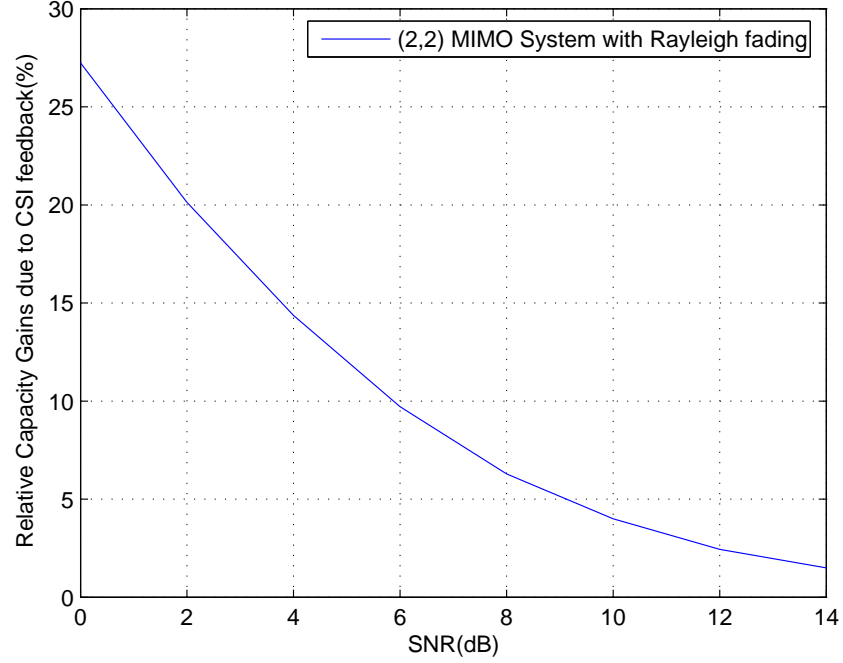


FIGURE 2.5. Relative capacity gain versus SNR.

$$RCG = \frac{C_{WF} - C_{EP}}{C_{EP}} \quad (2.19)$$

where C_{WF} is the capacity with water-filling scheme and C_{EP} is the capacity achieved with equal power allocation. Fig. 2.4 shows the channel capacity with water-filling and equal-power transmission. Fig. 2.5 shows the relative capacity gain of a (2, 2) MIMO system. If the transmitter has channel parameters, power is optimally allocated to the spatial channel based on the water-filling principle. If channel information is only available at the receiver, equal power allocation is applied. In the figure, it proves that the capacity gain due to CSI feedback disappears gradually with an increased SNR.

There are two asymptotic values to measure the average capacity C_A and the outage probability ε : spatial multiplexing order (O_{SP}) and diversity order (O_D), which are defined as

$$O_{SP} = \lim_{\rho \rightarrow \infty} \frac{C_A}{\log_2(\rho)} \tag{2.20}$$

$$O_D = - \lim_{\rho \rightarrow \infty} \frac{\log_2(\varepsilon)}{\log_2(\rho)}. \tag{2.21}$$

The spatial multiplexing order is the asymptotic rate at which the average capacity increases with the log scale of SNR. It is shown in Fig. 2.6 that a MIMO channel can provide a spatial multiplexing order as large as N_T if the number of transmit antennas is equal to the number of receive antennas (i.e., $N_T = N_R$).

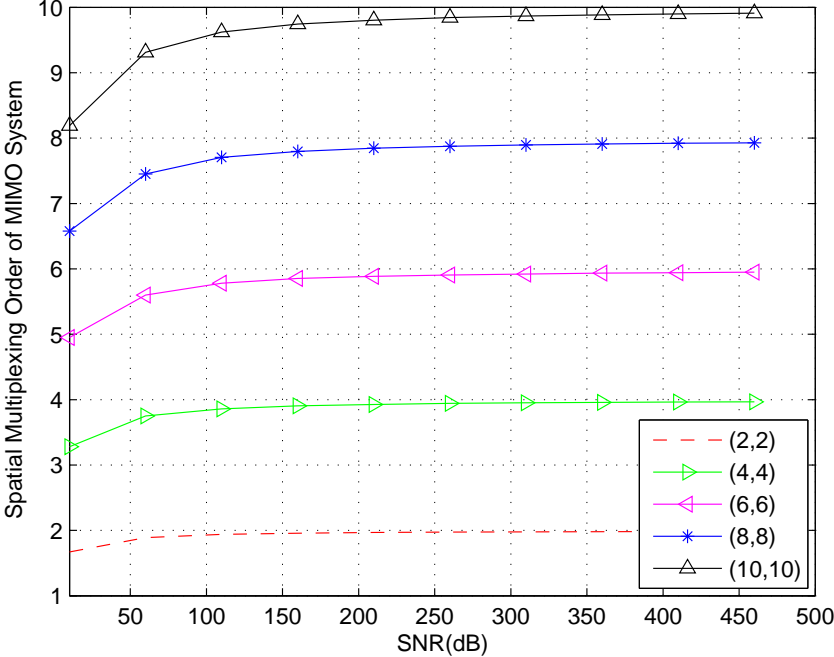


FIGURE 2.6. Spatial multiplexing order of spatially uncorrelated MIMO Rayleigh fading channels versus SNR.

2.1.2. MIMO Frequency-selective and Time-varying Channels

If the signal bandwidth is much smaller than the channel coherent bandwidth, then fading across the entire signal bandwidth is highly correlated. This is referred to as flat fading. On the other hand, if the channel coherence bandwidth is much smaller than the signal bandwidth, then individual frequencies might be attenuated and faded differently [37]. In this case, the channel is described as frequency-selective fading. It occurs if the channel delay spread is significant compared with the symbol period. The current symbol will collide with later ones, which results in ISI.

Consider a system with N_T transmit antennas and N_R receive antennas. The sub-channels are defined as the channels over which the signal is transmitted from the u -th ($1 \leq u \leq N_T$) transmit antenna to the v -th ($1 \leq v \leq N_R$) receive antenna. Since the signal is band-limited, the time-varying multipath channel can be represented by using the tapped-delay line model with time-varying coefficients but fixed tap spacing [87]. The delay spread of the channel determines the length of the tapped delay line and the tap spacing must be equal to or less than the reciprocal of the signal bandwidth. Each sub-channel is composed of $L + 1$ paths, where L depends on the ratio of the maximum delay spread of the channel to the OFDM sampling interval. With perfect sample timing, we can denote the discrete time multipath sub-channel from the u -th transmit antenna to the v -th receive antenna at time nT_s as

$$\underline{A}_{v,u}(n) = [A_{v,u}(n, 0), A_{v,u}(n, 1), \dots, A_{v,u}(n, L)]^T \quad (2.22)$$

where $(\cdot)^T$ denotes transpose and $A_{v,u}(n, l)$ denotes the tap gain of the l -th path at time index n . If L equals 0, the channel becomes a memoryless channel and the frequency response is flat, which results in flat fading.

2.1.3. Spatially Correlated and Uncorrelated MIMO Channels

Let $\mathbf{A}(n, l)$ denote the $N_R \times N_T$ uncorrelated MIMO fading channel matrix whose (v, u) -th element is $A_{v,u}(n, l)$. Assume that different paths are uncorrelated, i.e.,

$$E \{ \text{vec}\{\mathbf{A}(n, l_1)\} \text{vec}^H\{\mathbf{A}(n, l_2)\} \} = \mathbf{0}_{N_T N_R}, l_1 \neq l_2 \quad (2.23)$$

where $(\cdot)^H$ denotes Hermitian, $\mathbf{0}_{N_T N_R}$ represents $N_T N_R \times N_T N_R$ zero matrix, and $\text{vec}\{\mathbf{A}(n, l)\}$ is the $N_R N_T \times 1$ vector constructed by stacking all of the columns of matrix $\mathbf{A}(n, l)$.

If both the transmit and receive antennas are sufficiently separated under the rich-scattering environment [38], channel fading processes for different sub-channels are assumed to be independent and identically distributed (i.i.d.). In this case, the $N_T \times N_T$ transmitter correlation matrix \mathbf{T}_l and $N_R \times N_R$ receiver correlation matrix \mathbf{R}_l reduce to identity matrices, i.e., $\mathbf{T}_l = \mathbf{I}_{N_T}$ and $\mathbf{R}_l = \mathbf{I}_{N_R}$. The propagation scenario considered in this thesis is a typical cellular deployment: the base transceiver station (BTS) is located in the tower, which is sufficiently high without any obstruction or local scatterers. The spatial channels at the BTS are correlated and determined by the BTS antenna spacing and the angular spread observed at the BTS array [39]. However, the subscriber unit (SU) is surrounded by many local scatterers and the antenna spacing is large such that the SU antennas are spatially uncorrelated. In this thesis, we focus our analysis on the downlink case. Thus, the transmitter refers to BTS and the receiver refers to SU (i.e., $\mathbf{R}_l = \mathbf{I}_{N_R}$). An uniform linear array (ULA) at both the transmitter and receiver is assumed. Let $\bar{\theta}_l$ and $\gamma_l^2, l = 0, 1, \dots, L$, represent the mean of the departure angle and the variance of the departure angular spread for the l -th path, respectively. If there is no angular spread [39], the transmitter correlation matrix can be represented as

$$\mathbf{T}_l = \mathbf{a}(\bar{\theta}_l)\mathbf{a}^T(\bar{\theta}_l) \quad (2.24)$$

$$\mathbf{a}(\bar{\theta}_l) = \left[1, e^{j2\pi B \cos(\bar{\theta}_l)}, \dots, e^{j2\pi(N_T-1)B \cos(\bar{\theta}_l)} \right]^T \quad (2.25)$$

$$B = f_c b / c \quad (2.26)$$

where B is the relative antenna spacing, b is the absolute antenna spacing, c is the light speed, and f_c is the carrier frequency. If the angular spread is not zero, it is shown in [40] that the (m, n) -th element of transmitter correlation matrix \mathbf{T}_l can be approximated as

$$[\mathbf{T}_l]_{m,n} \approx e^{-j2\pi(n-m)B \cos(\bar{\theta}_l)} e^{(-0.5)(2\pi(n-m)B \sin(\bar{\theta}_l)\gamma_l)^2}. \quad (2.27)$$

The spatially correlated CSI matrix, $\mathcal{H}(n, l)$, is defined as [39]

$$\mathcal{H}(n, l) = \mathbf{R}_l^{1/2} \mathbf{A}(n, l) \mathbf{T}_l^{1/2} \quad (2.28)$$

where $(\cdot)^{1/2}$ denotes matrix square root. With perfect sample timing, we can denote the discrete time multipath channel at time nT_s as

$$\mathbf{h}_{v,u}(n) = [h_{v,u}(n, 0), h_{v,u}(n, 1), \dots, h_{v,u}(n, L)]^T \quad (2.29)$$

where $h_{v,u}(n, l)$ is the (v, u) -th element of matrix $\mathcal{H}(n, l)$. This model is assumed and verified by measurements in [44–47]. In this MIMO fading channel model, the rank of the CSI matrix $\mathcal{H}(n, l)$ is determined not only by the Rayleigh fading ($\mathbf{A}(n, l)$) but also by the fading correlation at the transmitter and receiver (\mathbf{T}_l and \mathbf{R}_l). If the angular spread of the l -th path is large, $\mathcal{H}(n, l)$ will most likely have high rank.

2.2. Simulation Model of MIMO Time-varying Channels

Mobile channel simulators are commonly used to test and evaluate the systems. Many approaches have been proposed for the modelling and simulation of

mobile radio channels. Among them, the Jakes model [48] has been widely used for Rayleigh fading channels. The channel of each pair of transmit and receive antennas is assumed to have $L + 1$ multipath components and fading processes are piecewise-constant approximated, which allows the channel coefficients to be constant in one sampling interval and change over different sampling intervals according to the spaced-time correlation function. Fading processes for different spatial sub-channels and different paths are all assumed to be independent. Also, the first and second order statistics of the channel do not change over the entire transmission horizon.

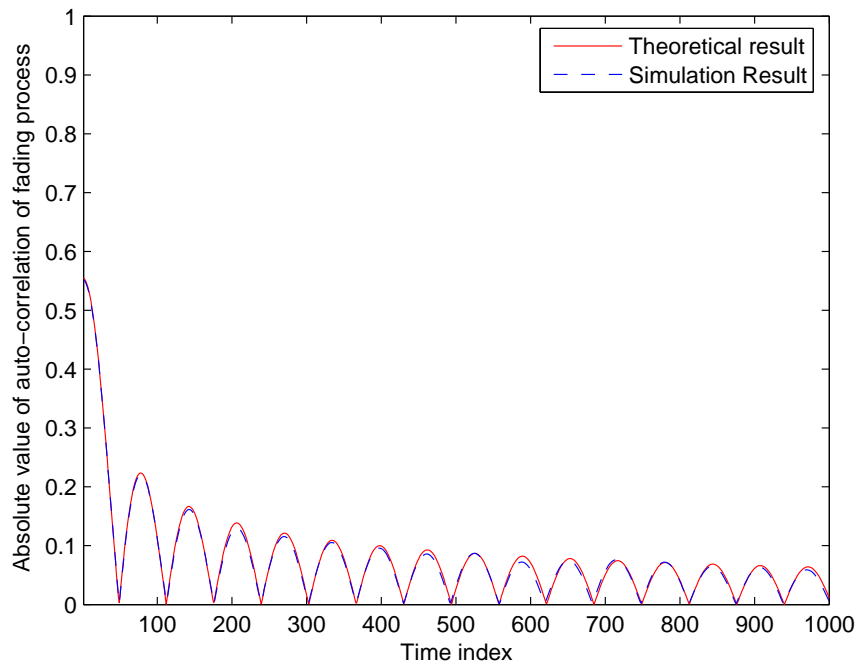


FIGURE 2.7. The theoretical and simulated auto-correlation of the modified Jakes model.

Since Jakes model is a deterministic model and has difficulties in generating uncorrelated multipath, different modified simulators are proposed in [49–51]. [49]

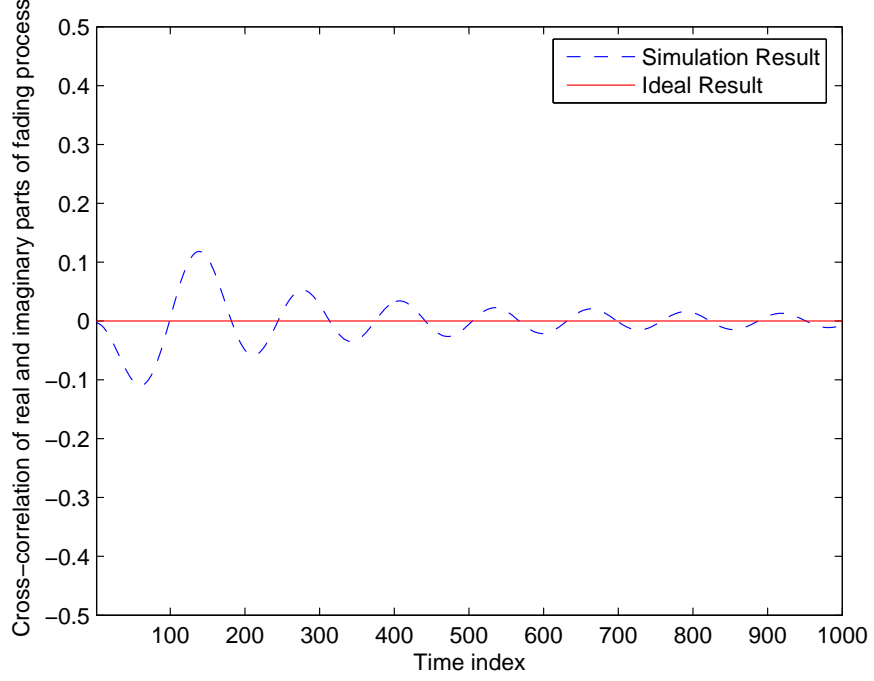


FIGURE 2.8. The ideal and simulated cross-correlation of real and imaginary parts of the modified Jakes model.

proposes a modified Jakes model to generate uncorrelated multipath waveforms based on Walsh-Hadamard codewords. This model assumes that N_r equal-strength rays arrive at a moving receiver with uniformly distributed arrival angle α_n ($n = 1, 2, \dots, N_r$) such that the n -th ray experiences a Doppler shift $\omega_n = 2\pi f_d \cos(\alpha_n)$, where f_d is the maximum Doppler shift. f_d can be calculated as $f_d = f_c v/c$, where v is the vehicle speed. By setting $\alpha_n = 2\pi(n - 0.5)/N_r$, the fading waveform can be modeled with N_1 complex oscillators ($N_1 = N_r/4$). The equal power oscillators are considered in order to eliminate the correlation. The waveform of the model is defined as

$$a(t) = \sqrt{\frac{2}{N_1}} \sum_{n=1}^{N_1} [\cos(\pi n/N_1) + j \sin(\pi n/N_1)] \cos(\omega_n t + \theta_n) \quad (2.30)$$

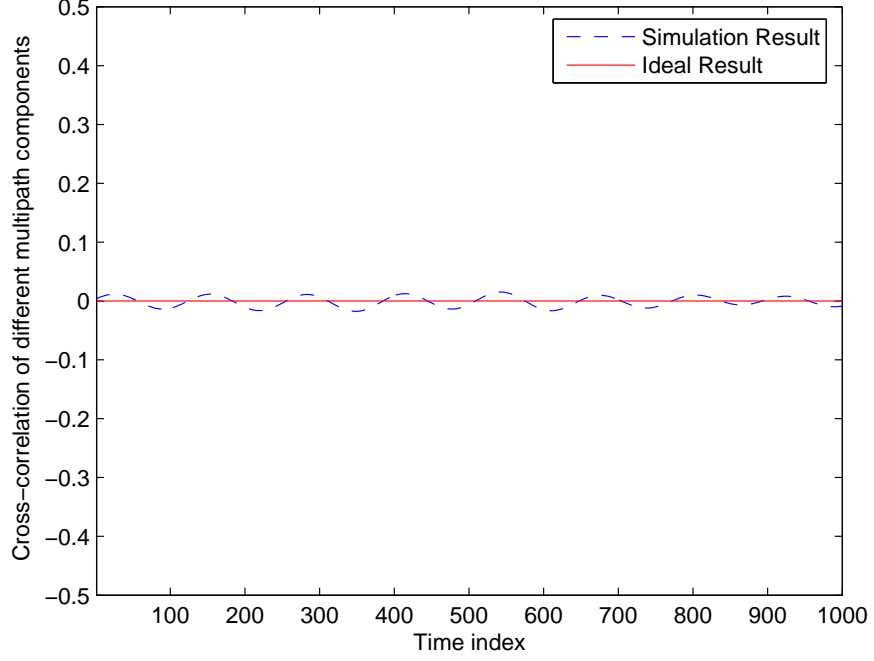


FIGURE 2.9. The ideal and simulated cross-correlation of different multipath components of the modified Jakes model.

where $\sqrt{\frac{2}{N_1}}$ is the normalization factor to ensure $E\{a(t)a^*(t)\} = 1$. In order to generate uncorrelated waveforms, Walsh-Hadamard codewords are used to weigh the oscillator values before summing. The l -th waveform is generated as

$$a(t, l) = \sqrt{\frac{2}{N_1}} \sum_{n=1}^{N_1} M(l, n) [\cos(\pi n/N_1) + j \sin(\pi n/N_1)] \cos(\omega_n t + \theta_n) \quad (2.31)$$

where $M(l, n)$ is the n -th value of the l -th Walsh-Hadamard code sequence. With a sampling interval of T_s , $A_{v,u}(n, l)$, the (v, u) -th element of matrix $\mathbf{A}(n, l)$, is determined by the value of $a(nT_s, l)$. The theoretical and simulated auto-correlations of the waveform are shown in Fig. 2.7. We can see the two results match very well. The ideal cross-correlation of the real and imaginary parts of the waveform is

zero and the simulated result is shown in Fig. 2.8. The simulated cross-correlation of the waveforms of different multipath components is shown in Fig. 2.9 and it is compared with the ideal result, which is zero as shown in the figure. The model [49] is considered in this thesis due to its better auto-correlation of the fading process. But it has a slightly inferior cross-correlation among different multipath components compared to the simulation model proposed in [50].

After obtaining uncorrelated channel coefficient, $A_{v,u}(n, l)$, for different multipath and distinct pair of transmit and receive antennas and having the knowledge of transmitter correlation matrix, the spatially correlated CSI matrix, $\mathcal{H}(n, l)$, can be obtained by Eq. (2.28).

3. PERFORMANCE MODELLING OF MIMO OFDM SYSTEMS VIA CHANNEL ANALYSIS

Implementation of high data rate WLAN has been a major focus of research in recent years. MIMO schemes [52–54] and OFDM [27] can be combined to operate at the high-throughput (HT) mode, or the diversity mode, or the combination of both in fading environments [55]. Such systems could achieve high spectral efficiency and/or a large coverage area that are critical for future-generation wireless local area networks.

Existing research has relied mainly on obtaining the error-rate performance curves to determine the throughput and diversity gains [56, 57] of various MIMO configurations, assuming Rayleigh fading and independent and identically distributed MIMO OFDM sub-channels. Alternatively, the relative capacity and throughput of different system configurations can be obtained by using the channel characteristics. If analytical characterizations of the channel are available, this approach will be more efficient than the former, as it does not require complex system-level simulations.

Common open-loop linear detection schemes include the ZF and MMSE schemes [2, 58]. A large condition number (i.e., the maximum-to-minimum-singular-value ratio, MMSVR) of the CSI matrix implies a high noise enhancement and causes the open-loop schemes to fail in exploiting the available capacity [59]. Thus, MMSVR could be a convenient and effective metric to characterize the performance of different MIMO configurations.

The importance and effectiveness of the eigenvalue distribution on MIMO system capacity and the overall system performance have been well recognized [60–63]. The eigenvalue analysis for MIMO OFDM systems can be used to reduce the overall system complexity [64, 65]. In this chapter, we derive the analytical

probability density function (pdf) of the MMSVR value, which can be used to predict the relative performance of different MIMO configurations. The pdf can also be used to estimate the lower bound on the noise enhancement [66] and the capacity of MIMO channels. We establish the relationship between MMSVR and the achievable data throughput. Simulation results verify the accuracy of the closed-form pdf expressions of MMSVR derived in this chapter.

This chapter is organized as follows. In Section 3.1, the MIMO OFDM system model and the open-loop ZF and MMSE detection schemes [2, 58] will be described. Section 3.2 introduces the channel model and then derives the pdf of the MMSVR of the channel matrix, while Section 3.3 provides simulation setup and discusses channel analysis simulation results for various MIMO configurations. Concluding remarks are made in Section 3.4.

3.1. System Model and Detection Schemes

3.1.1. System Model

Consider a MIMO OFDM system where the transmitter has N_T antennas, the receiver has N_R antennas, and all the transmitted symbols share N sub-carriers. The frequency domain transmitted sequence from the n -th ($n = 1, \dots, N_T$) transmit antenna is represented by $X_{n,k}$, where $k = 1, \dots, N$ represents the k -th OFDM sub-carrier. The sequence received by the m -th ($m = 1, \dots, N_R$) receive antenna is expressed as

$$Y_{m,k} = \sum_{n=1}^{N_T} H_{m,n,k} X_{n,k} + \zeta_{m,k} \quad (3.1)$$

where $H_{m,n,k}$ is the frequency response of the channel between the n -th transmit antenna and the m -th receive antenna for the k -th sub-carrier, $\zeta_{m,k}$ is the frequency

response of zero-mean additive white Gaussian noise (AWGN) with a one-sided power spectral density of \mathcal{N}_0 . Let us define the signal transmitted on the k -th sub-carrier from all the N_T transmit antennas as $\mathbf{X}_k = [X_{1,k}, X_{2,k}, \dots, X_{N_T,k}]^T$, where $(\cdot)^T$ denotes transpose. The received signal as a function of the respective CSI matrix \mathbf{H}_k can be expressed as

$$\begin{aligned} \mathbf{Y}_k &= [Y_{1,k}, Y_{2,k}, \dots, Y_{N_R,k}]^T \\ &= \begin{bmatrix} H_{1,1,k} & H_{1,2,k} & \cdots & H_{1,N_T,k} \\ & & \vdots & \\ H_{N_R,1,k} & H_{N_R,2,k} & \cdots & H_{N_R,N_T,k} \end{bmatrix} \mathbf{X}_k + \begin{bmatrix} \zeta_{1,k} \\ \zeta_{2,k} \\ \vdots \\ \zeta_{N_R,k} \end{bmatrix} \\ &= \mathbf{H}_k \mathbf{X}_k + \boldsymbol{\zeta}_k. \end{aligned} \quad (3.2)$$

We obtain the general system description by vertically stacking the received signal given in Eq. (3.2) for all N sub-carriers as

$$\begin{aligned} \mathbf{Y} &= [\mathbf{Y}_1^T, \mathbf{Y}_2^T, \dots, \mathbf{Y}_N^T]^T \\ &= \mathbf{H} \mathbf{X} + \boldsymbol{\zeta} \end{aligned} \quad (3.3)$$

where $\mathbf{X} = [\mathbf{X}_1^T, \mathbf{X}_2^T, \dots, \mathbf{X}_N^T]^T$, $\boldsymbol{\zeta} = [\boldsymbol{\zeta}_1^T, \boldsymbol{\zeta}_2^T, \dots, \boldsymbol{\zeta}_N^T]^T$, and $\mathbf{H} = \text{diag}[\mathbf{H}_1, \mathbf{H}_2, \dots, \mathbf{H}_N]$ is a block diagonal matrix.

3.1.2. Detection

Open-loop detection schemes require $N_R \geq N_T$ if the system operates at the spatial multiplexing mode. Zero-forcing (ZF) is the simplest open-loop method in which the estimates of the transmitted signals are obtained by multiplying the received signal \mathbf{Y} with the pseudo-inverse of the CSI matrix as

$$\hat{\mathbf{X}} = \mathbf{W}_{ZF} \mathbf{Y} = \mathbf{H}^+ \mathbf{Y} = \mathbf{X} + \boldsymbol{\xi} \quad (3.4)$$

where $(\cdot)^+$ represents the pseudo-inverse, $\mathbf{W}_{ZF} = \mathbf{H}^+$ is the weight matrix for the ZF scheme, and $\boldsymbol{\xi} = \mathbf{H}^+ \boldsymbol{\zeta}$. Note that the detection can be carried out on a sub-carrier by sub-carrier basis if there is no inter-carrier interference. This method requires channel estimates at the receiver, and since AWGN is not considered in the estimation process, it might result in a high noise enhancement. At high signal-to-noise ratios (SNR), the instantaneous noise power of the n -th data stream transmitted on the k -th sub-carrier is written as [67]

$$[E\{\boldsymbol{\xi}\boldsymbol{\xi}^\dagger\}]_{n \times k, n \times k} = \mathcal{N}_0 [\mathbf{W}\mathbf{W}^\dagger]_{n \times k, n \times k} \quad (3.5)$$

where $[\cdot]_{n \times k, n \times k}$ denotes the $(n \times k, n \times k)$ -th component of a matrix, $E\{\cdot\}$ denotes expectation, and \mathbf{W} could be either \mathbf{W}_{ZF} or \mathbf{W}_{MMSE} . For a particular CSI matrix \mathbf{H} , the instantaneous noise enhancement factor for the n -th data stream in the k -th sub-carrier is $[\mathbf{W}\mathbf{W}^\dagger]_{n \times k, n \times k}$. When the MMSVR of \mathbf{H} is large, the noise enhancement will be high.

3.2. Analysis of MIMO Channel

3.2.1. Channel Model

Spatial sub-channels (i.e., the channel from transmit antenna n to receive antenna m) are assumed to be independent. This assumption is valid if the antenna spacing is greater than half of the wavelength of the carrier under rich-scattering environment. We adopt the IEEE 802.11 model with an exponential power-delay profile [69]. The channel is modeled as a finite impulse response (FIR) filter where all the $L + 1$ paths are independent complex Gaussian random variables with zero

mean and average power ω_l^2 ($l = 0, 1, \dots, L$). The channel impulse response can be written as $h_l = a + jb$, where a and b are defined to be random variables obeying normal distribution with zero mean and variance of $\omega_l^2/2$. In this model, the power of multipath components decreases exponentially. To normalize the channel energy, the first multipath component is chosen as $\omega_0^2 = (1 - \beta)/(1 - \beta^{L+1})$, where $\beta = e^{-T_s/\tau_{rms}}$, $L = 10\tau_{rms}/T_s$, T_s represents the sampling period, and τ_{rms} is the root mean-square (RMS) delay spread of the channel. The energy of the l -th multipath component is then defined as $\omega_l^2 = \omega_0^2\beta^l$.

3.2.2. Analysis of Channel Characteristics

For the ZF detection scheme to work efficiently, some constraints must be met. First of all, the number of receive antennas N_R should not be, as mentioned earlier, less than the number of transmit antennas N_T . In the downlink of a practical WLAN system, however, it is preferred to have more antennas at the transmitter considering power consumption of the receiver. Moreover, the CSI matrix for each sub-carrier, \mathbf{H}_k , should not be an ill-conditioned¹ matrix since such a matrix will cause a high noise enhancement in detection. For open-loop operations, the system could run in the high throughput (HT) mode (the number of spatial streams equals the number of transmit antennas) when the received SNR is moderately high. If the channel is ill-conditioned, detection using the ZF scheme will experience a low instantaneous SNR, resulting in poor performance. In this case, it might be better

¹In this chapter, a non-square matrix is defined to be ill-conditioned if the minimum singular value of the channel matrix is significantly small compared to the maximum singular value.

to switch the system to operate at the diversity mode (the number of spatial streams is less than the number of transmit antennas).

Let the noise enhancement matrix for the k -th sub-carrier be $\mathbf{\Omega}_k, k = 1, \dots, N$. For a rank-two² ZF scheme in the HT mode, using the singular value decomposition (SVD) of the CSI matrix, we obtain $\mathbf{\Omega}_{ZF,k}$ as

$$\begin{aligned}
\mathbf{\Omega}_{ZF,k} &= \mathbf{W}_{ZF,k} \mathbf{W}_{ZF,k}^\dagger = \mathbf{H}_k^+ (\mathbf{H}_k^+)^{\dagger} = (\mathbf{H}_k^{\dagger} \mathbf{H}_k)^+ \\
&= (\mathbf{V}_k \mathbf{\Sigma}_k^{\dagger} \mathbf{U}_k^{\dagger} \mathbf{U}_k \mathbf{\Sigma}_k \mathbf{V}_k^{\dagger})^+ \\
&= \mathbf{V}_k (\mathbf{\Sigma}_k^{\dagger} \mathbf{\Sigma}_k)^+ \mathbf{V}_k^{\dagger} \\
&= \mathbf{V}_k \begin{bmatrix} 1/|\sigma_{k,1}|^2 & 0 \\ 0 & 1/|\sigma_{k,2}|^2 \end{bmatrix} \mathbf{V}_k^{\dagger} \\
&= |\sigma_{k,1}|^{-2} \mathbf{V}_k \begin{bmatrix} 1 & 0 \\ 0 & |\sigma_{k,1}|^2/|\sigma_{k,2}|^2 \end{bmatrix} \mathbf{V}_k^{\dagger} \tag{3.6}
\end{aligned}$$

where $\sigma_{k,1}$ and $\sigma_{k,2}$ ($\sigma_{k,1} \geq \sigma_{k,2} > 0$) represent the singular values of matrix \mathbf{H}_k . $1/|\sigma_{k,1}|^2$ and $1/|\sigma_{k,2}|^2$ also represent the noise enhancement factors for the two sub-channels. Let $\gamma_k = \sigma_{k,1}/\sigma_{k,2}$. A large γ_k value could arise either because $\sigma_{k,2}$ is small or because $\sigma_{k,1}$ is large. From simulation results, it is found that the latter is unlikely³, thus γ_k is a good indicator of noise enhancement, and if $\gamma_k \gg 1$, we can conclude that the channel is ill-conditioned for the k -th sub-carrier. For an open-

²The main focus of this chapter is on rank-two and rank-three CSI matrices since the emerging IEEE 802.11n MIMO WLAN standard is expected to have 2 to 4 transmit and 2 to 4 receive antennas.

³The probability of having $\sigma_{k,1}$ larger than five equals 8.71×10^{-9} for a 2×2 system, 1.05×10^{-7} for a 2×3 system, 1.17×10^{-6} for a 3×3 system, 8.59×10^{-6} for a 3×4 system, 5.81×10^{-5} for a 4×4 system and 2.92×10^{-4} for a 4×5 system.

loop system with a rank higher than two, the definition of γ_k can be generalized as $\sigma_{k,1}/\sigma_{k,u}$, where $u = \min(N_T, N_R)$, and $\sigma_{k,1}$, $\sigma_{k,u}$ are the maximum and minimum singular values, respectively.

MMSVR is also a good measure of the system capacity lower bound. Using the alternative capacity representation of [60], the capacity of the k -th carrier can be written as

$$C_k = \sum_{i=1}^u \log_2 \left(1 + \frac{\rho_k}{N_T} |\sigma_{k,i}|^2 \right) \quad (3.7)$$

where ρ_k is the SNR of the k -th sub-carrier. Considering $\sigma_{k,1} \geq \sigma_{k,2} \geq \dots \geq \sigma_{k,u} > 0$, a lower bound of the capacity can be written as

$$C_k \geq \log_2 \left(1 + \frac{\rho_k}{N_T} |\sigma_{k,1}|^2 \right) + (u-1) \log_2 \left(1 + \frac{\rho_k}{N_T} \frac{|\sigma_{k,1}|^2}{|\gamma_k|^2} \right). \quad (3.8)$$

As mentioned earlier, a large γ_k value is mostly due to a small $\sigma_{k,u}$ value. This fact combined with Eq. (3.8) clearly indicates that a high value of MMSVR results in a considerably lowered system capacity.

The Fourier transform of the channel impulse response of each OFDM carrier described in Section 3.2.1 has a Gaussian distribution. The singular values of the CSI matrix for the k -th OFDM carrier, \mathbf{H}_k , are the positive square-roots of the eigenvalues of the positive-definite Wishart matrix given as $\mathbf{Q}_k = \mathbf{H}_k^\dagger \mathbf{H}_k$, where $(\cdot)^\dagger$ represents Hermitian transpose. To obtain the pdf of γ_k , the joint pdf of the eigenvalues of \mathbf{Q}_k is needed. Let $\lambda_1 \geq \lambda_2 \geq \dots \geq \lambda_u$ be the eigenvalues of the positive-definite matrix \mathbf{Q}_k . The joint density function of $\lambda_1, \lambda_2, \dots, \lambda_u$ are obtained to be

$$f_\lambda(\lambda_1, \dots, \lambda_u) = K_{u,v}^{-1} e^{-\sum_i \lambda_i} \prod_i \lambda_i^{v-u} \prod_{i < j} (\lambda_i - \lambda_j)^2 \quad (3.9)$$

where $u = \min(N_T, N_R)$, $v = \max(N_T, N_R)$, and $K_{u,v}$ is a normalization factor [60]. From Eq. (3.9), we can calculate the joint density function of λ_1 and λ_u , $f_\lambda(\lambda_1, \lambda_u)$, from which the joint cumulative distribution function is obtained as

$$F_\lambda(\lambda_1, \lambda_u) = \int_0^{\lambda_1} \int_0^{\lambda_u} f_\lambda(\alpha, \beta) d\alpha d\beta. \quad (3.10)$$

Since the singular values of \mathbf{H}_k , σ_i , $i = 1, \dots, u$, are the square-root of the eigenvalues λ_i , $i = 1, \dots, u$, of the positive-definite matrix \mathbf{Q}_k , the joint cumulative distribution of σ_1 and σ_u is

$$\begin{aligned} F_\sigma(\sigma_1, \sigma_u) &= P(\sqrt{\lambda_1} \leq \sigma_1, \sqrt{\lambda_u} \leq \sigma_u) \\ &= P(0 \leq \lambda_1 \leq \sigma_1^2, 0 \leq \lambda_u \leq \sigma_u^2) \\ &= F_\lambda(\sigma_1^2, \sigma_u^2) - F_\lambda(0, \sigma_u^2) - \\ &\quad F_\lambda(\sigma_1^2, 0) + F_\lambda(0, 0). \end{aligned} \quad (3.11)$$

Using Eq. (3.11), the probability density function of γ , omitting the subscript for simplicity of notation in the sequel, can be derived as

$$f_\sigma(\sigma_1, \sigma_u) = \frac{d^2 F_\sigma(\sigma_1, \sigma_u)}{d\sigma_1 d\sigma_u} \quad (3.12)$$

$$\begin{aligned} f_\gamma(\gamma) &= f_\gamma\left(\frac{\sigma_1}{\sigma_u}\right) \\ &= \int_0^\infty |\sigma_u| f_\sigma(\sigma_u \gamma, \sigma_u) d\sigma_u. \end{aligned} \quad (3.13)$$

For 2×2 and 2×3 configurations, the distribution of the singular value ratios obtained using Eqs. (3.9)-(3.13) are

$$f_\gamma(\gamma)_{2 \times 2} = \frac{12\gamma(-1 + \gamma^2)^2}{(1 + \gamma^2)^4} \quad (3.14)$$

$$f_\gamma(\gamma)_{2 \times 3} = \frac{120\gamma^3(-1 + \gamma^2)^2}{(1 + \gamma^2)^6}. \quad (3.15)$$

Similarly for 3×3 and 3×4 systems, the distributions of γ obtained by using Eqs. (3.9)-(3.13) are

$$f_{\gamma}(\gamma)_{3 \times 3} = \frac{216(-1 + \gamma^2)^7(1 + \gamma^2)(11 + 20\gamma^2 + 11\gamma^4)}{(2 + 5\gamma^2 + 2\gamma^4)^6} \quad (3.16)$$

$$f_{\gamma}(\gamma)_{3 \times 4} = \frac{840\gamma^3(-1 + \gamma^2)^7(1 + \gamma^2)(A_{3 \times 4}(\gamma) + B_{3 \times 4}(\gamma))}{(2 + 5\gamma^2 + 2\gamma^4)^9} \quad (3.17)$$

where

$$A_{3 \times 4}(\gamma) = 4107\gamma^2 + 11562\gamma^4 + 15868\gamma^6 \quad (3.18)$$

$$B_{3 \times 4}(\gamma) = 454 + 11562\gamma^8 + 4107\gamma^{10} + 454\gamma^{12}. \quad (3.19)$$

The methodology of calculating the closed-form theoretical expressions for the pdf of γ can be easily extended to MIMO OFDM systems with a rank higher than three.

3.3. Numerical Examples and Discussion

In simulations, an RMS delay spread of $\tau_{rms} = 50\text{ns}$ and the maximum delay of $10\tau_{rms}$ are considered. Statistics are collected based on 10,000 channel realizations. Each channel tap is modeled as an independent complex Gaussian random variable. The CSI matrix is decomposed on a per OFDM carrier basis, and as defined in Section 3.2.2, γ_k is the ratio of the maximum and the minimum singular values of \mathbf{H}_k for the k -th sub-carrier. The parameters of OFDM symbols are chosen as in the IEEE 802.11a standard (i.e., 64 sub-carriers in one OFDM symbol with a sub-carrier frequency spacing of 312.5kHz).

The analytical and simulated pdf of γ_k , $k = 1, \dots, 64$, for a 2×2 system and a 2×3 system are shown in Fig. 3.1. For both cases, the simulation and analytical results match very well. Fig. 3.2 shows the simulation and theoretical results for the system with 3 transmit antennas.

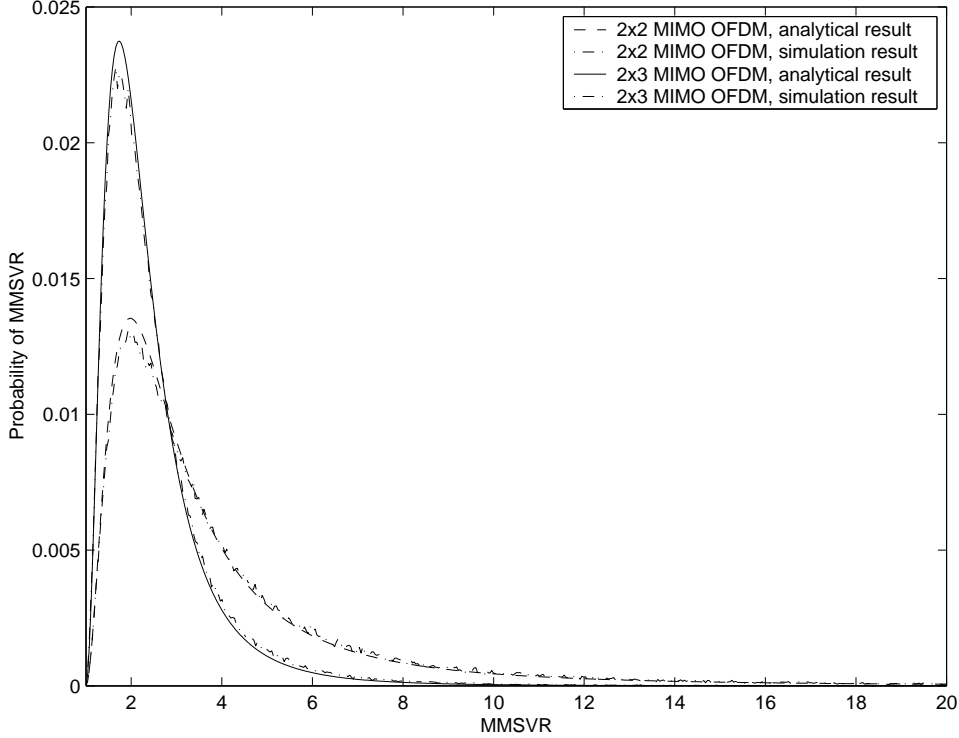


FIGURE 3.1. Analytical and simulated probability density of MMSVR for 2×2 and 2×3 MIMO OFDM configurations.

The pdf of γ leads directly to results showing which $N \times M$ MIMO configuration is an appropriate choice for the high-throughput mode. For instance, it is well known that an $N \times (M + 1)$ open-loop MIMO scheme outperforms an $N \times M$ system. The pdf of γ derived in this letter confirms this result. For example, the pdf of γ clearly demonstrates that a 2×2 spatial multiplexing system will experience a much higher probability of having an ill-conditioned channel compared to a 2×3 system. A 3×3 configuration is found to have a much higher probability of ill-conditioned channels compared to a 2×2 system.

The difference of noise enhancement between two MIMO configurations will result in different throughput. It is shown in [66] that the lower bound of the noise

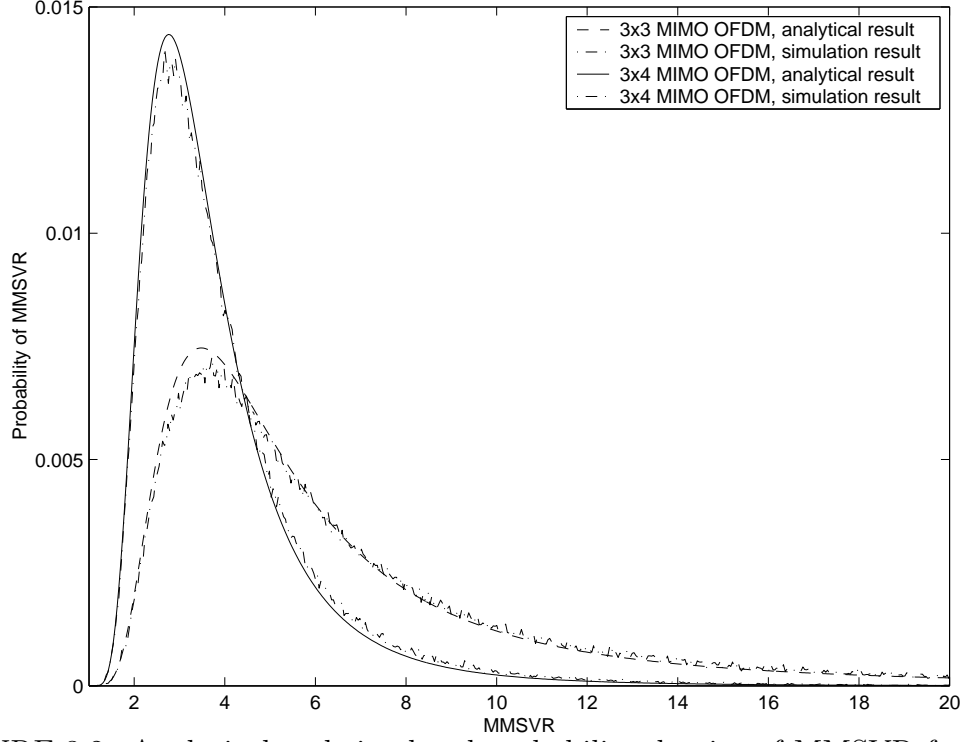


FIGURE 3.2. Analytical and simulated probability density of MMSVR for 3×3 and 3×4 MIMO OFDM configurations.

enhancement when ZF detection is adopted is given as the mean of the square of MMSVR. This bound can be calculated using the analytical expression of the pdf of MMSVR as

$$E\{\gamma_{N \times M}^2\} = \int_1^{\infty} \gamma^2 f_{\gamma}(\gamma_{N \times M}) d\gamma. \quad (3.20)$$

The mean value of $\gamma_{N \times M}^2$ is calculated to be 19.9636, 7.5452, 41.1853 and 17.9986 for 2×2 , 2×3 , 3×3 and 3×4 MIMO configurations, respectively. Using these results, the relative throughput gains can be estimated through channel analysis as $10 \log_{10} \left(E\{\gamma_{N \times N}^2\} - 10 \log_{10}(E\{\gamma_{N \times (N+1)}^2\}) \right)$. Figs. 3.3 and 3.4 show the upper

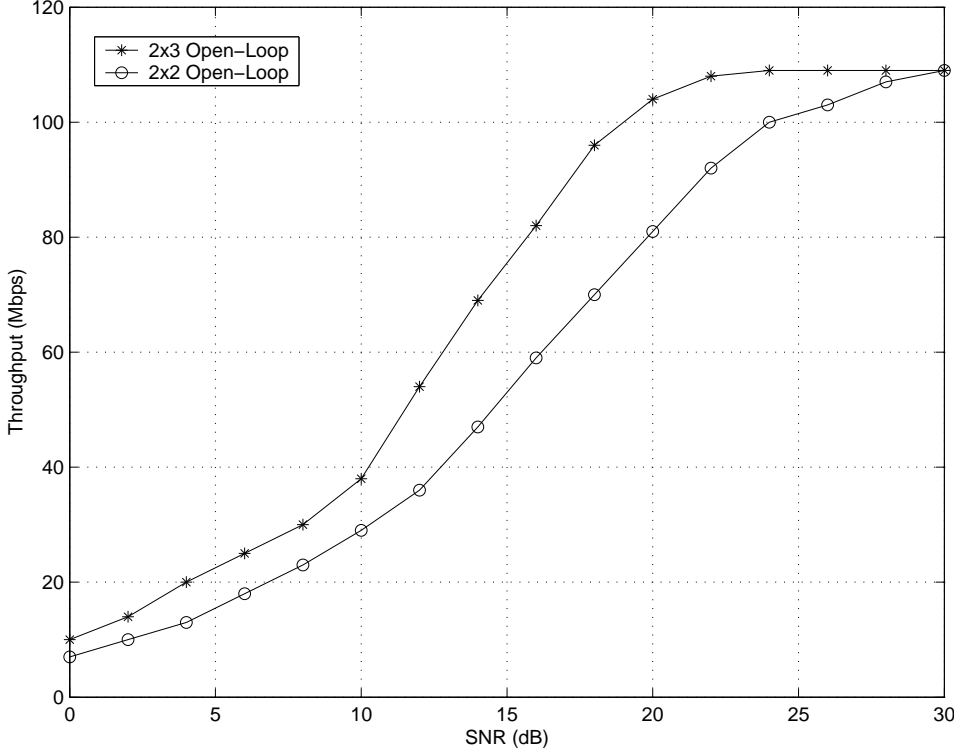


FIGURE 3.3. Throughput comparison of MIMO OFDM systems [70].

bound of the throughput curves of MIMO OFDM schemes versus SNR⁴. It is observed that for a throughput of 80Mbps, the 2×3 system attains an approximate 4.2dB gain over the 2×2 system, and the 3×4 has a gain of 3.6dB over the 3×3

⁴Five thousand channel realizations are created. For each realization, the throughput of each modulation coding scheme (MCS) is calculated. After obtaining the packet error rate (PER) using the i -th MCS, the corresponding throughput is calculated as $Throughput(i) = D(i) * (1 - PER(i))$, where $D(i)$ is data rate provided by the i -th MCS. The maximum throughput value over all MCS sets is adopted as the ideal hull throughput for a specific realization [70].

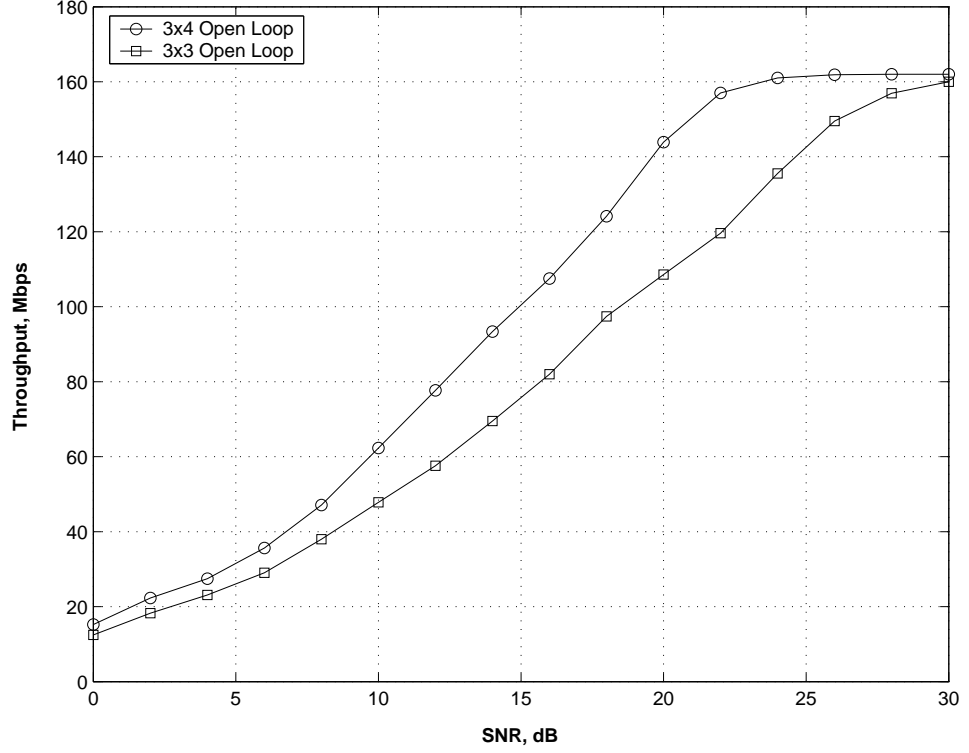


FIGURE 3.4. Throughput comparison of MIMO OFDM systems [70].

system. These results match well with the results obtained by using Eq. (3.20): 4.2257dB gain for 2×3 over 2×2 , and 3.5950dB gain for 3×4 over 3×3 . The improvement provided by an extra receive antenna is attributed to having fewer ill-conditioned channels.

3.4. Conclusion

We have derived the closed-form pdf expressions of the condition number (MMSVR) of the channel matrix for various MIMO configurations. These analytical results can be used to predict the relative performance of MIMO OFDM

systems without complicated system-level simulations. They can also be applied to determine the lower capacity bound of such systems. Through the channel analysis, it is clearly observed that an additional receive antenna could provide significant performance improvements. The analytical results and the gain/loss of different configurations predicted using the mean of the square of MMSVR matches well that obtained through system-level simulations. The results presented in this letter provide a simple and effective way for predicting the relative performances of different MIMO OFDM configurations.

4. DECISION-DIRECTED ESTIMATION OF MIMO TIME-VARYING RAYLEIGH FADING CHANNELS

MIMO communication systems have been shown to provide high spectral efficiencies [1]. If perfect channel coefficients are available at the receiver, a linear increase in ergodic capacity is achievable with MIMO systems [60, 71]. Perfect channel estimates, however, can be obtained only if the channel is either static for a long time (noise can be averaged out) or perfect (no noise). The rapid phase and amplitude variations inherent in a time-varying fading channel render perfect estimates impossible, regardless of the type of channel estimation method used. Channel estimation has been studied extensively for single-antenna systems (e.g., [72–76]). In [68] a pilot embedding method, where low-level pilots are transmitted concurrently with data, was proposed for turbo decoding in a MIMO system. The effects of pilot assisted channel estimation on the achievable data rates (capacity lower bound) over a frequency nonselective, quasi-static fading channel were analyzed in [77]. In this scheme, periodic pilot signals assigned to different transmit antennas are assumed to be mutually orthogonal. Although it avoids inter-antenna interference within the pilot periods, such scheme could significantly lower the spectral efficiency of the system. Throughput of a system with a maximum-likelihood channel estimator that employs periodic optimal training sequences for block and continuous flat fading channels was studied in [78]. In [79], an iterative method was derived to improve the estimation of channel parameters for a MIMO system, based on the assumption that data decisions have already been made. This method needs to invert a matrix of size $L \times L$, with L being the frame length per transmit antenna, for every frame. With practical frame lengths (e.g., $L = 130$, as applied in simulations in [79]), the computational load could be prohibitively high.

In this chapter, we derive a decision directed (DD) maximum *a posteriori* probability (MAP) channel estimation scheme for MIMO systems over time-varying fading channels. A zero-forcing receiver is applied to detect the spatially multiplexed symbols transmitted in the current symbol interval. The estimated symbols are then incorporated in the DD MAP channel predictor to obtain estimates of the channel coefficients in future symbol intervals. The proposed scheme does not rely on the assumption of a quasi-static fading model and can be applied in a time-varying environment. Compared to most existing schemes, it has a lower complexity and is capable of operating with significantly less pilot symbols.

4.1. System Model

Consider a communication system with N_T transmit and N_R receive antennas, denoted as an (N_T, N_R) system, over a time-varying, frequency-nonselctive Rayleigh fading channel. In the transmitter, data are serial-to-parallel converted and sent to N_T transmit antennas for simultaneous transmission. Each receive antenna responds to each transmit antenna through a statistically independent fading coefficient. The received signals are corrupted by additive white Gaussian noise (AWGN), which is statistically independent among different receive antennas. We focus on the baseband model of a system, which employs M -ary phase-shift keying (PSK) with zero inter-symbol interference (ISI) design. The results can be easily extended to a MIMO system employing a more general pulse-amplitude modulation (PAM) scheme. The u -th transmitted data stream (the signal from the u -th transmit antenna) is expressed as

$$x_u(t) = \sum_{i=-\infty}^{\infty} \sqrt{E_s} s_u(i) g(t - iT), \quad u = 1, \dots, N_T \quad (4.1)$$

where $s_u(i)$ is the i -th symbol of the u -th data stream, E_s is the energy per symbol, T is the symbol interval, and $g(t)$ is the transmitted Nyquist pulse applied to all transmitted data streams. Energy of $g(t)$ is normalized to unity, i.e., $\int_{-\infty}^{\infty} g^2(t)dt = 1$.

The time-varying fading channel introduces a random amplitude and phase shift to the transmitted signal. The fading channel process $h(t)$ is modeled as a normalized, zero-mean, complex wide-sense stationary Gaussian process with a spaced-time correlation function $\Phi(\Delta t)$ expressed as $\Phi(\Delta t) = E\{h(t)h^*(t + \Delta t)\}$, where $E\{\cdot\}$ denotes statistical expectation and $(\cdot)^*$ represents complex conjugate. In a typical mobile communication environment, the spaced-time correlation function of the channel can be modeled as $\Phi(\Delta t) = J_0(2\pi f_d \Delta t)$ [48], where f_d represents the maximum Doppler shift of the channel and $J_0(\cdot)$ is the zeroth order Bessel function of the first kind.

The received signal of the v -th antenna $r_v(t)$, $v = 1, \dots, N_R$, is the sum of signals transmitted from N_T transmit antennas and is expressed as

$$r_v(t) = \sum_{u=1}^{N_T} \sqrt{E_s} h_{v,u}(t) x_u(t) + \nu_v(t), \quad v = 1, \dots, N_R \quad (4.2)$$

where $h_{v,u}(t)$ represents the fading process for signals from the u -th transmit antenna to the v -th receive antenna and $\nu_v(t)$ is a complex zero-mean white Gaussian noise process with power spectral density N_0 . The received signal $r_v(t)$ is filtered by a matched filter, matched to $g(t)$, and then sampled at the symbol rate of each data stream.

Let the $N_T \times 1$ transmitted signal vector in the i -th symbol interval be $\mathbf{s}(i) = [s_1(i), s_2(i), \dots, s_{N_T}(i)]^T$, where $[\cdot]^T$ denotes transpose. The $N_R \times 1$ received signal vector at the i -th discrete-time interval is obtained as

$$\mathbf{r}(i) = \sqrt{E_s} \mathcal{H}(i) \mathbf{s}(i) + \boldsymbol{\nu}(i) \quad (4.3)$$

where $\boldsymbol{\nu}(i)$ is the complex zero-mean noise vector. The channel matrix $\boldsymbol{\mathcal{H}}(i)$ ($N_R \times N_T$) is expressed as

$$\begin{aligned} \boldsymbol{\mathcal{H}}(i) &= [\mathbf{h}_1(i) \ \mathbf{h}_2(i) \ \dots \ \mathbf{h}_{N_T}(i)] \\ &= \begin{bmatrix} h_{1,1}(i) & h_{1,2}(i) & \dots & h_{1,N_T}(i) \\ h_{2,1}(i) & h_{2,2}(i) & \dots & h_{2,N_T}(i) \\ \vdots & & & \vdots \\ h_{N_R,1}(i) & h_{N_R,2}(i) & \dots & h_{N_R,N_T}(i) \end{bmatrix} \end{aligned} \quad (4.4)$$

where $N_R \times 1$ column vectors $\mathbf{h}_u(i) = [h_{1,u}(i), h_{2,u}(i), \dots, h_{N_R,u}(i)]^T$, $u = 1, \dots, N_T$, represent the channel coefficients from the u -th transmit antenna to all N_R receive antennas. Each element of $\boldsymbol{\mathcal{H}}(i)$ is a zero-mean, complex Gaussian random variable of unit variance. In the discrete-time channel formulation adopted above, the fading process is piecewise-constant approximated in each symbol interval. It is assumed that the temporal variations of the fading processes, $h_{v,u}(t)$, are such that the piecewise-constant, discrete-time approximation is valid. The v -th component of $\mathbf{r}(i)$ represents the received signal from the v -th receive antenna and is expressed as $r_v(i) = \sum_{u=1}^{N_T} \sqrt{E_s} h_{v,u}(i) s_u(i) + \nu_v(i)$. Let us assume that $\hat{\boldsymbol{\mathcal{H}}}(i-L), \dots, \hat{\boldsymbol{\mathcal{H}}}(i-1)$, estimates of $\boldsymbol{\mathcal{H}}(i-L), \dots, \boldsymbol{\mathcal{H}}(i-1)$, and $\hat{\mathbf{s}}(i-L), \dots, \hat{\mathbf{s}}(i-1)$, estimates of $\mathbf{s}(i-L), \dots, \mathbf{s}(i-1)$, have been obtained. At the beginning of the transmission, these channel coefficients could be obtained by using pilot symbols. In the proposed channel estimation and data detection scheme, $\boldsymbol{\mathcal{H}}(i)$ is obtained using $\hat{\boldsymbol{\mathcal{H}}}(i-L), \dots, \hat{\boldsymbol{\mathcal{H}}}(i-1)$ and $\hat{\mathbf{s}}(i-L), \dots, \hat{\mathbf{s}}(i-1)$. Then, $\mathbf{s}(i)$ is detected using $\hat{\boldsymbol{\mathcal{H}}}(i)$. After that, $\hat{\boldsymbol{\mathcal{H}}}(i-L+1), \dots, \hat{\boldsymbol{\mathcal{H}}}(i)$ and $\hat{\mathbf{s}}(i-L+1), \dots, \hat{\mathbf{s}}(i)$ are used to estimate $\boldsymbol{\mathcal{H}}(i+1)$. Periodic pilot blocks can be inserted in the data stream to improve estimation quality and to stop error propagation when the receiver is operating in the decision directed mode.

4.2. Channel Estimation and Data Detection

4.2.1. Decision-directed Channel Estimation

Due to inter-antenna interference, it is impossible to solve for $\hat{\mathcal{H}}(i)$ based on the received signal model given in Eq. (4.3) even if an estimate of symbol vector $\mathbf{s}(i)$ is available. Let us assume that estimates of previous symbols, $\hat{\mathbf{s}}_u(i-L)$, $\hat{\mathbf{s}}_u(i-L+1)$, \dots , $\hat{\mathbf{s}}_u(i-1)$, and channel coefficients in previous symbol intervals, $\hat{h}_{v,u}(i-L)$, $\hat{h}_{v,u}(i-L+1)$, \dots , $\hat{h}_{v,u}(i-1)$, have been made. To estimate $h_{v,u}(i)$, $u = 1, \dots, N_T$, $v = 1, \dots, N_R$, we consider a sliding window approach in which $\hat{h}_{v,u}(i)$ is derived from the received signals $\mathbf{r}(l)$, $l = i-L, \dots, i-1$, and symbol decisions within a window of L symbols preceding the current symbol. Specifically, $y_{v,u}(l)$ is constructed as

$$y_{v,u}(l) = \left[r_v(l) - \sum_{\substack{k=1 \\ k \neq u}}^{N_T} \sqrt{E_s} \hat{h}_{v,k}(l) \hat{s}_k(l) \right] / \hat{s}_u(l) \quad (4.5)$$

$$u = 1, \dots, N_T, \quad v = 1, \dots, N_R, \quad l = (i-L), (i-L+1), \dots, (i-1).$$

Note that the v -th element of $\mathbf{r}(l)$, $r_v(l)$, consists of the desired signal, the inter-antenna interference, and a noise term. Ideally, if the channel is noiseless, feedback symbol decisions are correct, and channel estimates are perfect, then $y_{v,u}(l)$ in Eq. (4.5) equals exactly $\sqrt{E_s} h_{v,u}(l)$, the desired component needed for the decision-directed channel estimation. In a practical time-varying fading environment, there will be decision and channel estimation errors, and $y_{v,u}(l)$ does not perfectly represent the desired signal component $\sqrt{E_s} h_{v,u}(l)$.

Let us define an $L \times 1$ vector $\mathbf{y}_{vu}(i, L)$ and an $(L+1) \times 1$ vector $\mathbf{x}(i, L)$ as

$$\mathbf{y}_{vu}(i, L) = [y_{v,u}(i-L), y_{v,u}(i-L+1), \dots, y_{v,u}(i-1)]^T \quad (4.6)$$

$$\mathbf{x}(i, L) = \begin{bmatrix} \mathbf{y}_{vu}(i, L) \\ h_{v,u}(i) \end{bmatrix}. \quad (4.7)$$

The covariance matrix of zero-mean vector $\mathbf{x}(i, L)$ can be written as $\mathbf{F}_x = E\{\mathbf{x}(i, L)\mathbf{x}^H(i, L)\} = \begin{bmatrix} \mathbf{F}_{x11} & \mathbf{f}_{x12} \\ \mathbf{f}_{x21} & f_{x22} \end{bmatrix}$, where $(\cdot)^H$ denotes conjugate transpose and

$$\mathbf{F}_{x11} = E\{\mathbf{y}_{vu}(i, L)\mathbf{y}_{vu}^H(i, L)\} \quad (4.8)$$

$$\mathbf{f}_{x12} = E\{\mathbf{y}_{vu}(i, L)h_{v,u}^H(i)\} \quad (4.9)$$

$$\mathbf{f}_{x21} = E\{h_{v,u}(i)\mathbf{y}_{vu}^H(i, L)\} = \mathbf{f}_{x12}^H \quad (4.10)$$

$$f_{x22} = E\{h_{v,u}(i)h_{v,u}^H(i)\}. \quad (4.11)$$

Given the availability of $\mathbf{y}_{vu}(i, L)$, estimate of $h_{v,u}(i)$ can be obtained by maximizing its conditional probability density function $p\{h_{v,u}(i)|\mathbf{y}_{vu}(i, L)\}$ as

$$\hat{h}_{v,u}(i) = \max_{h_{v,u}(i)} p\{h_{v,u}(i)|\mathbf{y}_{vu}(i, L)\}. \quad (4.12)$$

For Rayleigh channels being considered, the $(L+1) \times 1$ vector $\mathbf{x}(i, L)$ is complex Gaussian¹. Therefore, the conditional probability density function can be written as [72]

$$\begin{aligned} p\{h_{v,u}(i)|\mathbf{y}_{vu}(i, L)\} &= \frac{p\{\mathbf{y}_{vu}(i, L), h_{v,u}(i)\}}{p\{\mathbf{y}_{vu}(i, L)\}} \\ &= \frac{\frac{1}{\pi^{L+1}|\mathbf{F}_x|} e^{-\mathbf{x}^H(i, L)\mathbf{F}_x^{-1}\mathbf{x}(i, L)}}{\frac{1}{\pi^L|\mathbf{F}_{x11}|} e^{-\mathbf{y}_{vu}^H(i, L)\mathbf{F}_{x11}^{-1}\mathbf{y}_{vu}(i, L)}} \end{aligned} \quad (4.13)$$

¹Under normal operation conditions, there will be occasional erroneous decisions on previously sent symbols $\hat{s}_u(l)$. However, a decision error does not affect the Gaussian distribution of $\mathbf{x}(i, L)$. This is because both the channel and noise components are zero-mean complex Gaussian (Rayleigh magnitude and uniform phase between $0-2\pi$) and a feedback decision error only introduces a rotation to the phase of the channel coefficient and noise component of $y_{v,u}(l)$.

where $|\cdot|$ denotes the determinant of a matrix. By using the matrix inversion lemma [101], \mathbf{F}_x^{-1} is expressed as

$$\mathbf{F}_x^{-1} = \begin{bmatrix} \mathbf{F}_{x11} & \mathbf{f}_{x12} \\ \mathbf{f}_{x21} & f_{x22} \end{bmatrix}^{-1} = \begin{bmatrix} \mathbf{F}_{xi11} & \mathbf{f}_{xi12} \\ \mathbf{f}_{xi21} & f_{xi22} \end{bmatrix} \quad (4.14)$$

where

$$\mathbf{F}_{xi11} = (\mathbf{F}_{x11} - \mathbf{f}_{x12}f_{x22}^{-1}\mathbf{f}_{x21})^{-1} \quad (4.15)$$

$$f_{xi22} = (f_{x22} - \mathbf{f}_{x21}\mathbf{F}_{x11}^{-1}\mathbf{f}_{x12})^{-1} \quad (4.16)$$

$$\mathbf{f}_{xi12} = -\mathbf{F}_{xi11}\mathbf{f}_{x12}f_{x22}^{-1} \quad (4.17)$$

$$\mathbf{f}_{xi21} = -f_{xi22}\mathbf{f}_{x21}\mathbf{F}_{x11}^{-1}. \quad (4.18)$$

Note that \mathbf{F}_x and \mathbf{F}_{x11} are fixed and thus independent of $\mathbf{x}(i, L)$. Therefore, maximizing the conditional probability density function is equivalent to minimizing the following quadratic function

$$\lambda = \mathbf{x}^H(i, L)\mathbf{F}_x^{-1}\mathbf{x}(i, L) - \mathbf{y}_{vu}^H(i, L)\mathbf{F}_{x11}^{-1}\mathbf{y}_{vu}(i, L). \quad (4.19)$$

By letting the conjugate derivative of λ with respect to $h_{v,u}(i)$ to zero, we obtain the decision-directed maximum *a posteriori* probability estimate of $h_{v,u}(i)$ as²

$$\hat{h}_{v,u}(i) = \mathbf{w}^H\mathbf{y}_{vu}(i, L) \quad (4.20)$$

where $\mathbf{w} = (\mathbf{f}_{x21}\mathbf{F}_{x11}^{-1})^H$ is the $L \times 1$ tap weight vector. This procedure needs to be done for all elements of $\mathcal{H}(i)$ to form the estimated channel matrix $\hat{\mathcal{H}}(i)$. It is

²Because received signals and decisions of symbols in previous symbol periods are used to predict the current channel state, the scheme derived is actually a channel predictor. Although the term ‘‘channel estimation’’ is usually used to broadly refer to the procedure from which the channel state is obtained through either prediction or estimation [72], it is more precise to describe $\hat{h}_{v,u}(i)$ derived in this chapter as a ‘‘predictor channel estimate’’, a term adopted in [73].

assumed that all elements of $\mathcal{H}(i)$ are identically distributed. Thus, tap weight \mathbf{w} is common for all coefficients (any combination of v and u). If significant changes in the channel statistics (e.g., the Doppler shift) have occurred, however, \mathbf{f}_{x21} and \mathbf{F}_{x11} (thus \mathbf{w}) must be updated to reflect such changes.

The DD MAP channel prediction procedure is illustrated in Fig. 4.1. When applied to the special case of a single-antenna system, the channel estimate derived in this chapter is similar to the linear minimum mean-square error (MMSE) estimate [72, 74]. The tap weight is the same, but the MAP predictor estimate derived in this chapter combines previous received signals scaled by the corresponding symbol decisions which form $\hat{h}_{v,u}(i)$, whereas the MMSE estimate given in [72, 74] combines estimates (e.g., obtained via a maximum likelihood approach) of past channel trajectory up to time $i - 1$.

4.2.2. Detection

Given the received signal in Eq. (4.3), $\mathbf{s}(i)$ can be detected using several algorithms such as the maximum likelihood (ML) detection [80, 81], MMSE detection, zero-forcing (ZF) detection [82, 83], and the BLAST scheme [7, 84]. The ZF scheme has the lowest complexity and supports orthogonal matrix triangularization (QR decomposition) implementation. Moreover, at high signal-to-noise ratios (SNR), performance of the ZF scheme approaches that of the MMSE scheme. For these reasons, the ZF scheme will be adopted in this chapter for data detection.

In the ZF scheme, the decision vector for the N_T spatially multiplexed symbols in the i -th interval is written as

$$\boldsymbol{\beta}(i) = \hat{\mathcal{H}}^\dagger(i)\mathbf{r}(i) \quad (4.21)$$

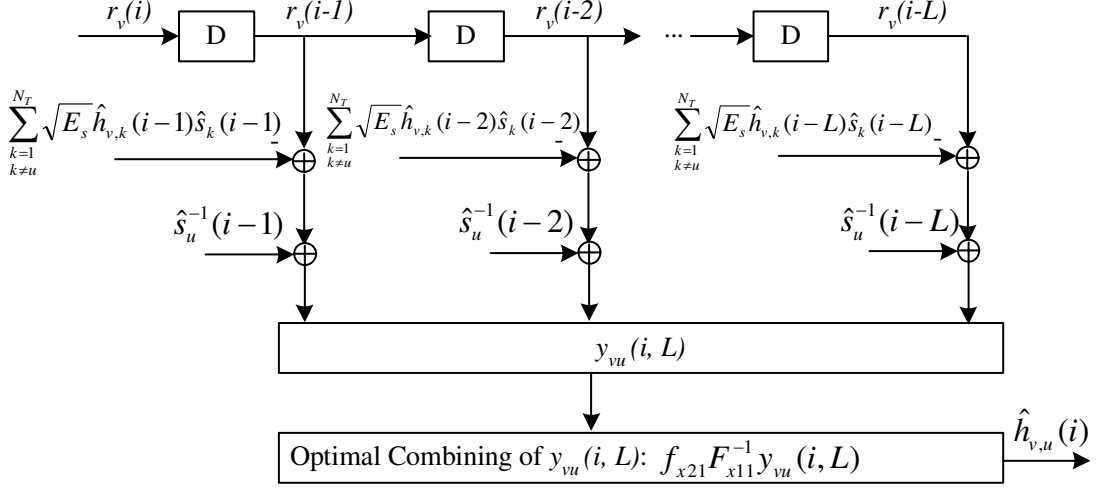


FIGURE 4.1. The DD MAP channel predictor for MIMO systems.

where $(\cdot)^+$ denotes the pseudoinverse. Because we consider an overdetermined system ($N_R \geq N_T$), $\hat{\mathcal{H}}^+(i)$, omitting symbol index i , can be calculated as $\hat{\mathcal{H}}^+ = [\hat{\mathcal{H}}^H \hat{\mathcal{H}}]^{-1} \hat{\mathcal{H}}^H$. If channel estimates are perfect (i.e., $\hat{\mathcal{H}} = \mathcal{H}$), then $\beta(i) = \sqrt{E_s} \mathbf{s}(i) + \xi(i)$, where $\xi(i) = \mathcal{H}^+(i) \nu(i)$ is the noise component after the zero-forcing operation.

4.3. Numerical Examples and Discussion

For all numerical examples, binary phase-shift keying (BPSK) with a data rate of $R_b = 1\text{Mbps}$ is chosen. Bit decisions for the BPSK system are obtained by slicing the real part of $\beta(i)$ given in Eq. (4.21) as $\hat{\mathbf{s}}(i) = \text{sgn}\{\Re[\beta(i)]\}$, where $\Re(\cdot)$ denotes the real part. The Doppler shift is calculated based on a center frequency $f_c = 2.0\text{GHz}$. Fading processes among all transmit and receive antennas

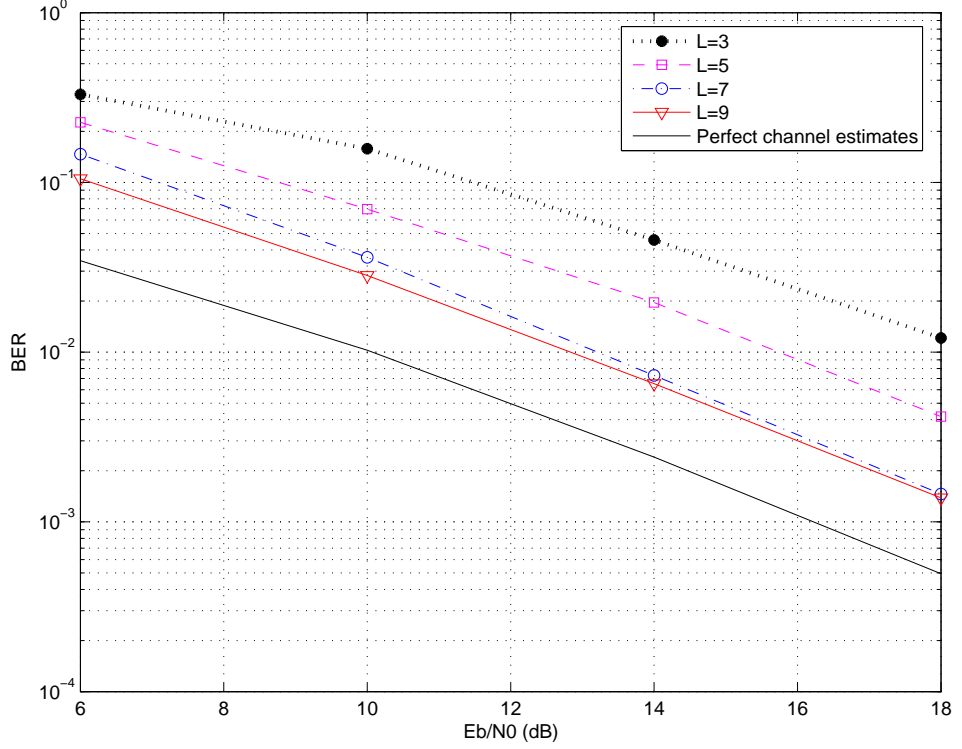


FIGURE 4.2. BER versus E_b/N_0 with different memory depth L .

are assumed independent and identically distributed; their first and second order statistics do not change over the entire transmission horizon. Although the proposed DD MAP scheme does not require periodic pilot bits in principle, errors introduced in applying Eq. (4.5) will accumulate over bits. Therefore, periodic pilot bits are added, but with a large block length of $K = 600$ bits unless explicitly specified otherwise. Let P ($N_T \leq P \ll K$) represent the number of pilot bits in each pilot period. For small values of P , the fading rates of interest are such that the channel remains approximately constant during one pilot period. The received signals in the pilot period are written in an $N_R \times P$ matrix as $\mathbf{Y}_p = [\mathbf{r}(1), \mathbf{r}(2), \dots, \mathbf{r}(P)] = \mathcal{H}_p \mathbf{S}_p + \mathbf{V}_p$, where $\mathbf{r}(p)$ was given in Eq. (4.3), \mathcal{H}_p is the channel coefficient matrix

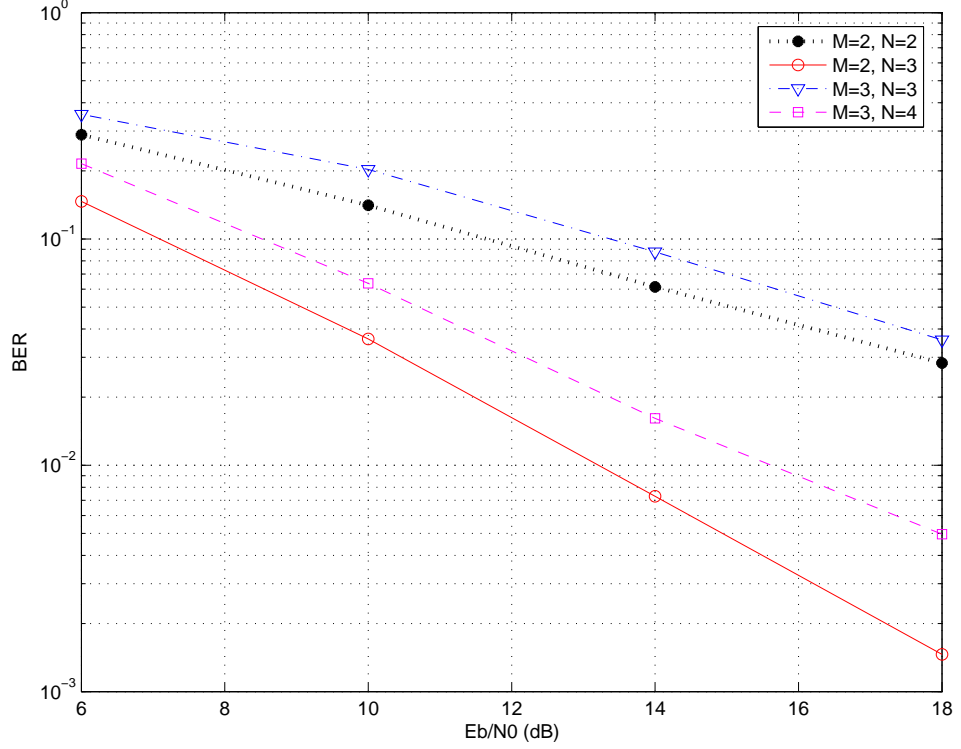


FIGURE 4.3. BER versus E_b/N_0 for different number of transmit and receive antennas.

in the pilot period, $\mathbf{S}_p = [\mathbf{s}(1), \mathbf{s}(2), \dots, \mathbf{s}(P)]$, and $\mathbf{V}_p = [\boldsymbol{\nu}(1), \boldsymbol{\nu}(2), \dots, \boldsymbol{\nu}(P)]$. Hence, channel estimates in the pilot period are obtained as $\hat{\mathcal{H}}_p = \mathbf{Y}_p \mathbf{S}_p^+$.

Memory depth (window length) L for the DD MAP channel predictor affects the error performance. Fig. 4.2 shows the bit error rate (BER) versus bit-energy-to-noise-density ratio (E_b/N_0) curves of a (2, 3) system with different values of L . The maximum Doppler shift is $f_d = 74\text{Hz}$ ($f_d T_b = 7.4 \times 10^{-5}$), which is obtained based on a vehicular speed of $v = 40\text{Km/h}$. BER curves shown are for memory depths of $L = 3, 5, 7$, and 9. For comparison purposes, the error rate curve with perfect channel estimates is also shown in the aforementioned figure. With the set of system parameters applied, error performance improves significantly when L increases from

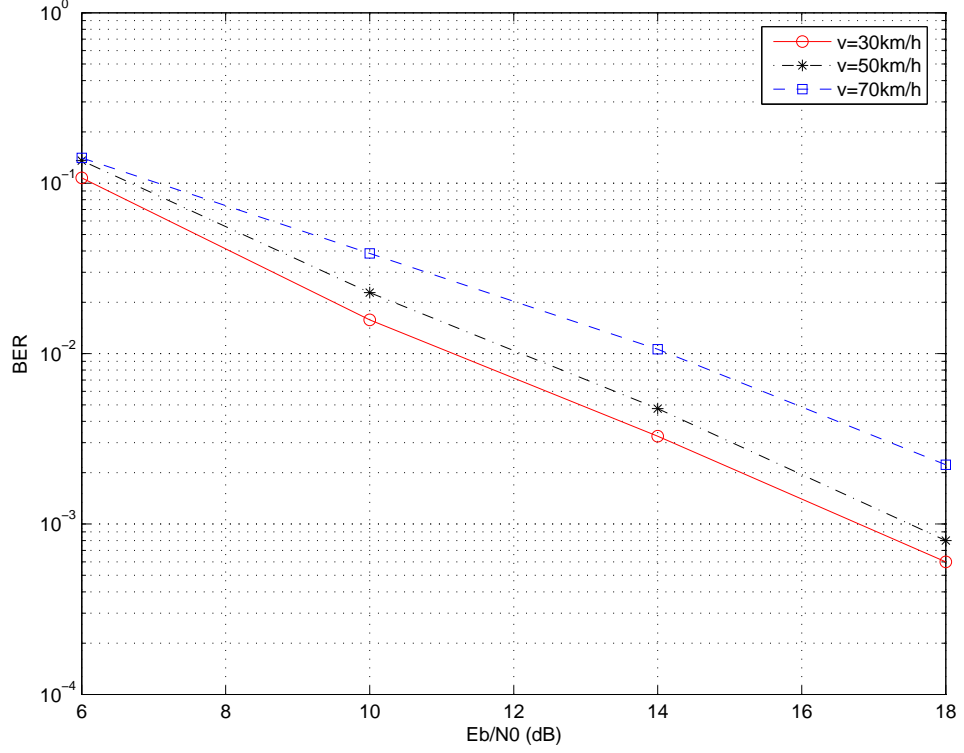


FIGURE 4.4. BER versus E_b/N_0 with different fading rates.

3 to 7. However, when L increases to over 7, performance improvement is negligible. With $L = 9$ and other parameters adopted for a target BER of 10^{-3} , the proposed scheme performs approximately 2.5dB worse than the case when all coefficients of the matrix channel are perfectly known to the receiver.

Since channel estimation depends on the accuracy of inter-antenna interference cancellation using Eq. (4.5), it is expected that the performance will degrade when the number of transmit antennas increases. Fig. 4.3 shows the BER versus E_b/N_0 curves with $L = 7$ and $(N_T, N_R) = (2, 2), (2, 3), (3, 3),$ and $(3, 4)$. Other parameters applied are the same as adopted for Fig. 4.2. Under ideal conditions, the ZF detection should yield the same error performance for cases of $(N_T, N_R) = (2, 2)$

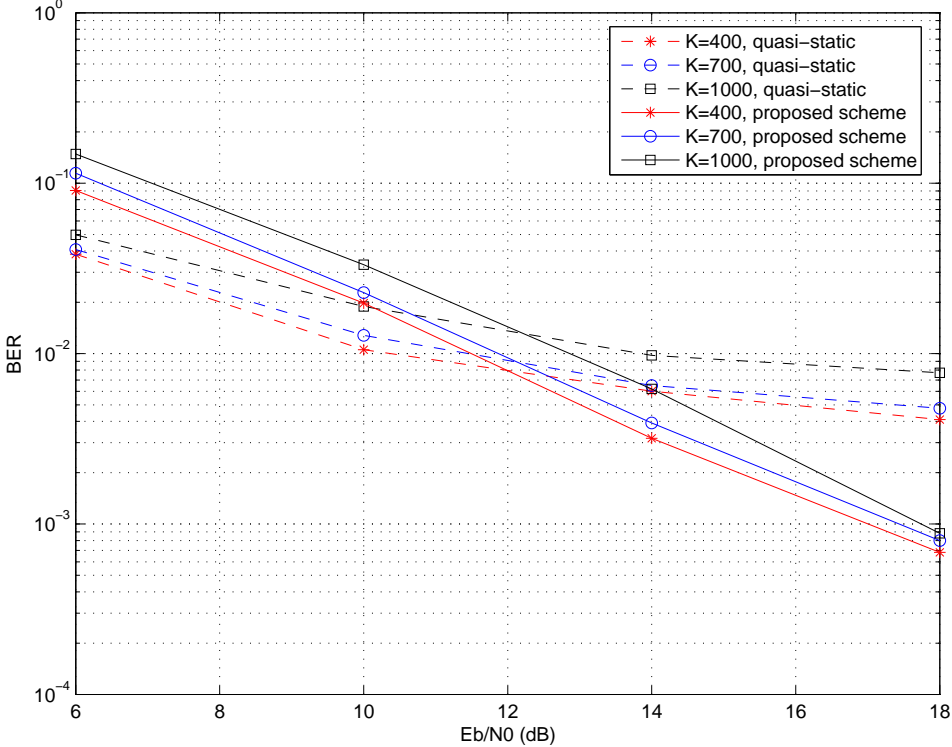


FIGURE 4.5. Performance comparison of the proposed scheme and the scheme with the channel treated as block fading.

and $(N_T, N_R) = (3, 3)$, if the received signal energy per symbol per antenna is the same [67]. With actual channel estimates, it is observed that a $(3, 3)$ system performs worse than a $(2, 2)$ system.

The fading rate quantified by the Doppler shift affects the performance of any channel estimation schemes. If channel phase and magnitude remain constant over a number of bits, accurate channel estimates are possible. As the fading rate increases, estimation quality deteriorates. Fig. 4.4 shows BER versus E_b/N_0 curves of a $(2, 3)$ system with $L = 7$ and $v = 30, 50,$ and 70Km/h . Performance degradation from $v = 30\text{Km/h}$ to $v = 50\text{Km/h}$ is considerably less significant than that from $v = 50\text{Km/h}$ to $v = 70\text{Km/h}$.

The rationale behind the quasi-static fading model is that the channel remains approximately constant over one block of data. If this were true, a simple method would be to apply the channel estimates obtained using pilot symbols embedded with data for data detection in the whole block. This scheme will not work well when the system is operating over a time-varying fading channel. Fig. 4.5 compares the performance of a (2, 3) system employing the proposed scheme with that of the scheme based on the quasi-static fading model described above. Fading rate is calculated based on $v = 50\text{Km/h}$ and block lengths of $K = 400, 700,$ and 1000 are evaluated. The proposed scheme performs worse in the low E_b/N_0 region (high BER values), but the scheme based on the quasi-static model reaches an error floor between 10^{-2} to 10^{-3} with the set of system parameters applied. The major factor causing this behavior of the proposed scheme in the low E_b/N_0 region is that higher error rates result in worse estimates of $\mathbf{y}_{vu}(i, L)$.

4.4. Conclusion

A decision directed maximum *a posteriori* probability channel estimation scheme for symbol-by-symbol detection in MIMO systems has been derived. This scheme has a low complexity and can be applied to time-varying Rayleigh fading channels with an arbitrary spaced-time correlation function. Numerical results indicate that a long memory depth is unnecessary for a system to work well. The channel estimation quality deteriorates as the number of transmit antennas increases. The fading rate has a high impact on system performance, and the proposed scheme is more appropriate for channels with low to medium normalized Doppler shifts. Large block length between adjacent pilot blocks can be deployed with the proposed scheme. This results in minimum overhead for pilot symbols. The schemes based

on the quasi-static channel model reach an error floor whereas the proposed scheme works very well at high E_b/N_0 values.

5. CHANNEL ESTIMATION FOR MOBILE MIMO OFDM SYSTEM

OFDM is attractive for wideband communications because of its ability to transform a frequency-selective channel into a series of frequency-flat sub-channels. This scheme allows the system to transmit data reliably in a time-dispersive, or frequency-selective, channel without the need of a complex time-domain equalizer. MIMO communication techniques [1] can be applied with OFDM to increase spectral efficiency. It has recently become one of the most significant technical breakthroughs to solve the bottleneck of high data rate requirement and it is the key technology in the emerging high data rate standards such as IEEE 802.16 and IEEE 802.11n. In MIMO OFDM systems, flexible transmission and signal processing techniques can be implemented to provide high quality measured by the bit-error rate (BER) and/or high data rate by exploiting either the diversity gain and/or the spatial multiplexing gain. Realizing these gains requires knowledge of CSI at the receiver, which is often obtained through channel estimation.

There exist two main types of channel estimation schemes: non-blind (or pilot assisted) schemes, in which a portion of the bandwidth is allocated to training symbols [24, 28], and blind approaches, which can be implemented by exploiting the statistical properties [21] or the deterministic information of the transmitted symbol (e.g., finite alphabet, constant modulus, etc.) [22, 23]. For pilot assisted schemes, CSI can be estimated by exploiting the frequency correlation and/or the time correlation of the pilot and data symbols. The estimates are in general reliable, but pilot symbols imply signaling overhead. On the other hand, blind channel estimation requires a long data observation interval. The slow convergence rate limits the application of the statistical approach to mobile channels and a high computation complexity due to the maximization process restricts the deterministic

approach. In [25], channel estimation algorithms based on comb-type pilots with improvements through interpolation at data frequencies were studied. Performance bound of a pilot assisted least square (LS) channel estimator over a multipath slowly fading channel was derived in [26]. When applied to OFDM systems over fast-fading channels, however, this scheme can not perform well due to the large normalized Doppler shift. A Kalman filter based scheme to estimate the state-transition matrix of time-varying MIMO OFDM channels and a scheme based on minimizing the mean-square error (MSE) of a cost function were developed in [29, 30] and [31, 27], respectively. ICI and rapid channel variations make channel estimation more challenging in mobile channels. In order to mitigate ICI effects, various detection structures were proposed and compared in [24]. These schemes generally have a high complexity. In [28], an iterative multistage channel estimator with iterative ICI cancellation to maximize the signal-to-noise-plus-ICI ratio was derived.

In this chapter, we investigate pilot assisted channel estimation for MIMO OFDM systems in the presence of ICI due to the nature of time-varying channels. We firstly apply phase shift orthogonal (PSO) pilot sequences [86] for different transmit antennas to minimize the MSE of the LS channel estimates. As the LS scheme requires the inversion of a large-size matrix (up to $M \times M$ with M being the number of sub-carriers dedicated to pilot symbols) every OFDM symbol interval in fast-fading channels, its complexity becomes prohibitively high. Thus, we derive an expectation-maximization (EM) based LS channel estimator to avoid matrix inversions. Fast-fading causes severe ICI in OFDM systems with large number of densely spaced sub-carriers. This interference becomes particularly disturbing at normal freeway speed for such systems. With the estimate of the channel for the current symbol interval and initially detected symbols, the ICI component is estimated and removed before detecting the transmitted symbols. The detected

symbols are then fed back to the channel estimator for more accurate estimation of the channel states in the next iteration.

Maximum *a posteriori* probability (MAP) channel estimation algorithms generate optimal results. However, for many applications, the computational complexity could be prohibitively high as it needs to invert large-size matrices. This chapter develops an iterative channel estimation and data detection scheme for mobile MIMO OFDM systems for which ICI cannot be neglected. The major contribution is on deriving a low-complexity MAP channel estimator while maintaining high data-detection performances for time-varying channels. In the proposed scheme, channel estimates are initially obtained by using an LS algorithm that operates on pilot symbols only. To avoid matrix inversion, we derive an expectation maximization (EM) algorithm to obtain the LS solutions. Then, a successive interference cancellation (SIC) scheme is incorporated in the data detection process. With the initial channel estimate and the temporary data decisions, the ICI component is approximated and cancelled from the received signal. In fast fading channels, LS estimates based on pilot symbols only might not be sufficient to provide a high detection performance. Once the temporary data decisions and channel estimates are available, performance could be significantly improved by using a MAP estimator. In order to lower the complexity, we derive an EM-based MAP estimator by exploiting the channel statistical information and employing low-rank approximation. The temporary symbol decisions and the received signal after ICI cancellation are finally processed by the derived EM-based MAP estimator to refine CSI and data detection.

Most of the existing research on MIMO detection has assumed uncorrelated MIMO spatial channels. However, the channel can be correlated due to the small angular spread and/or antenna spacing. We optimize data transmission by ex-

exploiting the long-term correlation characteristics and incorporate it in the iterative process. We provide extensive simulation results to evaluate the error performance of the proposed scheme, including comparison with that of the LS scheme and the ideal case – time-invariant channels and perfect channel estimates. We show that the proposed scheme does not have an error floor even under high Doppler shifts and in the presence of a high spatial correlation.

5.1. System Model

Consider an (N_T, N_R) MIMO system, where N_T and N_R represent the number of transmit and receive antennas, respectively. A sub-channel is defined as the channel transmitted from the u -th ($1 \leq u \leq N_T$) transmit antenna to the v -th ($1 \leq v \leq N_R$) receive antenna. If the antennas are sufficiently separated under the rich-scattering environment [38], channel fading processes for different sub-channels can be assumed to be independent and identically distributed (i.i.d.). OFDM with N sub-carriers is followed by a spatial multiplexing block and serial-to-parallel (S/P) converts the incoming OFDM signals into N_T streams for simultaneous transmission through the transmit antennas. Since the signal is band-limited, the time-varying multipath channel can be represented by using the tapped-delay line model with time-varying coefficients, but fixed tap spacing [87]. The delay spread of the channel determines the length of the tapped delay line and the tap spacing must be equal to or less than the reciprocal of the signal bandwidth. The impulse response of the channel is described by $A_{v,u}(n, l)$, which denotes the tap gain of the l -th path at time index n for the sub-channel transmitted from the u -th antenna to the v -th receive antenna. The maximum tap delay is assumed to be less than or equal to the OFDM guard interval. In this chapter, we assume an

exponentially decaying multipath power profile, which determines the power distribution among the taps. The power profile is also assumed to be the same for all the sub-channels. Thus, fading coefficient $A_{v,u}(n, l)$ is modeled as a zero-mean, complex, wide sense stationary Gaussian process with a spaced-time correlation function $\Phi(n_2 - n_1, l_2 - l_1)$ expressed as [85]

$$\begin{aligned}\Phi(n_2 - n_1, l_2 - l_1) &= E\{A_{v,u}(n_1, l_1)A_{v,u}^*(n_2, l_2)\} \\ &= \epsilon \cdot J_0(2\pi f_d T_s(n_2 - n_1)) \cdot e^{-l_1/L} \delta(l_2 - l_1)\end{aligned}\quad (5.1)$$

where

$$\epsilon = \frac{1 - e^{-1/L}}{1 - e^{-(L+1)/L}} \quad (5.2)$$

is a normalization factor to ensure $\epsilon \cdot \sum_l e^{-l/L} = 1$, $E\{\cdot\}$ denotes statistical expectation, $\{\cdot\}^*$ represents complex conjugate, $\delta(\cdot)$ represents the Dirac delta function, $J_0(\cdot)$ is the zeroth order Bessel function of the first kind, f_d is the maximum Doppler shift of the channel in Hz, and T_s is the sampling interval. f_d can be calculated as $f_d = f_c v/c$, where f_c is the carrier frequency, v is the vehicle speed, and c is the light speed. The total number of taps is assumed to be $L + 1$, which depends on the ratio of the maximum delay of the channel to the OFDM sampling interval. Let $\mathbf{A}(n, l)$ denote the $N_R \times N_T$ MIMO fading channel matrix whose (v, u) -th element is $A_{v,u}(n, l)$. It is assumed that the fading among different paths is uncorrelated. The $N_R \times N_R$ receiver correlation matrix is assumed to be identity and the $N_T \times N_T$ transmitter correlation matrix is denoted by \mathbf{T}_l . The spatially correlated CSI matrix, $\mathcal{H}(n, l)$, is defined as

$$\mathcal{H}(n, l) = \mathbf{A}(n, l) \mathbf{T}_l^{1/2}. \quad (5.3)$$

With perfect sample timing, we can denote the discrete time multipath channel at time nT_s along the delay paths as

$$\mathbf{h}_{v,u}(n) = [h_{v,u}(n, 0), h_{v,u}(n, 1), \dots, h_{v,u}(n, L)]^T \quad (5.4)$$

where $h_{v,u}(n, l)$ is the (v, u) -th element of matrix $\mathcal{H}(n, l)$. The discrete Fourier transform of $\mathbf{h}_{v,u}(n)$ is expressed as

$$\underline{H}_{v,u}(n) = \mathbf{F}\mathbf{h}_{v,u}(n) \quad (5.5)$$

where \mathbf{F} is an $N \times (L + 1)$ matrix with $\mathbf{F}[k, l] = e^{-j2\pi kl/N}$, $0 \leq k \leq N - 1$, $0 \leq l \leq L$. The k -th element of the $N \times 1$ vector $\underline{H}_{v,u}(n)$, $H_{v,u}(k, n)$, represents the frequency response of the channel for the k -th sub-carrier. In this model, the channel coefficients are assumed to be constant in one sampling interval, which is much shorter than one OFDM symbol duration, and change over different sampling interval according to the spaced-time correlation function. In discrete time, the signal transmitted from the u -th antenna can be represented as

$$s_u(n) = \sqrt{\frac{E_s}{N}} \sum_{k=0}^{N-1} d_u(k) \cdot e^{j2\pi nk/N} \quad (5.6)$$

where $d_u(k)$ is the transmitted data at the k -th sub-carrier from the u -th antenna and E_s is the symbol energy per sub-carrier. The signal received by the v -th antenna is expressed as

$$y_v(n) = \sum_{u=1}^{N_T} \sum_{l=0}^L h_{v,u}(n, l) s_u(n - l) + w_v(n) \quad (5.7)$$

where $w_v(n)$ is the zero-mean additive white Gaussian noise (AWGN) with variance N_0 . Since the guard interval is not less than the maximum delay of the channel, there is no inter-symbol-interference (ISI). For simplicity of notation, we let the symbol energy per sub-carrier be normalized to 1. After removing the guard interval, the received signal can be expressed as

$$y_v(n) = \frac{1}{\sqrt{N}} \sum_{u=1}^{N_T} \sum_{k=0}^{N-1} d_u(k) H_{v,u}(k, n) e^{j2\pi nk/N} + w_v(n) \quad (5.8)$$

where again $H_{v,u}(k, n)$ is the k -th element of $\underline{H}_{v,u}(n)$ given in Eq. (5.5). After performing the Fourier transform on the received signal $y_v(n)$, the signal at the k -th sub-carrier can be expressed as

$$Y_v(k) = \frac{1}{N} \sum_{u=1}^{N_T} \left[d_u(k) \sum_{n=0}^{N-1} H_{v,u}(k, n) + \sum_{m=0, m \neq k}^{N-1} d_u(m) \sum_{n=0}^{N-1} H_{v,u}(m, n) e^{j2\pi n(m-k)/N} \right] + W_v(k) \quad (5.9)$$

where the second term on the right-hand side represents the ICI component and

$$W_v(k) = \frac{1}{\sqrt{N}} \sum_{n=0}^{N-1} w_v(n) e^{-j2\pi nk/N}. \quad (5.10)$$

Let $\zeta_{v,u}(k)$ represent the ICI component caused by time-varying fading and $\bar{H}_{v,u}(k)$ denote the mean value of the channel response for the k -th sub-carrier. Eq. (5.9) can be rewritten as

$$\begin{aligned} Y_v(k) &= \sum_{u=1}^{N_T} [d_u(k) \bar{H}_{v,u}(k) + \zeta_{v,u}(k)] + W_v(k) \\ &= \sum_{u=1}^{N_T} d_u(k) \bar{H}_{v,u}(k) + \zeta_v(k) + W_v(k) \end{aligned} \quad (5.11)$$

where

$$\bar{H}_{v,u}(k) = \frac{1}{N} \sum_{n=0}^{N-1} H_{v,u}(k, n). \quad (5.12)$$

The impulse response of the sub-channel from transmit antenna u to receive antenna v is expressed as

$$\bar{\mathbf{h}}_{v,u} = [\bar{h}_{v,u}(0), \bar{h}_{v,u}(1), \dots, \bar{h}_{v,u}(L)]^T \quad (5.13)$$

where

$$\begin{aligned} \bar{h}_{v,u}(l) &= \sum_{k=0}^{N-1} \bar{H}_{v,u}(k) e^{j2\pi kl/N} \\ &= \frac{1}{N} \sum_{n=0}^{N-1} h_{v,u}(n, l). \end{aligned} \quad (5.14)$$

Most of the recent work (e.g., [22, 27]) has adopted the quasi-static model, assuming that $h_{v,u}(n, l)$ remains approximately constant over one OFDM symbol duration. Under this assumption, there is no ICI. However, if the Doppler shift is high and especially when the OFDM system has large number of densely spaced sub-carriers, this assumption is no longer valid. In this thesis, a more appropriate assumption is made such that the channel coefficients are assumed to be constant in one sampling interval and change over different sampling interval according to the spaced-time correlation function.

5.2. EM-Based LS Channel Estimation

EM-based LS is a pilot assisted channel estimation scheme to initially estimate the channel coefficients for MIMO OFDM systems in the presence of ICI due to the nature of time-varying channels. Let p_s and M denote the pilot sub-carrier spacing and the number of sub-carriers dedicated to pilot symbols, respectively. The received pilot vector at receive antenna v , $\underline{Y}_{v(p)}$, and transmitted pilot matrix, $\mathbf{D}_{u(p)}$, from transmit antenna u are written as

$$\underline{Y}_{v(p)} = [Y_v(0), Y_v(p_s), Y_v(2p_s), \dots, Y_v((M-1)p_s)]^T \quad (5.15)$$

$$\mathbf{D}_{u(p)} = \text{diag}[d_u(0), d_u(p_s), d_u(2p_s), \dots, d_u((M-1)p_s)] \quad (5.16)$$

where $\text{diag}[\cdot]$ denotes a diagonal matrix. From Eqs. (5.11) and (5.13), the received vector of the v -th antenna can be expressed as

$$\underline{Y}_{v(p)} = \mathbf{Q}_{(p)} \cdot \mathbf{h}_v + \boldsymbol{\zeta}_{v(p)} + \underline{W}_{v(p)} \quad (5.17)$$

where

$$\mathbf{Q}_{(p)} = [\mathbf{D}_{1(p)}\mathbf{F}_{(p)}, \mathbf{D}_{2(p)}\mathbf{F}_{(p)}, \dots, \mathbf{D}_{N_T(p)}\mathbf{F}_{(p)}] \quad (5.18)$$

$$\mathbf{h}_v = [\bar{\mathbf{h}}_{v,1}^T, \bar{\mathbf{h}}_{v,2}^T, \dots, \bar{\mathbf{h}}_{v,N_T}^T]^T \quad (5.19)$$

and $\mathbf{F}_{(p)}$ is an $M \times (L + 1)$ DFT matrix with $\mathbf{F}_{(p)}[k, l] = e^{-j2\pi kl/N}$, $k = 0, p_s, 2p_s, \dots, (M - 1)p_s$, $0 \leq l \leq L$. The k -th elements of $M \times 1$ vectors $\mathbf{\zeta}_{v(p)}$ (i.e., $\zeta_v(k)$) and $\underline{W}_{v(p)}$ (i.e., $W_v(k)$) were defined in Eqs. (5.10) and (5.11), respectively. The least square (LS) estimate of \mathbf{h}_v is simply obtained as

$$\hat{\mathbf{h}}_v = (\mathbf{Q}_{(p)})^+ \underline{Y}_{v(p)} \quad (5.20)$$

where $(\cdot)^+$ denotes the pseudo-inverse. Since $\mathbf{Q}_{(p)}$ is an $M \times N_T(L + 1)$ matrix, it will have a unique LS channel estimate as long as the number of pilot sub-carriers M is not less than N_T times the number of channel delay taps $(L + 1)$. Calculating the inverse of an $N_T(L + 1) \times N_T(L + 1)$ square matrix could be computationally extensive. Thus, it is favorable to ignore the channel taps whose magnitudes are small, like the method of significant tap catching method (STCM) proposed in [88]. With L_r significant taps ($L_r < L + 1$), the computation complexity can be reduced to the inversion of an $N_T L_r \times N_T L_r$ square matrix. However, an irreducible error floor is introduced since the power-delay profile cannot be completely represented by the L_r taps [89, 90].

We derive an EM-based LS channel estimation scheme to provide a more reliable channel estimate than the STCM scheme and at the same time avoid the inversion of large-size matrices. This algorithm transforms the estimation process for multiple-input channels into a series of independent single-input single-output (SISO) channel estimation. Since the received signal is decomposed and estimated for each sub-channel, it can be implemented more efficiently compared with other algorithms.

E-step: for $u = 1, 2, \dots, N_T$,

$$\underline{\hat{Y}}_{v,u(p)}^{(g)} = \mathbf{D}_{u(p)} \mathbf{F}_{(p)} \hat{\mathbf{h}}_{v,u}^{(g)} \quad (5.21)$$

$$\hat{\mathbf{r}}_{v,u(p)}^{(g)} = \underline{\hat{Y}}_{v,u(p)}^{(g)} + \beta_u \left[\underline{Y}_{v(p)} - \sum_{u=1}^{N_T} \underline{\hat{Y}}_{v,u(p)}^{(g)} \right] \quad (5.22)$$

where superscript g represents the g -th sub-iteration and $\sum_{u=1}^{N_T} \beta_u = 1$. Typically, $\beta_u, u = 1, \dots, N_T$, are chosen as $\beta_1 = \dots = \beta_{N_T}$.

M-step: in order to minimize the detection error, the estimated channel coefficient can be expressed as

$$\hat{\mathbf{h}}_{v,u}^{(g+1)} = \mathbf{F}_{(p)}^H \mathbf{D}_{u(p)}^{-1} \hat{\mathbf{r}}_{v,u(p)}^{(g)}. \quad (5.23)$$

Since $\mathbf{D}_{u(p)}$ is a diagonal matrix, $\mathbf{D}_{u(p)}^{-1}$ can be obtained via division only. The channel estimates can be initially set as $\hat{\mathbf{h}}_{v,u}^{(0)} = \mathbf{1}_{L+1}, (1 \leq v \leq N_R, 1 \leq u \leq N_T)$, where $\mathbf{1}_{L+1}$ is an $(L+1) \times 1$ vector whose elements are all 1's. Increasing the number of sub-iterations G will result in better quality of the channel estimates. However, as will be shown in the numerical examples section, for most common MIMO OFDM configurations and fading rates, the performance saturates quickly as G increases; thus, a large G is typically unnecessary.

5.3. Low-complexity MAP Channel Estimation

The transmitted data could be detected by simply employing the EM-based LS estimates of the channel coefficients. However, in fast time-varying fading channels, the performance will be significantly improved by employing a MAP channel estimator. A major problem with applying a MAP estimator is the need of data matrix inversion for every OFDM symbol. We investigate an EM-based MAP estimator which takes the temporary symbol decisions and the received signals after ICI cancellation to refine CSI. The received signal of the v -th antenna at the k -th

sub-carrier $Y_v(k)$ is expressed by Eq. (5.11). The received vector on all sub-carriers at antenna v can be expressed as

$$\underline{Y}_v = \mathbf{D} \cdot \mathbf{H}_v + \underline{\zeta}_v + \underline{W}_v \quad (5.24)$$

$$\mathbf{D} = [\mathbf{D}_1, \mathbf{D}_2, \dots, \mathbf{D}_{N_T}] \quad (5.25)$$

$$\mathbf{D}_u = \text{diag}[d_u(0), d_u(1), \dots, d_u(N-1)] \quad (5.26)$$

$$\mathbf{H}_v = [(\mathbf{H}_{v,1})^T, (\mathbf{H}_{v,2})^T, \dots, (\mathbf{H}_{v,N_T})^T]. \quad (5.27)$$

The u -th element of \mathbf{H}_v is $\mathbf{H}_{v,u} = \mathbf{F} \bar{\mathbf{h}}_{v,u}$, where $\bar{\mathbf{h}}_{v,u}$, $u = 1, 2, \dots, N_T$ was defined in Eq. (5.13) and \mathbf{F} is an $N \times (L+1)$ DFT matrix defined in Eq. (5.5). The k -th elements of vectors \underline{Y}_v , $\underline{\zeta}_v$, and \underline{W}_v (i.e., $Y_v(k)$, $\zeta_v(k)$, and $W_v(k)$) have been defined in Eqs. (5.9), (5.10), and (5.11), respectively. Since the EM algorithm can decompose the MIMO channels into a series of SISO channels, the received vector at antenna v can be expressed as

$$\underline{Y}_v = \sum_{u=1}^{N_T} \underline{Y}_{v,u} \quad (5.28)$$

where

$$\underline{Y}_{v,u} = \mathbf{D}_u \mathbf{H}_{v,u} + \underline{\xi}_{v,u} \quad (5.29)$$

and $\underline{\xi}_{v,u}$ is the component consisting of AWGN and ICI for the sub-channel transmitted from the u -th antenna to the v -th receive antenna. By exploiting the channel statistical information and employing low rank approximation, an expectation maximization (EM) based MAP channel estimator of MIMO OFDM systems is derived to achieve excellent performance without the need of any matrix inversion.

5.3.1. MAP Channel Estimation

Maximum *a posteriori* probability (MAP) algorithm achieves optimal estimates of the channel parameters. It maximizes the probability density function (pdf) of $\mathbf{H}_{v,u}$ conditioned on the received signal and the transmitted data matrix as [72]

$$\hat{\mathbf{H}}_{v,u} = \arg \max_{\mathbf{H}_{v,u}} f(\mathbf{H}_{v,u} | \underline{Y}_{v,u}, \mathbf{D}_u) \quad (5.30)$$

where $f(\cdot)$ denotes the pdf. It was shown in [72] that the MAP estimate of the parameter, $\hat{\mathbf{H}}_{v,u}$, can be expressed as

$$\begin{aligned} \hat{\mathbf{H}}_{v,u} &= \boldsymbol{\mu} + \mathbf{R}_H \mathbf{D}_u^H (\mathbf{D}_u \mathbf{R}_H \mathbf{D}_u^H + \mathbf{R}_N)^{-1} (\underline{Y}_{v,u} - \mathbf{D}_u \boldsymbol{\mu}) \\ &= \left[\mathbf{R}_H \mathbf{D}_u^H (\mathbf{D}_u \mathbf{R}_H \mathbf{D}_u^H + \mathbf{R}_N)^{-1} \right] \cdot \underline{Y}_{v,u} + \\ &\quad \left[\mathbf{I} - \mathbf{R}_H \mathbf{D}_u^H (\mathbf{D}_u \mathbf{R}_H \mathbf{D}_u^H + \mathbf{R}_N)^{-1} \mathbf{D}_u \right] \cdot \boldsymbol{\mu} \end{aligned} \quad (5.31)$$

where $\boldsymbol{\mu}$ and \mathbf{R}_H denote, respectively, the mean and covariance matrix of $\mathbf{H}_{v,u}$, and \mathbf{R}_N is the covariance matrix of vector $\boldsymbol{\xi}_{v,u}$. For most common OFDM systems, the number of sub-carrier is a large number (e.g., 128). Therefore, the ICI component, $\zeta_{v,u}(k)$, can be approximated as a Gaussian random variable by invoking the central limit theorem [100]. Once the Doppler shift is estimated, the variance of ICI, σ_{ICI}^2 , can be estimated as [24]

$$\begin{aligned} \sigma_{ICI}^2 &= \frac{1}{N^2} \sum_{m=0, m \neq k}^{N-1} \sum_{n_1=0}^{N-1} \sum_{n_2=0}^{N-1} E \left\{ H_{v,u}(m, n_1) H_{v,u}^*(m, n_2) \right\} \cdot e^{\frac{j2\pi(n_1 - n_2)(m - k)}{N}} \\ &= \frac{1}{N^2} \sum_{m=0, m \neq k}^{N-1} \sum_{n_1=0}^{N-1} \sum_{n_2=0}^{N-1} J_0 \left(\frac{2\pi f_d T (n_1 - n_2)}{N} \right) \cdot e^{\frac{j2\pi(n_1 - n_2)(m - k)}{N}} \\ &= \frac{1}{N^2} \sum_{m=0, m \neq k}^{N-1} \left(N + 2 \sum_{n=1}^{N-1} (N - n) J_0(2\pi f_d T_s n) \cos \left(2\pi(m - k) \frac{n}{N} \right) \right). \end{aligned} \quad (5.32)$$

$\boldsymbol{\xi}_{v,u}$ is assumed to be zero mean with covariance matrix of $\sigma^2 \mathbf{I}_N$, where \mathbf{I}_N is $N \times N$ identity matrix and $\sigma^2 = \sigma_{ICI}^2 + \sigma_{AWGN}^2 / N_T$. Eq. (5.31) can be rewritten as

$$\begin{aligned}
\hat{\mathbf{H}}_{v,u} &= \mathbf{R}_H \mathbf{D}_u^H (\mathbf{D}_u \mathbf{R}_H \mathbf{D}_u^H + \sigma^2 \mathbf{I})^{-1} \cdot \underline{Y}_{v,u} \\
&= \mathbf{R}_H (\mathbf{D}_u \mathbf{R}_H + \sigma^2 \cdot (\mathbf{D}_u^H)^{-1})^{-1} \cdot \underline{Y}_{v,u} \\
&= \mathbf{R}_H (\mathbf{R}_H + \sigma^2 \cdot (\mathbf{D}_u^H \mathbf{D}_u)^{-1})^{-1} \mathbf{D}_u^{-1} \cdot \underline{Y}_{v,u}.
\end{aligned} \tag{5.33}$$

5.3.2. Low Rank Approximated MAP Channel Estimation

Since the transmitted data \mathbf{D}_u changes every OFDM symbol interval, the system complexity could be prohibitively high due to the frequent inversion of large-size matrices. It was shown in [91] that the instantaneous matrix $(\mathbf{D}_u^H \mathbf{D}_u)^{-1}$ can be replaced with $E\{(\mathbf{D}_u^H \mathbf{D}_u)^{-1}\}$ at the expense of a negligible performance degradation. Assuming a normalized constellation power and equally probable constellation points, we can easily show that $E\{(\mathbf{D}_u^H \mathbf{D}_u)^{-1}\} = \alpha \mathbf{I}$, where \mathbf{I}_N is an $N \times N$ identity matrix and α equals 1, 1.8889, and 2.6854 for QPSK, 16-QAM, and 64-QAM, respectively. Thus, Eq. (5.33) can be approximated as

$$\begin{aligned}
\hat{\mathbf{H}}_{v,u} &= \mathbf{R}_H (\mathbf{R}_H + \sigma^2 \cdot E\{(\mathbf{D}_u^H \mathbf{D}_u)^{-1}\})^{-1} \mathbf{D}_u^{-1} \cdot \underline{Y}_{v,u} \\
&= \mathbf{R}_H (\mathbf{R}_H + \sigma^2 \alpha \mathbf{I})^{-1} \mathbf{D}_u^{-1} \cdot \underline{Y}_{v,u} \\
&= \mathbf{R}_H \mathbf{R} \cdot \hat{\mathbf{H}}_{v,u,LS} \\
&= \mathbf{\Gamma} \cdot \hat{\mathbf{H}}_{v,u,LS}
\end{aligned} \tag{5.34}$$

where $\mathbf{\Gamma} = \mathbf{R}_H \mathbf{R}$ and $\mathbf{R} = \mathbf{R}_H + \sigma^2 \alpha \mathbf{I}$. Furthermore, $\mathbf{\Gamma}$ can be optimally approximated by an $N \times N$ matrix, $\mathbf{\Gamma}_m$, with low rank. It was proven in [92] that an optimal rank reduction can be achieved by minimizing the trace of the extra covariance as

$$\min_{\mathbf{\Gamma}_m} tr[(\mathbf{\Gamma} - \mathbf{\Gamma}_m) \mathbf{R} (\mathbf{\Gamma} - \mathbf{\Gamma}_m)^T]. \tag{5.35}$$

The solution of above equation is to make $\mathbf{\Gamma}_m \mathbf{R}^{1/2}$ the best low rank approximation of $\mathbf{\Gamma} \mathbf{R}^{1/2}$. After applying singular value decomposition (SVD) of matrix \mathbf{R}_H , $\mathbf{R}_H = \mathbf{U} \mathbf{\Lambda} \mathbf{U}^H$, $\mathbf{\Gamma} \mathbf{R}^{1/2}$ can be expressed as

$$\begin{aligned}
\mathbf{\Gamma} \mathbf{R}^{1/2} &= \mathbf{R}_H \mathbf{R}^{-1/2} \\
&= \mathbf{R}_H (\mathbf{R}_H + \sigma^2 \alpha \mathbf{I})^{-1/2} \\
&= \mathbf{U} \mathbf{\Lambda} \mathbf{U}^H (\mathbf{U} (\mathbf{\Lambda} + \sigma^2 \alpha \mathbf{I}) \mathbf{U}^H)^{-1/2} \\
&= \mathbf{U} \mathbf{\Lambda} (\mathbf{\Lambda} + \sigma^2 \alpha \mathbf{I})^{-1/2} \mathbf{U}^H
\end{aligned} \tag{5.36}$$

where $\mathbf{\Lambda}$ is a diagonal matrix with elements of $\lambda_m, m = 0, 1, \dots, N - 1$. Let $\mathbf{X} = \mathbf{\Lambda} (\mathbf{\Lambda} + \sigma^2 \alpha \mathbf{I})^{-1/2}$ and $\mathbf{\Delta} = \mathbf{X} (\mathbf{\Lambda} + \sigma^2 \alpha \mathbf{I})^{-1/2}$. The low-rank approximated channel estimate is derived as

$$\begin{aligned}
\hat{\mathbf{H}}_{v,u} &= \mathbf{U} \mathbf{X}_m \mathbf{U}^H (\mathbf{U} (\mathbf{\Lambda} + \sigma^2 \alpha \mathbf{I}) \mathbf{U}^H)^{-1/2} \cdot \hat{\mathbf{H}}_{v,u,LS} \\
&= \mathbf{U} \mathbf{X}_m (\mathbf{\Lambda} + \sigma^2 \alpha \mathbf{I})^{-1/2} \mathbf{U}^H \cdot \hat{\mathbf{H}}_{v,u,LS} \\
&= \mathbf{U} \mathbf{\Delta}_m \mathbf{U}^H \cdot \mathbf{D}_u^{-1} \underline{Y}_{v,u}
\end{aligned} \tag{5.37}$$

where \mathbf{X}_m and $\mathbf{\Delta}_m$ are the $N \times N$ diagonal matrices whose first $L + 1$ diagonal elements are the same as those of \mathbf{X} and $\mathbf{\Delta}$, respectively. The rest of the diagonal elements of \mathbf{X}_m and $\mathbf{\Delta}_m$ are all 0's. Thus the first $L + 1$ diagonal elements of $\mathbf{\Delta}_m$ are represented as $\frac{\lambda_m}{\lambda_m + \sigma^2 \alpha}, m = 0, 1, 2, \dots, L$.

5.3.3. EM-based MAP Channel Estimation

Since the signal power is not changed by the transmitter correlation matrix, the (m, n) -th element of the covariance matrix \mathbf{R}_H can be derived as

$$[\mathbf{R}_H]_{m,n} = E \{ \bar{H}_{v,u}(m) \bar{H}_{v,u}^*(n) \}$$

$$\begin{aligned}
&= E \left\{ \sum_{l_1=0}^L \bar{h}_{v,u}(l_1) e^{-\frac{j2\pi ml_1}{N}} \sum_{l_2=0}^L \bar{h}_{v,u}(l_2) e^{-\frac{j2\pi nl_2}{N}} \right\} \\
&= \frac{1}{N^2} E \left\{ \sum_{l=0}^L \sum_{n_1=0}^{N-1} h_{v,u}(n_1, l) \sum_{n_2=0}^{N-1} h_{v,u}(n_2, l) e^{-\frac{j2\pi(m-n)l}{N}} \right\} \\
&= \frac{1}{N^2} E \left\{ \sum_{l=0}^L \left(\sum_{n_1=0}^{N-1} \sum_{n_2=0}^{N-1} A_{v,u}(n_1, l) A_{v,u}(n_2, l) \right) e^{-\frac{j2\pi(m-n)l}{N}} \right\} \\
&= \epsilon \sum_{l=0}^L e^{-l/L} e^{-\frac{j2\pi(m-n)l}{N}} \cdot \frac{1}{N^2} \sum_{n_1=0}^{N-1} \sum_{n_2=0}^{N-1} J_0(2\pi f_d T_s(n_2 - n_1)) \quad (5.38)
\end{aligned}$$

It is assumed that the normalized Doppler shift is less than 0.05. Thus, the value of $J_0(2\pi f_d T_s(n_2 - n_1))$ is close to 1. $[\mathbf{R}_H]_{m,n}$ can be approximated as $\epsilon \sum_{l=0}^L e^{-l/L} e^{-\frac{j2\pi(m-n)l}{N}}$, where the normalization factor ϵ is defined in Eq. (5.2). After performing SVD of matrix \mathbf{R}_H , we can obtain the unitary matrix \mathbf{U} and the singular values $\lambda_m, m = 0, 1, 2, \dots, L$.

The EM-based MAP algorithm can be efficiently implemented as

E-step: for $u = 1, 2, \dots, N_T$,

$$\hat{\underline{Y}}_{v,u}^{(g)} = \mathbf{D}_u \mathbf{U} \Delta_{mi} \mathbf{U}^H \mathbf{F} \hat{\mathbf{h}}_{v,u}^{(g)} \quad (5.39)$$

$$\hat{\mathbf{r}}_{v,u}^{(g)} = \hat{\underline{Y}}_{v,u}^{(g)} + \beta_u \left[\underline{Y}_v - \sum_{u=1}^{N_T} \hat{\underline{Y}}_{v,u}^{(g)} \right] \quad (5.40)$$

where, as the EM-based LS scheme, superscript g represents the g -th sub-iteration and $\beta_u, u = 1, \dots, N_T$, satisfy $\sum_{u=1}^{N_T} \beta_u = 1$ and are typically chosen as $\beta_1 = \dots = \beta_{N_T}$. Δ_{mi} is the pseudo-inverse of diagonal matrix Δ_m ; the $L+1$ non-zero diagonal elements of Δ_{mi} equal $\frac{\lambda_m + \sigma^2 \alpha}{\lambda_m}, m = 0, 1, 2, \dots, L$.

M-step: in order to minimize the detection error, the estimated channel coefficient can be expressed as

$$\hat{\mathbf{h}}_{v,u}^{(g+1)} = \mathbf{F}^H \mathbf{U} \Delta_m \mathbf{U}^H \mathbf{D}_u^{-1} \hat{\mathbf{r}}_{v,u}^{(g)}. \quad (5.41)$$

Since \mathbf{D}_u is a diagonal matrix, its inversion can be obtained by division only. No matrix inversion is required for the proposed EM-based MAP channel estimator. This scheme can achieve optimal performance with relatively low complexity.

6. DATA DETECTION FOR MOBILE MIMO OFDM SYSTEMS

The ultimate goal of a receiver is to detect the transmitted symbols with minimum probability of detection error based on the received signal, which is distorted by the noise and channel. For MIMO OFDM systems, the interference between signals simultaneously transmitted from the multiple transmit antennas considerably increases the detection complexity. Maximum likelihood (ML) is an optimal detector. However, the implementation is restricted by the significant increase in complexity, which exponentially grows with the number of transmit antennas [36]. Thus, several suboptimal detectors have been developed, e.g., zero-forcing (ZF) and minimum-mean-square error (MMSE) linear detectors. Both ZF and MMSE can decouple spatial interference by matrix inversion. While reducing the detection complexity, these receivers suffer a loss in diversity gain. It has been shown that these receivers achieve a receive diversity order of $N_R - N_T + 1$ instead of the usual N_R [82, 52]. Alternative nonlinear receivers have also been considered, e.g., successive interference cancellation (SIC) [7, 93] detection. Signals transmitted from multiple antennas are detected in an optimal order and the interference is successively cancelled from the received signal. In reality, the receiver is designed by balancing the detection performance and the system complexity.

Based on the channel estimation schemes (LS, EM-based LS, EM-based MAP, etc.) of MIMO OFDM systems described in Chapter 5, the $(L + 1) \times 1$ vector of the channel multipath fading, $\hat{\mathbf{h}}_{v,u}$, can be estimated. Thus the estimate of the channel frequency response at the k -th sub-carrier, $\hat{H}_{v,u}(k)$ ($v = 1, 2, \dots, N_R$ and $u = 1, 2, \dots, N_T$), can be obtained for all the sub-channels by applying Eq. (5.5). Let $\hat{\mathbf{H}}(k)$ denote an $N_R \times N_T$ channel matrix whose (v, u) -th element is $\hat{H}_{v,u}(k)$ and let $\underline{\mathbf{Y}}(k)$ denote an $N_R \times 1$ received vector whose v -th element is $Y_v(k)$.

From Eq. (5.11), the received vector at the k -th sub-carrier of MIMO systems can be expressed as

$$\underline{Y}(k) = \hat{\mathbf{H}}(k)\mathbf{d}(k) + \mathbf{N}(k) \quad (6.1)$$

where $\mathbf{d}(k)$ is a $N_T \times 1$ transmitted vector whose u -th element is $d_u(k)$ and $\mathbf{N}(k)$ is a $N_R \times 1$ noise vector whose v -th element is $\zeta_v(k)$ plus $W_v(k)$.

6.1. ZF and MMSE Detection

A linear approach to recover $\mathbf{d}(k)$ from $\underline{Y}(k)$ is to use a $N_T \times N_R$ weight matrix \mathbf{W} (either \mathbf{W}_{ZF} or \mathbf{W}_{MMSE}), which linearly combines the elements of $\underline{Y}(k)$ to estimate the transmitted symbols, i.e., $\hat{\mathbf{d}}(k) = \mathbf{W}\underline{Y}(k)$. By inverting the channel with the weight matrix, the ZF algorithm nulls out the interference introduced from the channel matrix. The ZF weight matrix is defined as

$$\mathbf{W}_{ZF} = \hat{\mathbf{H}}(k)^\dagger = \left(\hat{\mathbf{H}}(k)^H \hat{\mathbf{H}}(k) \right)^{-1} \hat{\mathbf{H}}(k)^H \quad (6.2)$$

where $(\cdot)^H$ denotes Hermitian, $(\cdot)^{-1}$ denotes matrix inversion, $(\cdot)^\dagger$ denotes matrix pseudo-inversion. The drawback of the ZF detection scheme is that nulling out the interference without considering the noise will increase the noise power significantly, which results in performance degradation. The analysis is mainly described in Chapter 3. To avoid this noise enhancement, MMSE detection scheme minimizes the mean-square of the detection error, i.e., $J(\mathbf{W}) = E \left\{ (\mathbf{d}(k) - \hat{\mathbf{d}}(k))^H (\mathbf{d}(k) - \hat{\mathbf{d}}(k)) \right\}$, with respect to \mathbf{W} . The optimum weight can be derived as

$$\mathbf{W}_{MMSE} = \left(\hat{\mathbf{H}}(k)^H \hat{\mathbf{H}}(k) + \sigma_{AWGN}^2 \mathbf{I}_{N_T} \right)^{-1} \hat{\mathbf{H}}(k)^H \quad (6.3)$$

where σ_{AWGN}^2 is the variance of AWGN noise, \mathbf{I}_{N_T} is the $N_T \times N_T$ identity matrix. In the MMSE scheme, the decision vector for the N_T spatially multiplexed symbols on the k -th sub-carrier is obtained as

$$\hat{\mathbf{d}}(k) = \left(\hat{\mathbf{H}}(k)^H \hat{\mathbf{H}}(k) + \sigma_{AWGN}^2 \mathbf{I}_{N_T} \right)^{-1} \hat{\mathbf{H}}(k)^H \underline{Y}(k), \quad k = 0, 1, \dots, N-1 \quad (6.4)$$

where $\hat{\mathbf{d}}(k)$ is an $N_T \times 1$ vector whose u -th element is the estimate of the symbol transmitted from the u -th antenna at the k -th sub-carrier, $\hat{d}_u(k)$, $u = 1, 2, \dots, N_T$.

6.2. ICI-based MMSE Detection

The MMSE scheme would have worked were the channel a slow-fading one, as in such scenario ICI would have been very mild and could be neglected. In a fast-fading channel with high Doppler shift, however, the received signal could be corrupted severely by ICI. Thus, Eq. (6.4) must be modified to incorporate ICI to the MMSE process, forming the ICI-based MMSE to improve the detection accuracy in the first iteration when the ICI approximation and cancellation has yet not begun. Data detection quality in this initial phase of the iterative process will affect the receiver performance.

Since for most common OFDM configurations, the number of sub-carrier is a large number (e.g., 128), the ICI component, $\zeta_{v,u}(k)$, can be approximately as a Gaussian random variable by invoking the the central limit theorem [100]. The variance of $\zeta_v(k)$ can be determined by exploiting the ICI power and the number of transmit antenna as shown in Eq. (5.9) and Eq. (5.11). Once Doppler shift is estimated, the variance of $\zeta_v(k)$, $N_T \sigma_{ICI}^2$, can be estimated by Eq. (5.32). The improved decision vector for the k -th sub-carrier employing the ICI-based MMSE algorithm is obtained as

$$\hat{\mathbf{d}}(k) = \left(\hat{\mathbf{H}}(k)^H \hat{\mathbf{H}}(k) + (\sigma_{AWGN}^2 + N_T \sigma_{ICI}^2) \mathbf{I}_{N_T} \right)^{-1} \hat{\mathbf{H}}(k)^H \underline{Y}(k) \quad (6.5)$$

where $\hat{\mathbf{d}}(k)$ is an $N_T \times 1$ vector whose u -th element is $\hat{d}_u(k)$, $u = 1, 2, \dots, N_T$.

In OFDM, a stream of symbols are modulated on many equally spaced parallel sub-carriers [17]. Modulation and demodulation are efficiently implemented by IFFT and FFT. However, the orthogonality of the transmitted symbols is maintained only if the channel is time-invariant [28]. This section describes how the ICI is generated due to the nature of time-varying channel. It is shown that ICI can cause a significant effect on a system with large number of densely spaced sub-carriers even for a slowly fading channel. Data detection can be improved based on the analysis and iterative cancellation of ICI.

In the presence of severe ICI, the ultimate solution would be to cancel it in the detection process. The channel transfer function can be approximately expressed by using the first-order Taylor series expansion as [28]

$$H_{v,u}(k, n) = H_{v,u}(k, n_0) + H'_{v,u}(k, n_0)(n - n_0). \quad (6.6)$$

Then, $\zeta_{v,u}(k)$ given in Eq. (5.11) can be rewritten as

$$\zeta_{v,u}(k) = \sum_{m=0}^{N-1} H_{v,u}(m, n_0)' \Xi_k(m) d(m) \quad (6.7)$$

$$\Xi_k(m) = \frac{1}{N} \sum_{n=0}^{N-1} (n - n_0) e^{j2\pi n(m-k)/N}, \quad k = 0, 1, \dots, N-1, \quad m = 0, 1, \dots, N-1. \quad (6.8)$$

Let Ξ be an $N \times N$ matrix whose (k, m) -th element is $\Xi_k(m)$, $k, m = 0, 1, \dots, N-1$. With the initial estimate of the channel and the temporary symbol decisions for all the sub-carriers, the ICI component is approximated as

$$\hat{\zeta}_{v,u} = \Xi \mathbf{H}'_{v,u} \hat{\mathbf{d}}_u \quad (6.9)$$

$$\hat{\mathbf{d}}_u = [\hat{d}_u(0), \hat{d}_u(1), \dots, \hat{d}_u(N-1)]^T \quad (6.10)$$

$$\hat{\boldsymbol{\zeta}}_{v,u} = [\hat{\zeta}_{v,u}(0), \hat{\zeta}_{v,u}(1), \dots, \hat{\zeta}_{v,u}(N-1)]^T \quad (6.11)$$

$$\mathbf{H}'_{v,u} = \text{diag}[H'_{v,u}(0, n_0), H'_{v,u}(1, n_0), \dots, H'_{v,u}(N-1, n_0)]. \quad (6.12)$$

The first order derivative of the channel response, $H'_{v,u}(k, n_0)$, can be estimated by calculating the difference of $\bar{H}_{v,u}(k)$ between two consecutive OFDM symbols [28]. The ICI component is then cancelled before the next iteration of data detection as

$$\hat{\mathbf{Y}}_v = \mathbf{Y}_v - \sum_{u=1}^{N_T} \hat{\boldsymbol{\zeta}}_{v,u} \quad (6.13)$$

where $\mathbf{Y}_v = [Y_v(0), Y_v(1), \dots, Y_v(N-1)]^T$. Once the ICI component is cancelled from the received signal, both channel estimation and data detection should be significantly improved. The block diagram of the proposed iterative EM-based LS channel estimation and ICI-based MMSE detection scheme for MIMO OFDM systems is shown in Fig. 6.1. Recall that for each transmit antenna, N data symbols are transmitted over the N orthogonal sub-carriers during one OFDM symbol period. In the proposed receiver, an EM-based LS channel estimation scheme described in Chapter 5 is used to estimate the channel coefficients for all the sub-channels employing the output signals of the FFT block. Then, MMSE detection is performed based on the ICI power, which can be calculated by exploiting the knowledge of the Doppler shift. Once the temporary hard decisions of the transmitted symbols are available, the ICI component can be approximated and cancelled from the received signal. Thus, a refined received signal is constructed for the next iteration. This iterative process of EM-based channel estimation, MMSE detection, and ICI approximation and cancellation will continue until certain performance criteria are met. The performance gain and the impact of various choices of the algorithm

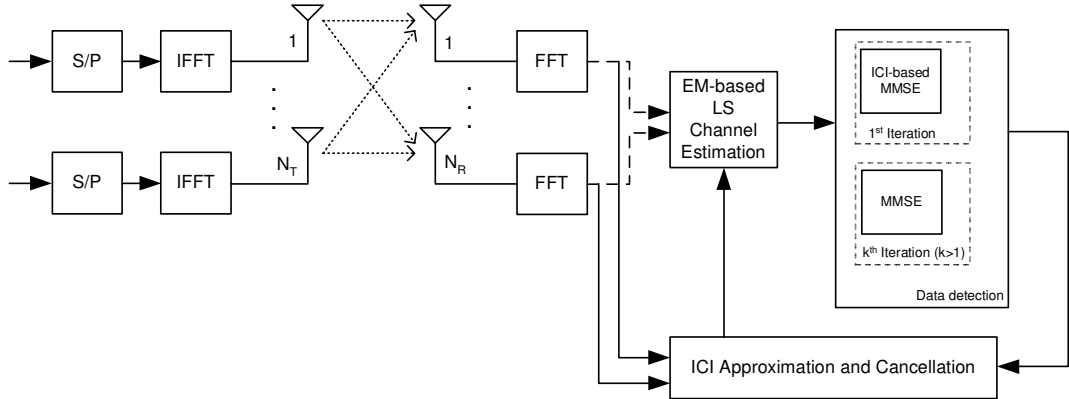


FIGURE 6.1. Block diagram of the proposed iterative EM-based LS channel estimation and ICI-based MMSE detection for MIMO OFDM systems.

and system related parameters with the proposed scheme will be presented and discussed through numerical examples.

6.3. SIC Detection

Successive interference cancellation (SIC) uses the detect-and-cancel strategy similar to that of decision-feedback equalizer. Either ZF or MMSE can be used for detecting the signal component used for interference cancellation. It has been shown that the capacity of MIMO systems decreases in the presence of high transmit and/or the receive correlations [45, 94]. We will assess the performance and robustness of the proposed channel estimation schemes in both independent and highly correlated spatial channels. In highly correlated channels, an adaptive precoder is needed to optimally adjust the signal power and phase for each antenna

by exploiting the long-term spatial correlation characteristics of the MIMO channel. For systems with 2 transmit antennas, a precoder is designed to optimize the multiple antenna transmission such that data transmitted from different antennas have the same error probability. The 2×2 precoder matrix is given as [93]

$$\mathbf{M} = \begin{bmatrix} \sqrt{P_1} & 0 \\ 0 & \sqrt{P_2}e^{-j\psi} \end{bmatrix} \quad (6.14)$$

where $\psi = 2\pi B \cos(\bar{\theta}_l)$, $P_1 = \frac{(1+\rho)^2}{1+(1+\rho)^2}$, $P_2 = \frac{1}{1+(1+\rho)^2}$, and ρ is the modulus of the antenna correlation coefficient expressed as $\rho = e^{(-0.5)(2\pi B \sin(\bar{\theta}_l)\gamma_l)^2}$. For the special case of independent MIMO channels, $\rho = 0$ and $\psi = 0$, which result in equal power allocation ($P_1 = P_2 = 1/2$) and zero phase-shift. Details of optimal precoder design for MIMO systems with more than 2 transmit antennas can be found in [93].

Upon obtaining the CSI matrix $\mathcal{H}(n, l)$ including spatial correlation effects by using the proposed scheme described in Section 5.2 or Section 5.3, $\mathbf{A}(n, l)$ can be calculated through Eq. (5.3) for any transmit correlation matrix \mathbf{T}_l . After applying a linear zero-forcing filter to the $N_R \times 1$ received vector of the k -th sub-carrier, i.e., $\mathbf{g}(k) = \mathbf{A}(n, l)^\dagger \underline{\mathbf{Y}}(k)$, the symbol transmitted from the first antenna can be estimated by the dot product of the first column of $\mathbf{T}_l^{1/2}$ and $\mathbf{g}(k)$.

$$\hat{d}_1(k) = [\mathbf{T}_l^{1/2}(:, 1)]^H \mathbf{g}(k) / \sqrt{P_1}. \quad (6.15)$$

Then, the interference coming from the first detected symbol can be subtracted from $\mathbf{g}(k)$ before detecting the next symbol as

$$\hat{\mathbf{g}}(k) = \mathbf{g}(k) - \sqrt{P_1} \mathbf{T}_l^{1/2}(:, 1) \hat{d}_1(k). \quad (6.16)$$

The symbol transmitted from the second antenna can be estimated as

$$\hat{d}_2(k) = (\mathbf{T}_l^{1/2}(:, 2))^H \hat{\mathbf{g}}(k) / (\sqrt{P_2}e^{-j\psi}). \quad (6.17)$$

The block diagram of the iterative EM-based MAP channel estimation and SIC data detection for MIMO OFDM systems is shown in Fig. 6.2. In the transmitter, the adaptive MIMO precoder [93] utilizes spatial multiplexing scheme and optimally adjusts the signal power and phase for each antenna by exploiting the long term spatial correlation characteristics of the MIMO channels. Modulation and demodulation of OFDM are efficiently implemented by the means of inverse fast Fourier transform (IFFT) and fast Fourier transform (FFT). In the receiver, we propose an EM-based least square (LS) channel estimation scheme to initially estimate the channel coefficients for all the sub-channels by employing the output signals of the OFDM demodulation. Data is detected by successive interference cancellation (SIC) scheme. Once the temporary hard decisions of the transmitted symbols are available, the ICI component can be approximated and cancelled from the received signal. The received signals after ICI cancellation, the detected symbols and the statistical information of the channels are feedback to the EM-based MAP scheme to obtain more accurate channel parameters.

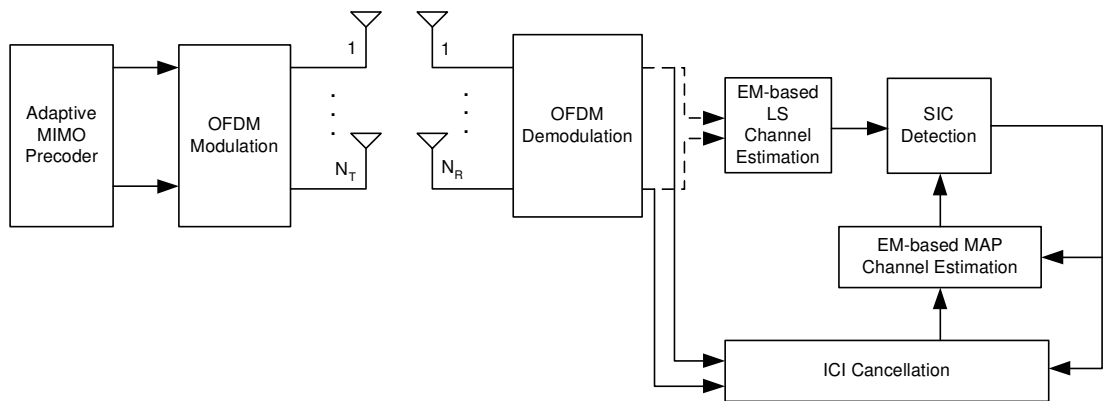


FIGURE 6.2. Block diagram of simplified MAP channel estimation and data detection for MIMO OFDM systems.

6.4. Numerical Examples and Discussion

Error performance of iterative EM-based LS channel estimation and ICI-based MMSE detection for MIMO OFDM systems is shown in Fig. 6.3 – Fig. 6.8. Simulation results are obtained with $N = 128$ sub-carriers employing QPSK modulation. A cyclic prefix of 16 samples is inserted at the beginning of each OFDM symbol to avoid ISI. One pilot sub-carrier is inserted after every 4 data sub-carriers. Thus, the pilot spacing in the frequency domain equals $4/(NT_s)$. Since the multipath spread of the channel is assumed to be LT_s , the coherence bandwidth is approximately equal to $1/(LT_s)$. Let R be the ratio of the pilot spacing to the channel coherence bandwidth. That is, $R = \frac{4L}{N}$. Since the grid density of the pilot symbols must satisfy the 2-D sampling theorem in order to recover channel parameters [95], the pilot spacing must not be greater than half of the coherence bandwidth, which results in $R \leq 0.5$. Thus, $R = 0.4375$ will be adopted unless explicitly specified otherwise (e.g., in Fig. 6.6).

It was shown in [86] that to minimize the MSE of the LS channel estimate, the pilot sequence must be equipowered, equispaced, and phase-shift orthogonal for each transmit antenna in frequency-selective environments. Let us define $X_{u_1, u_2} = \mathbf{F}_{(p)}^H \mathbf{D}_{u_1(p)}^H \mathbf{D}_{u_2(p)} \mathbf{F}_{(p)}$, $u_1, u_2 = 1, 2, \dots, N_T$, to measure the orthogonality among the training sequences, where $\mathbf{D}_{u(p)}$ and $\mathbf{F}_{(p)}$ were defined in Section 5.2. It is required that

$$X_{u_1, u_1} = \mathbf{I}_{L+1} \quad (6.18)$$

$$X_{u_1, u_2} = \mathbf{0}_{(L+1) \times (L+1)}, u_1 \neq u_2 \quad (6.19)$$

where \mathbf{I} is the identity matrix and $\mathbf{0}$ is matrix whose elements are 0's. The rows of the Hadamard matrix satisfy the above criteria and will be used as the training sequences for different transmit antennas.

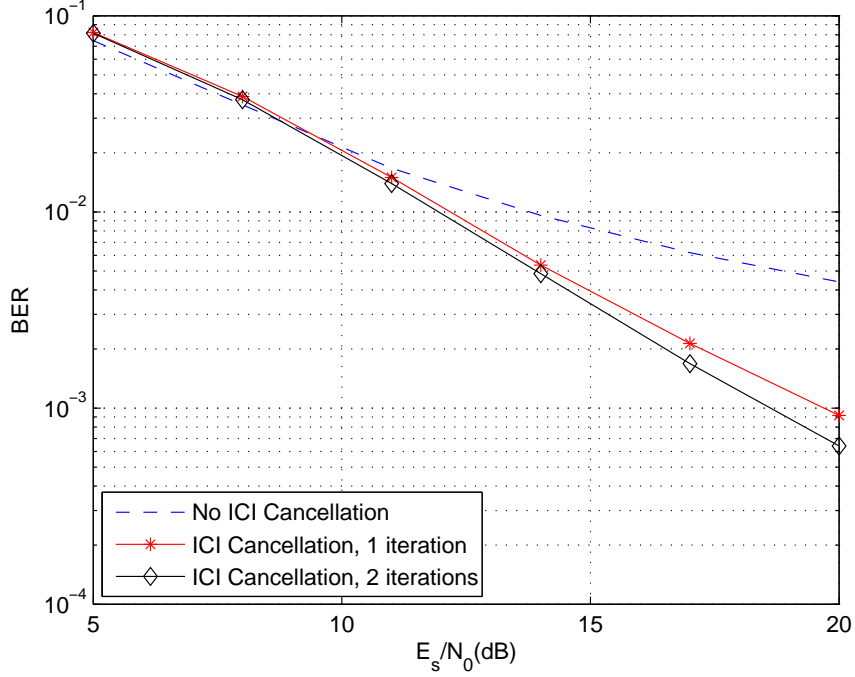


FIGURE 6.3. BER versus E_s/N_0 with and without ICI cancellation ($(N_t, N_r) = (2, 3)$, $f_d T = 0.113$, and $G = 9$).

Since the normalized Doppler shift $f_d T$, where T is the OFDM symbol duration, describes the channel fading rapidity for a given data rate better than the absolute Doppler shift f_d , $f_d T$ will be used for measuring fading rates. Values of $f_d T$ are chosen similar to those adopted in [86]. The channel is assumed to have 15 multipath components ($L = 14$) (unless explicitly specified otherwise) with an exponentially decaying power-delay profile. If both the transmitter and the receiver antennas are sufficiently separated under the rich-scattering environment [38], channel fading processes for different sub-channels are assumed to be independent and identically distributed (i.i.d.). In simulations, fading processes are piecewise-constant approximated, allowing the channel coefficients to be constant

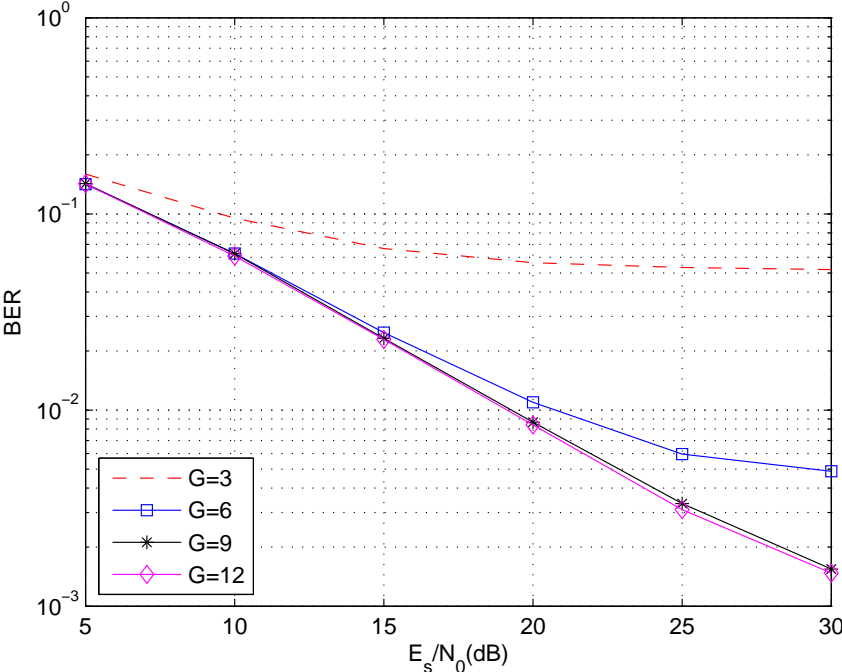


FIGURE 6.4. The effect of the number of sub-iterations in the EM process $((N_t, N_r) = (2, 2), f_d T = 0.0452$, after 2 iterations of ICI cancellation).

in one sampling interval and change over different sampling intervals according to the spaced-time correlation function given in Eq. (5.1). The deterministic method described in [48] has been widely used in simulations to generate frequency-flat Rayleigh fading channel coefficients with controllable normalized Doppler shifts. However, it is difficult to generate uncorrelated multipath components using this approach. Furthermore, there are known problems with the auto-correlation of the fading process generated using this model. Thus, many modified simulators have been proposed [49–51]. We adopt the model in [49] in our simulations because it results in better auto-correlation properties of the fading process than the one in [48].

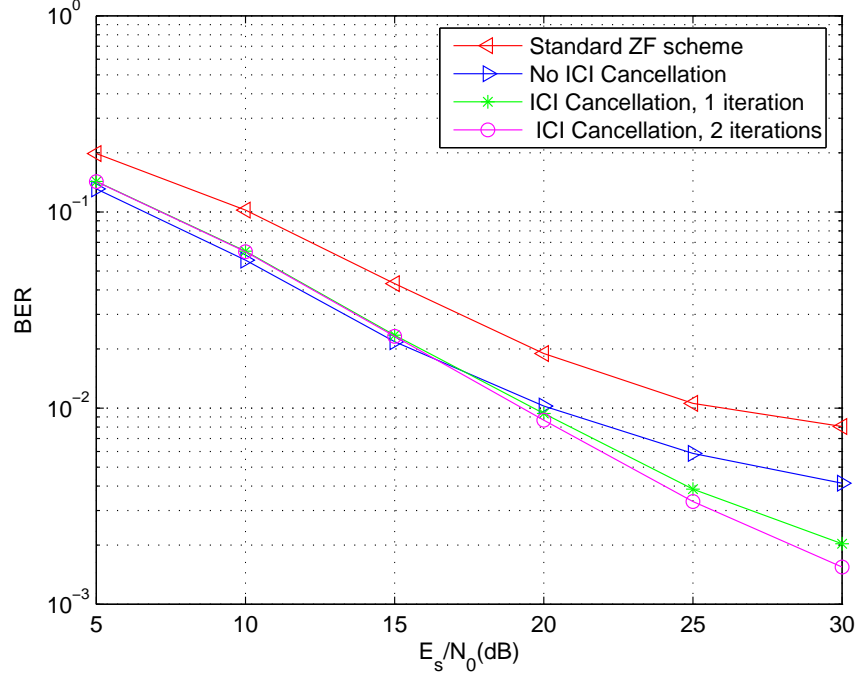


FIGURE 6.5. Comparison of the proposed scheme with a common ZF detection scheme ($(N_t, N_r) = (2, 2)$ and $f_d T = 0.0452$).

The number of sub-iterations in the EM process G , as mentioned in Section 5.2, affects the receiver performance. As will be shown later in Fig. 6.4, for common system configurations, performance improvements will saturate at $G = 9$ sub-iterations. Hence, in the EM process for all simulations, $G = 9$ with step sizes of $\beta_1 = \beta_2 = \dots = \beta_{N_T} = 1/N_T$ will be adopted unless explicitly specified otherwise. Fig. 6.3 compares the bit-error-rate (BER) performances of the proposed iterative scheme for a (2,3) MIMO system at a fading rate of $f_d T = 0.113$. The curve corresponding to the case of no ICI cancellation is obtained by employing the EM-based channel estimates combined with a common MMSE data detection. Not considering ICI in the MMSE detection process obviously causes an error floor.

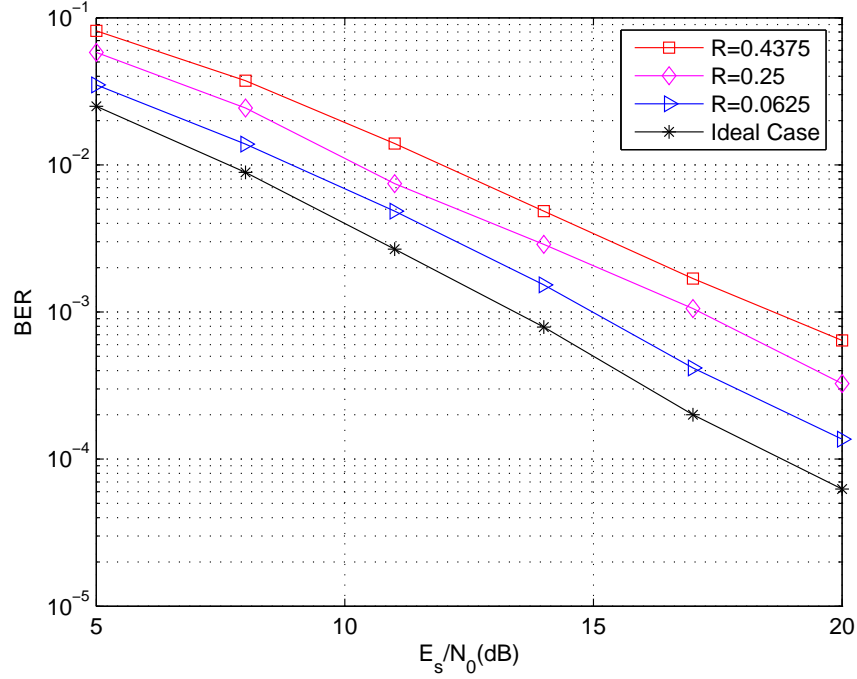


FIGURE 6.6. The effect of the ratio of pilot spacing to channel coherence bandwidth R ($(N_t, N_r) = (2, 3)$ and $f_d T = 0.113$).

The proposed scheme with only two iterations improves the system performance significantly. However, performance improvements are insignificant with more than two iterations. Thus, in all the rest of the simulations BER curves will be obtained after two iterations, except in Fig. 6.5.

In terrestrial digital video broadcasting (DVB-T) systems, normalized Doppler shift of 0.0452 corresponds to the vehicle speeds of 304.72km/h for the 2k mode (2048 sub-carriers) and 76.18km/h for the 8k mode (8192 sub-carriers) [28]. Fig. 6.4 shows the BER performance with different number of sub-iterations (G) of EM algorithm for a (2,2) MIMO OFDM system at a fading rate of $f_d T = 0.0452$. There is a huge improvement if G is increased from 3 to 9; however the improvement

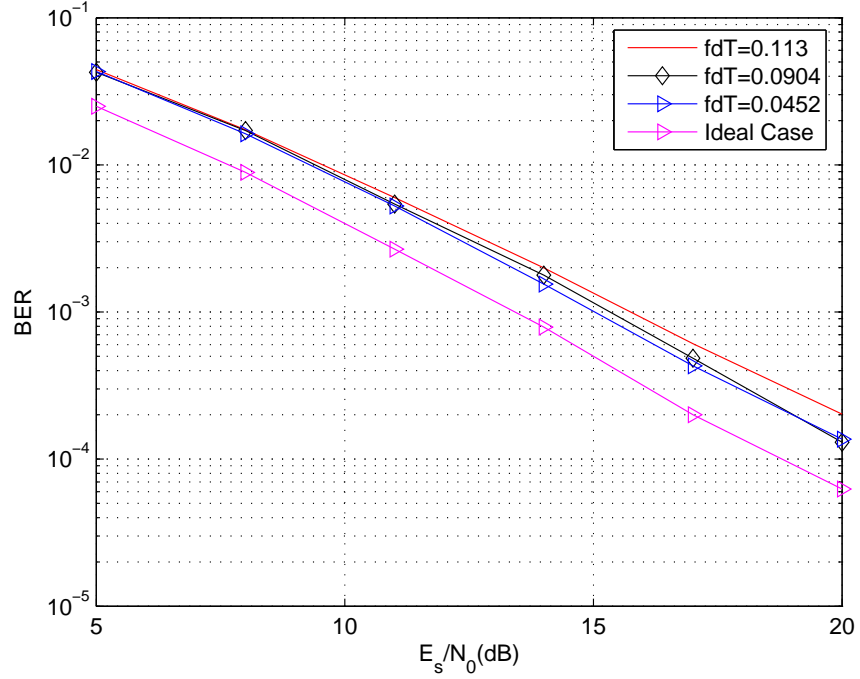


FIGURE 6.7. Performance comparison between the proposed scheme and the ideal case ($(N_t, N_r) = (2, 3)$ and $L = 5$).

is negligible beyond $G = 9$ sub-iterations. Fig. 6.5 compares the performance of the ICI-based MMSE with phase-shift orthogonal training sequence (POTS) with that of the common ZF detection scheme with orthogonal training sequence (OTS). Significant performance gains of the proposed scheme over the common ZF scheme are observed for a (2,2) MIMO system at a medium normalized Doppler shift of $f_dT = 0.0452$.

The effect of the ratio R defined at the beginning of this section on the BER performance for a (2,3) MIMO system operating at a fading rate of $f_dT = 0.113$ is shown in Fig. 6.6. As expected, the lower the ratio, the better the performance. However with the same channel scenario and system configuration, a lower value

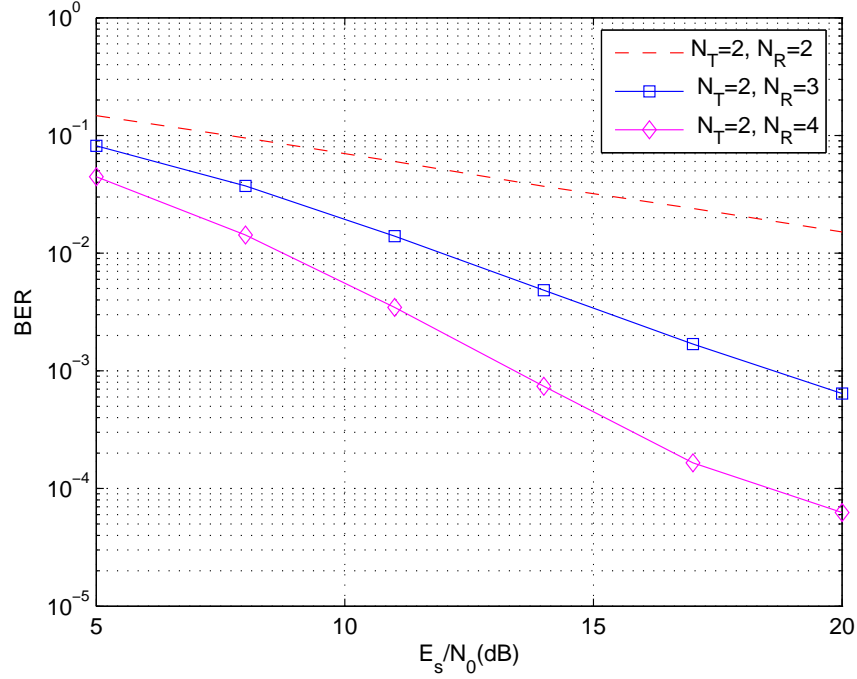


FIGURE 6.8. The effect of antenna configurations ($f_d T = 0.113$ and $R = 0.4375$).

of R results in a lower spectral efficiency. It will be useful to see the performance gap between the proposed scheme with that of the ideal case, which is defined as zero Doppler shift (thus, no ICI) and perfect knowledge of channel coefficients. In simulation for the ideal case, fading coefficients are generated based on the quasi-static model. The BER performance with different Doppler shifts is shown in Fig. 6.7 for a (2,3) MIMO system and the channel has five multipath components ($L = 4$). The performance gap is within 3dB compared to the ideal case with $f_d T$ as high as 0.113.

Fig. 6.8 shows the BER versus E_s/N_0 curves with $f_d T = 0.113$ and $R = 0.4375$ for different numbers of transmit and receive antennas: $(N_T, N_R) =$

(2, 2), (2, 3), (2, 4). Under the same system configuration and fading rate, the proposed scheme achieves about 4dB gain over the scheme given in [86] for a (2,4) MIMO system at the BER of 1.2×10^{-3} . Also, as expected, a (2, 4) system performs much better than a (2, 2) or a (2, 3) system, as it has the highest diversity gain provided by large difference between the number of receive and transmit antennas.

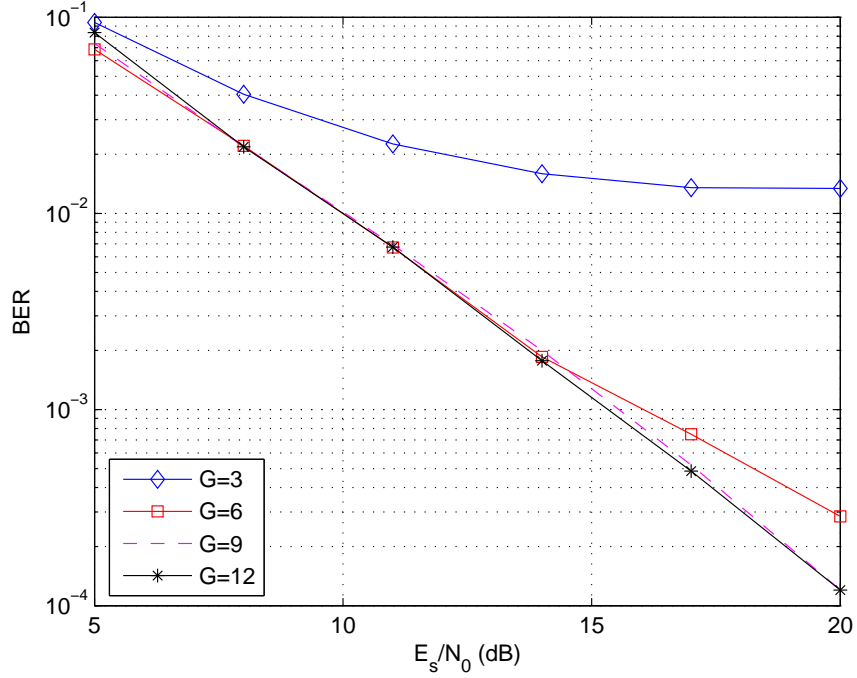


FIGURE 6.9. The effect of the number of sub-iterations in the EM process ($N_T = 2$, $N_R = 3$, uncorrelated spatial channels).

Error performance of iterative EM-based MAP channel estimation and SIC detection for MIMO OFDM systems is shown in Fig. 6.9 – Fig. 6.14. Simulation results are obtained with $N = 128$ sub-carriers employing QPSK modulation. A cyclic prefix of 16 samples is inserted at the beginning of each OFDM symbol to avoid ISI. One pilot sub-carrier is inserted after every 4 data sub-carriers. R is defined as the ratio of the pilot spacing to the channel coherence bandwidth. That

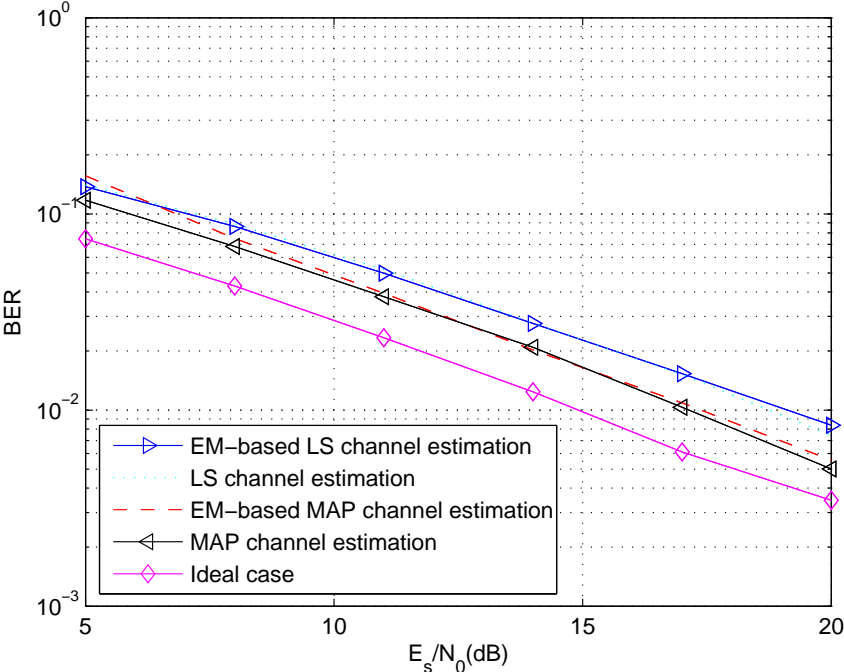


FIGURE 6.10. Performance comparison of various channel estimation schemes ($N_T = 2, N_R = 2$, uncorrelated spatial channels).

is, $R = \frac{4L}{N}$. Fading processes for different sub-channels are all assumed to be independent and identically distributed for spatially uncorrelated MIMO channels. In terrestrial digital video broadcasting 2k mode (DVB-T) systems, if the vehicle speed is 134.8km/h, the normalized Doppler shift is 0.02 [28]. Thus, $f_d T = 0.02$ is considered to be a fairly large Doppler shift for the simulated mobile environment. In simulations, fading processes are piecewise-constant approximated, allowing the channel coefficients to be constant in one sampling interval and change over different sampling intervals according to the spaced-time correlation function given in Eq. (5.1).

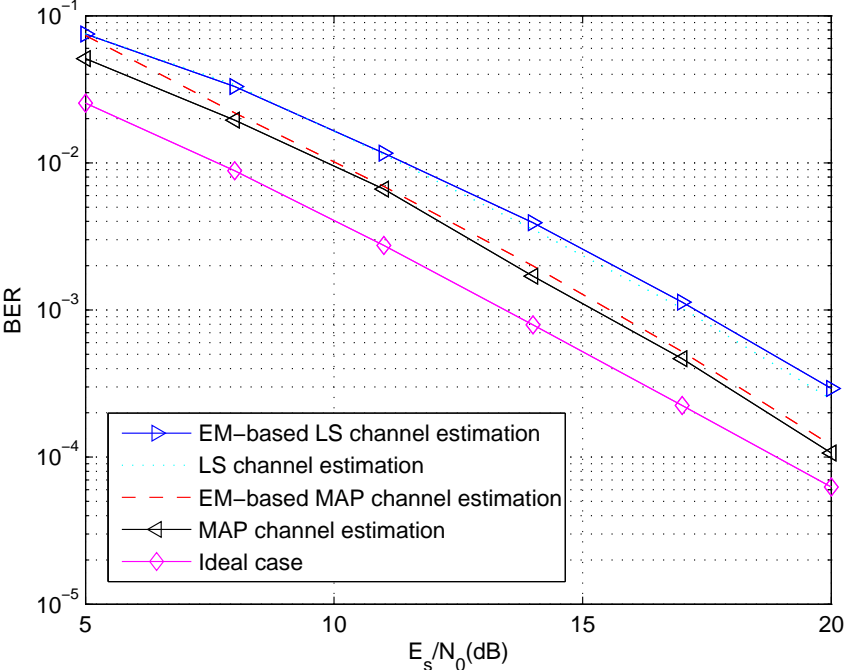


FIGURE 6.11. Performance comparison of various channel estimation schemes ($N_T = 2$, $N_R = 3$, uncorrelated spatial channels).

The number of sub-iterations in the EM process G , as mentioned in Section 5.3.3, affects the receiver performance. As will be shown later in Fig. 6.9, for common system configurations, performance improvements will saturate at $G = 9$ sub-iterations. Hence, in the EM process for all simulations, $G = 9$ with step sizes of $\beta_1 = \beta_2 = \dots = \beta_{N_T} = 1/N_T$ will be adopted unless explicitly specified otherwise. Figs. 6.10 and 6.11 compare the error performances when the receiver employs an LS, a MAP, an EM-LS, and an EM-MAP channel estimator for 2, 2) (i.e., $N_T = 2$, $N_R = 2$) and (2, 3) MIMO OFDM systems. Performance of the ideal case – zero Doppler shift (thus, no ICI) and perfect knowledge of channel coefficients – is used as the baseline performance. The EM-MAP scheme performs

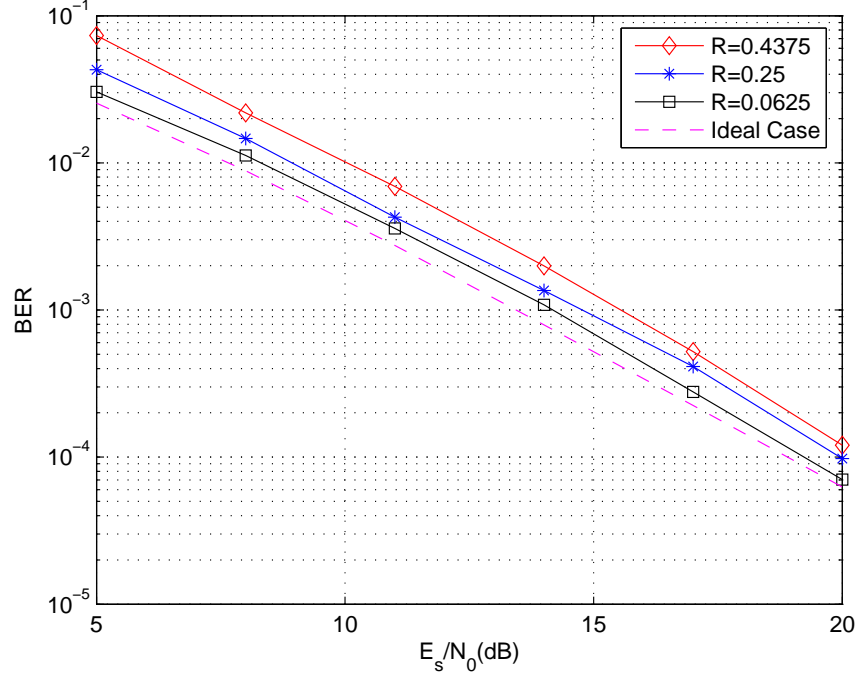


FIGURE 6.12. The effect of the ratio of pilot spacing to channel coherence bandwidth ($N_T = 2$, $N_R = 3$, uncorrelated spatial channels).

almost the same as the normal MAP scheme, but the latter is computationally much more extensive than the former. Approximately 2dB improvement is observed with the EM-based MAP estimator over the EM-based LS estimator.

The effect of the ratio of pilot spacing to the channel coherent bandwidth on the BER performance for a (2, 3) MIMO OFDM system operating at a fading rate of $f_d T = 0.02$ is shown in Fig. 6.12. As expected, the lower the ratio, the better the performance. However with the same channel scenario and system configuration, a lower value of R results in a lower spectral efficiency. The performance gap between the proposed scheme with that of the ideal case increases with larger R .

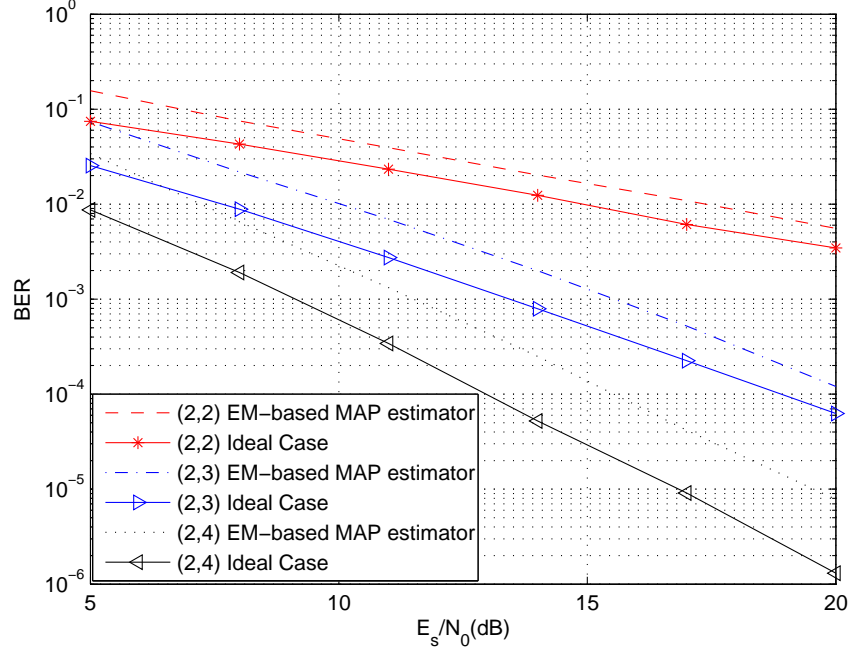


FIGURE 6.13. Performance of the proposed scheme with different antenna configurations ($R = 0.4375$, uncorrelated spatial channels).

Fig. 6.13 shows the BER versus E_s/N_0 curves with the EM-based MAP channel estimator under $f_d T = 0.02$, $R = 0.4375$, and different numbers of transmit and receive antennas: (2, 2), (2, 3), (2, 4). The error performance is also compared with the ideal case. For all cases simulated, performance of the proposed scheme is within about 2dB of that of the ideal case. In order to demonstrate the robustness of the proposed algorithm in the presence of high spatial correlations, the error performance of a (2, 2) system with different spatial correlation coefficients ($|\rho| = 0.75, 0.93, 0.993, 1$) is presented in Fig. 6.14. With the knowledge of channel correlation matrix, a precoder is applied for transmit power and phase optimization. Combined with the proposed EM-MAP estimator and the iterative detection

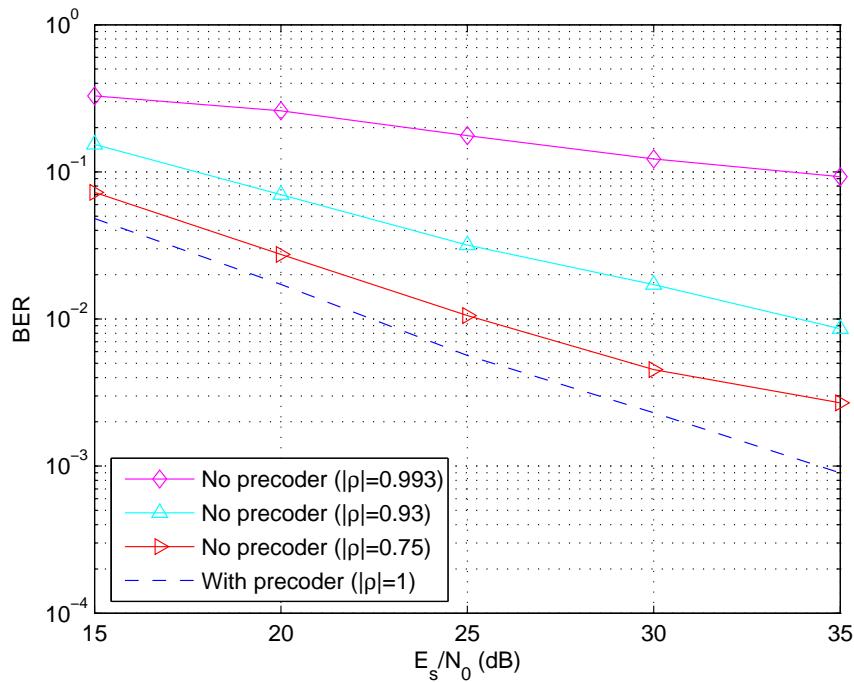


FIGURE 6.14. Performance of the proposed scheme in the presence of high spatial correlation ($N_T = 2$, $N_R = 2$, $f_d T = 0.04$).

scheme, no error floors are observed even under high spatial correlation and fast fading ($f_d T = 0.04$).

6.5. Conclusion

We have proposed an iterative EM-based LS and ICI-based MMSE detection scheme for MIMO OFDM systems over time-varying fading channels. This scheme incorporates an EM algorithm to avoid inversions of large-size matrices in obtaining the LS channel estimates. This significantly reduces the computational complexity while the LS performance is still maintained. To improve data detection performance, variance of ICI caused by time-varying fading is taken into consid-

eration in the MMSE process of the initial iteration. The ICI component is then approximated and cancelled in the iterative channel estimation and data detection process.

An iterative EM-based MAP channel estimation and SIC detection is proposed for MIMO OFDM systems. The initially detected symbols and the received signals after ICI cancellation are processed by the EM-based MAP estimator to refine the channel state information (CSI). Simulation results under different channel environments, MIMO configurations, and other algorithm-related parameters demonstrate the great robustness of the proposed scheme to fast fading and spatial correlations. With a fading rate as high as $f_d T = 0.02$, the proposed EM-MAP scheme achieves an error performance that is within about 2dB of the ideal case – zero Doppler shift (thus no ICI) and perfect knowledge of channel state information. We also observe a 2dB gain of the proposed EM-based MAP scheme over the least square (LS) scheme at medium normalized Doppler shifts.

7. CONCLUSIONS

7.1. Summary

In this thesis, we have proposed solutions to address various challenging physical layer issues of mobile MIMO OFDM systems, including channel analysis and modelling, channel estimation, and data detection. There are four main contributions in this thesis.

Firstly, we have derived the closed-form pdf expressions of the condition number (MMSVR) of the channel matrix for various MIMO configurations. These analytical results can be used to predict the relative performance of MIMO OFDM systems without complicated system-level simulations. They can also be applied to determine the lower capacity bound of such systems. Through the channel analysis, it is clearly observed that an additional receive antenna could provide significant performance improvements. The analytical results indicating the gain/loss of different configurations predicted using the mean of the square of MMSVR match the results obtained through system-level simulations very well. The analysis presented in Chapter 3 provides a simple and effective way to predict the relative performances of different MIMO OFDM configurations.

Secondly, a decision directed maximum *a posteriori* probability (MAP) channel estimation scheme for symbol-by-symbol detection in MIMO systems has been derived. This scheme has a low complexity and can be applied to time-varying Rayleigh fading channels with an arbitrary spaced-time correlation function. Numerical results indicate that a long memory depth is unnecessary for a system to work well. The channel estimation quality deteriorates as the number of transmit antennas increases. The fading rate has a high impact on system performance and the proposed scheme is more appropriate for the channels with low to medium

Doppler shifts. Large block length between adjacent pilot blocks can be deployed with the proposed scheme. This results in minimum overhead for pilot symbols. The schemes based on the quasi-static channel model reach an error floor whereas the proposed scheme works very well at high E_b/N_0 values.

In Sections 5.2 and 6.2, we have derived an expectation maximization (EM) based LS channel estimation and ICI-based MMSE data detection in MIMO OFDM systems over time-varying fading channels, respectively. The proposed scheme incorporates an EM algorithm to avoid inversions of large-size matrices in obtaining the LS channel estimates. This significantly reduces the computational complexity while the LS performance is still maintained. To improve data detection performance, variance of ICI caused by time-varying fading is taken into consideration in the MMSE process of the initial iteration. The ICI component is then approximated and cancelled in the iterative channel estimation and data detection process. We have provided a comprehensive performance evaluation of the proposed scheme with different channel environments, MIMO configurations, algorithm parameters such as the number of sub-iterations in the EM process, and detection schemes. Comparison is made between the proposed scheme and existing schemes under similar system setup and channel conditions. The proposed scheme was found to have superior performance than existing schemes in fast-fading environments.

Finally, in order to minimize the MSE of the channel estimates and reduce the complexity of the implementation simultaneously, an EM-based MAP channel estimator is proposed in Section 5.3. The channel parameters are initially obtained by an EM-based least square (LS) estimator. Then a successive interference cancellation (SIC) scheme described in Section 6.3 is considered for the data detection. With the estimate of the channel and the detected data for the current symbol interval, ICI component is approximated and removed from the received

signals. The detected symbols and the received signals after ICI cancellation are fed back to the MAP estimator to refine the CSI. 2dB gain is observed by our proposed EM-based MAP scheme over LS scheme at medium normalized Doppler shift ($f_d T = 0.02$). Performance comparison is made between the proposed scheme and the ideal case with no Doppler shift and perfect channel estimation. The proposed scheme achieves excellent performance in fast fading channels with relatively low complexity. The system performance is also analyzed over the spatially correlated channels. By exploiting only the long term correlation characteristics, the signal is optimally transmitted and can be successively detected with no error floor.

7.2. Future Research

Most of the design and analysis in this thesis is based on open-loop MIMO OFDM systems, which implies no feedback of channel information. However, it has been shown that channel adaptive transmit beam-forming can improve considerably the performance of MIMO systems [10, 102] by optimally using the available CSI information at the transmitter. Furthermore, if only limited feedback bits are available per fading block due to the limited bandwidth of the feedback link, the effect on the optimal transmission should be analyzed.

BIBLIOGRAPHY

- [1] G. J. Foschini, "On limits of wireless communications in a fading environment when using multiple antennas," *Wireless Personal Communications*, vol. 6, pp. 311–335, Mar. 1998.
- [2] D. Gesbert, M. Shafi, D. Shiu, P. Smith and A. Naguib, "From theory to practice: an overview of MIMO space-time coded wireless systems," *IEEE Journal on Selected Areas in Communications*, vol. 21, pp. 281–302, Apr. 2003.
- [3] S. M. Alamouti, "A simple transmit diversity technique for wireless communications," *IEEE Journal on Selected Areas in Communications*, vol. 16, pp. 1451–1458, Oct. 1998.
- [4] W. Su, Z. Safar, M. Olfat and K. Liu, "Obtaining full-diversity space-frequency codes from space-time codes via mapping," *IEEE Transactions on Signal Processing*, vol. 51, pp. 2905–2916, Nov. 2003.
- [5] W. Su, Z. Safar and K. Liu, "Full-rate full-diversity space-frequency codes with optimum coding advantage," *IEEE Transactions on Information Theory*, vol. 51, pp. 229–249, Jan. 2005.
- [6] M. Fozunbal, S. W. McLaughlin and R. W. Schafer, "On space-time-frequency coding over MIMO-OFDM systems," *IEEE Transactions on Wireless Communications*, vol. 4, pp. 320–331, Jan. 2005.
- [7] G. D. Golden, C. J. Foschini, R. A. Valenzuela and P. W. Wolniansky, "Detection algorithm and initial laboratory results using V-blast space-time communication architecture," *IEE Electronics Letters*, vol. 35, pp. 14–16, Jan. 1999.
- [8] P. W. Wolniansky, G. J. Foschini, G. D. Golden and R. A. Valenzuela, "V-BLAST: an architecture for realizing very high data rates over the rich-scattering wireless channel," *Signals, Systems, and Electronics, 1998. ISSSE 98*, pp. 295–300, Oct. 1998.
- [9] K. Mukkavilli, A. Sabharwal, E. Erkip and B. Aazhang, "On beamforming with finite rate feedback in multiple antenna systems," *IEEE Transactions on Information Theory*, vol. 49, pp. 2562–2579, Oct. 2003.
- [10] A. Narula, M. J. Lopez, M. D. Trott and G. W. Wornell, "Efficient use of side information in multiple-antenna data transmission over fading channels," *IEEE Journal on Selected Areas in Communications*, vol. 16, pp. 1423–1436, October 1998.

- [11] C. N. Chuah, D. Tse, J. M. Kahn and R. Valenzuela, "Capacity scaling in MIMO wireless systems under correlated fading," *IEEE Transactions on Information Theory*, vol. 48, pp. 637–650, Mar. 2002.
- [12] C. N. Chuah, J. M. Kahn and D. Tse, "Capacity of indoor multiantenna array systems in indoor wireless environment," in *Proc. GLOBECOM*, 98, Sydney, Australia, 1998, pp. 1894–1899.
- [13] Y. G. Li, J. H. Winters and N. R. Sollenberger, "MIMO-OFDM for wireless communications: signal detection with enhanced channel estimation," *IEEE Transactions on Communications*, vol. 50, pp. 1471–1477, Sep. 2002.
- [14] L. J. Cimini, "Analysis and simulation of a digital mobile channel using orthogonal frequency division multiplexing," *IEEE Transactions on Communications*, vol. 33, pp. 665–675, Jul. 1985.
- [15] V. Mignone and A. Morello, "CD3-OFDM: A novel demodulation scheme for fixed and mobile receivers," *IEEE Transactions on Communications*, vol. 44, pp. 1144–1151, Sep. 1996.
- [16] S. B. Weinstein and P. M. Ebert, "Data transmission by frequency-division multiplexing using the discrete fourier transform," *IEEE Transactions on Communications*, vol. 19, pp. 628–634, Oct. 1971.
- [17] J. A. C. Bingham, "Multicarrier modulation for data transmission: an idea whose time has come," *IEEE Transaction on Communications*, vol. 28, pp. 5–14, May 1990.
- [18] J. Gao and H. Liu, "Decision-directed estimation of MIMO time-varying Rayleigh fading channels," *IEEE Transactions on Wireless Communications*, vol. 4, pp. 1412–1417, Jul. 2005.
- [19] J. Gao, O. C. Ozdural, S. Ardalán and H. Liu, "Performance modeling of MIMO OFDM systems via channel analysis," *to appear in IEEE Transaction on Wireless Communications*.
- [20] J. Gao and H. Liu, "Iterative channel estimation and data detection for mobile MIMO-OFDM systems," *submitted to IEEE Transactions on Wireless Communications*.
- [21] B. Muquet and M. de Courville, "Blind and semi-blind channel identification methods using second order statistics for OFDM systems," *IEEE Int. Conf. Acoustics, Speech, and Signal Processing*, vol. 5, pp. 2745–2748, Mar. 1999.

- [22] M. C. Necker and G. L. Stuber, "Totally blind channel estimation for OFDM on fast varying mobile radio channels," *IEEE Transactions on Wireless Communications*, vol. 3, pp. 1514–1525, Sep. 2004.
- [23] N. Chotikakamthorn and H. Suzuki, "On identifiability of OFDM blind channel estimation," in *Proc. Vehicular Technology Conference*, Amsterdam, Netherlands, vol. 4, pp. 2358–2361, Sep. 1999.
- [24] Y.-S Choi, P. J. Voltz and F. A. Cassara, "On channel estimation and detection for multicarrier signals in fast and selective Rayleigh fading channels," *IEEE Transactions on Communications*, vol. 49, pp. 1375–1387, Aug. 2001.
- [25] S. Coleri, M. Ergen, A. Puri and A. Bahai, "Channel estimation techniques based on pilot arrangement in OFDM systems," *IEEE Transactions on Broadcasting*, vol. 48, pp. 223–229, Sep. 2002.
- [26] T. L. Tung and K. Yao, "Channel estimation and optimal power allocation for a multiple-antenna OFDM system," *EURASIP Journal on Applied Signal Processing*, vol. 2002, pp. 330–339, Mar. 2002.
- [27] G. L. Stuber, J. R. Barry, S. W. McLaughlin, Y. Li, M. A. Ingram and T.G. Pratt, "Broadband MIMO-OFDM wireless communications," *Proceedings of the IEEE*, vol. 92, pp. 271–294, Feb. 2004.
- [28] S. Tomasin, A. Gorokhov, H. Yang and J. Linnartz, "Iterative interference cancellation and channel estimation for mobile OFDM," *IEEE Transactions on Wireless Communications*, vol. 4, pp. 238–245, Jan. 2005.
- [29] D. Schafhuber, G. Matz, and F. Hlawatsch, "Kalman tracking of time-varying channels in wireless MIMO-OFDM systems," in *Proc. 37th Asilomar Conf. Signals, Systems, Computers, Pacific Grove, CA*, Nov. 2003, pp. 1261–1265.
- [30] K. Han, S. Lee, J. Lim, and K. Sung, "Channel estimation for OFDM with fast fading channels by modified kalman filter," *IEEE Transactions on Consumer Electronics*, vol. 50, pp. 443–449, May. 2004.
- [31] Y. Li, "Simplified channel estimation for OFDM systems with multiple transmit antennas," *IEEE Transactions on Wireless Communications*, vol. 1, pp. 67–75, Jan. 2002.
- [32] P. Vandenameele, L. Pene, M. Engler, B. Gyrelinckx and H. Man, "A combined OFDM/SDMA approach," *IEEE Journal on Selected Areas in Communications*, vol. 18, pp. 2312–2321, Nov. 2000.

- [33] S. Sun, I. Wiemer, C. K. Ho and T. T. Tjhung, "Training sequence assisted channel estimation for MIMO OFDM," *IEEE Wireless Communications and Networking Conference*, vol. 1, pp. 38–43, Mar. 2003.
- [34] Y. Teng, K. Mori and H. Kobayashi, "Performance of DCT interpolation-based channel estimation method for MIMO-OFDM systems," *IEEE International Symposium on Communications and Information Technology*, vol. 1, pp. 622–627, Oct. 2004.
- [35] W. T. A. Lopes and M. S. Alencar, "Performance of a rotated QPSK based system in a fading channel subject to estimation errors," *Microwave and Optoelectronics Conference, 2001. IMOC 2001*, pp. 27–30, Aug. 2001.
- [36] V. Tarokh, N. Seshadri and A. R. Calderbank, "Space-time codes for high data rate wireless communication: performance criterion and code construction," *IEEE Transactions on Information Theory*, vol. 44, pp. 744–765, Mar. 1998.
- [37] J. G. Proakis, *Digital communications*. McGraw Hill, 2000.
- [38] V. Pohl, V. Jungnickel, T. Haustein, and C. V. Helmolt, "Antenna spacing in MIMO indoor channels," in *Proc. of IEEE Vehicular Technology Conference*, pp. 749–753, May 2002.
- [39] H. Bolckei, D. Gesbert and A. J. Paulraj, "On the capacity of OFDM-based spatial multiplexing systems," *IEEE Transactions on Communications*, vol. 50, pp. 225–234, Feb. 2002.
- [40] D. Asztely, "On antenna arrays in mobile communication systems: fast fading and GSM base station receiver algorithms," *Royal Institute of Technology*, Stockholm, Sweden, IR-S3-SB-9611, 1996.
- [41] C. Chuah, D. Tse, J. Kahn and R. A. Valenzuela, "Capacity scaling of MIMO wireless systems under correlated fading," *IEEE Transactions on Information Theory*, vol. 48, pp. 637–650, Mar. 2002.
- [42] J. H. Kotecha and A. M. Sayeed, "Transmit signal design for optimal estimation of correlated MIMO channels," *IEEE Transactions on Signal Processing*, vol. 52, pp. 546–557, Feb. 2004.
- [43] R. B. Ertel, P. Cardieri, K. W. Sowerby, T. S. Rappaport and J. H. Reed, "Overview of spatial channel models for antenna array communication systems," *IEEE Personal Communications*, pp. 10–22, Feb. 1998.
- [44] C. N. Chua, J. M. Kahn and D. Tse, "Capacity of multi-antenna array systems in indoor wireless environment," *Proc. IEEE Global Telecommunication Conference*, pp. 1894–1899, Nov. 1998.

- [45] D. Shiu, G. Foschini, M. Gans and J. Kahn, "Fading correlation and its effect on the capacity of multielement antenna systems," *IEEE Transactions on Communications*, vol. 48, pp. 502–512, Mar. 2000.
- [46] D. Chizhik, F. Rashid-Farrokhi, J. Ling and A. Lozano, "Effect of antenna separation on the capacity of BLAST in correlated channels," *IEEE Communication Letters*, vol. 4, pp. 337–339, Nov. 2000.
- [47] K. Yu, M. Bengtsson, B. Ottersten, P. Karlsson and M. Beach, "Second order statistics of NLOS indoor MIMO channels based on 5.2 Ghz measurements," *Proc. IEEE Global Telecommunication Conference*, vol. 1, pp. 156–160, Nov. 2001.
- [48] W. C. Jakes, *Microwave mobile communications*. New York, NY: John Wiley and Sons, Inc., 1974.
- [49] P. Dent, G. E. Bottomley and T. Croft, "Jakes fading model revisited," *Electronics Letters*, vol. 29, pp. 1162–1163, Jun. 1993.
- [50] Y. Zheng and C. Xiao, "Simulation models with correct statistical properties for Rayleigh fading channels," *IEEE Transactions on communications*, vol. 51, pp. 920–928, Jun. 2003.
- [51] Y. Li and X. Huang, "The simulation of independent Rayleigh faders," *IEEE Transactions on communications*, vol. 50, pp. 1503–1514, Sep. 2002.
- [52] A. Pualraj, D. Gore, R. Nabar, and H. Bölcskei, "An overview of MIMO communications - a key to gigabit wireless," *Proceedings of the IEEE*, vol. 92, pp. 198–218, Feb. 2004.
- [53] A. Goldsmith, S. Jafar, N. Jindal and S. Vishwanath, "Capacity limits of MIMO channels," *IEEE Journal on Selected Areas in Communications*, vol. 21, pp. 684–702, Jun. 2003.
- [54] "Supplement to IEEE standard for information technology telecommunications and information exchange between systems - local and metropolitan area networks - specific requirements. Part 11: wireless LAN Medium Access Control (MAC) and Physical Layer (PHY) specifications: high-speed physical layer in the 5 GHz band," *IEEE Std 802.11a-1999*, Dec. 1999.
- [55] A. van Zelst and T. Schenk, "Implementation of a MIMO OFDM-based wireless LAN system," *IEEE Transactions on Signal Processing*, vol. 52, pp. 483–494, Feb. 2004.

- [56] L. Zheng and D. N. C. Tse, "Diversity and multiplexing: a fundamental tradeoff in multiple-antenna channels," *IEEE Transactions on Information Theory*, vol. 49, pp. 1073–1096, May 2003.
- [57] R. Heath and A. Paulraj, "Switching between multiplexing and diversity based on constellation distance," *Proc. of Allerton Conference on Communication, Control and Computing*, Oct. 2000.
- [58] B. Bjerke and J. Proakis, "Multiple-antenna diversity techniques for transmission over fading channels," *Proc. of IEEE Wireless Communications and Networking Conference*, vol. 3, pp. 1038–1042, Sep. 1999.
- [59] H. Artes, D. Seethaler and F. Hlawatsch, "Efficient detection algorithms for MIMO channels: A geometrical approach to approximate ML detection," *IEEE Transactions on Signal Processing*, vol. 51, pp. 2808–2820, Nov. 2003.
- [60] I. E. Telatar, "Capacity of multi-antenna Gaussian channels," *European Transactions on Telecommunication Related Technology*, vol. 10, pp. 585–595, Nov. 1999.
- [61] M. Chiani, M. Z. Win and A. Zanella, "The distribution of eigenvalues of a Wishart matrix with correlation and application to MIMO capacity," *Proc. of IEEE Globecom'03*, pp. 1802–1805, Nov. 2003.
- [62] C. Martin and B. Ottersten, "Asymptotic eigenvalue distribution and capacity for MIMO channels under correlated fading," *IEEE Transactions on Wireless Communication*, vol. 3, pp. 1350–1359, Jul. 2004.
- [63] R. K. Malik, "The pseudo-Wishart distribution and its application to MIMO systems," *IEEE Transactions on Information Theory*, vol. 49, pp. 2761–2769, Oct. 2003.
- [64] D. Huang and K. B. Letaief, "Pre-DFT processing using eigen-analysis for coded OFDM with multiple receive antennas," *IEEE Transactions on Communications*, vol. 52, pp. 2019–2027, Nov. 2004.
- [65] D. Huang and K. B. Letaief, "Symbol based space diversity for coded OFDM systems," *IEEE Transactions on Wireless Communications*, vol. 3, pp. 117–127, Jan. 2004.
- [66] C. Mecklenbrauker and M. Rupp, "Generalized Alamouti codes for trading quality of service against data rate in MIMO UMTS," *Eurasip Journal of Applied Signal Processing: Special Issue on MIMO Comm. and Signal Processing*, pp. 662–675, May 2004.

- [67] H. Liu, "Error performance of MIMO systems in frequency selective Rayleigh fading channels," *Proc. of IEEE Globecom'03*, vol. 4, pp. 2104–2108, Dec. 2003.
- [68] H. Zhu, B. Farhang-Boroujeny and C. Schlegel, "Pilot embedding for joint channel estimation and data detection in MIMO communication systems," *IEEE Communications Letters*, vol. 7, pp. 30–32, Jan. 2003.
- [69] S. Halford, K. Halford, and M. Webster, "Evaluating the performance of HRb proposals in the presence of multipath," *doc: IEEE 802.11-00/282r2*, Sep. 2000.
- [70] A. Maltsev and A. Davydov, "MIMO-OFDM system performance," *TR 03-05 Intel Nizhny Novgorod Labs (INNLL)*, Nov. 2003.
- [71] J. Baltarsee, G. Fock and H. Meyr, "Achievable rate of MIMO channels with data-aided channel estimation and perfect interleaving," *IEEE Journal on Selected Areas in Communications*, vol. 19, pp. 2358–2368, Dec. 2001.
- [72] H. Meyr, M. Moeneclaey, and S. A. Fechtel, *Digital Communication Receivers: Synchronization, Channel Estimation, and Signal Processing, Ch. 14*. John Wiley & Sons, Inc., 1998.
- [73] A. Svensson, "1 and 2 stage decision feedback coherent detectors for DQPSK in fading channels," *Proc. of IEEE Vehicular Technology Conference'95*, vol. 2, pp. 644–648, Jul. 1995.
- [74] B. Lindoff, C. Östberg, and H. Eriksson, "Channel estimation for the W-CDMA system, performance and robustness analysis from a terminal perspective," *Proc. of IEEE Vehicular Technology Conference'99*, vol. 2, pp. 1565–1569, May 1999.
- [75] P. D. Alexander and A. J. Grant, "Iterative decoding and channel estimation," *IEEE International Symposium on Information Theory*, pp. 171, Jun. 2000.
- [76] M. C. Valenti and B. D. Woerner, "Iterative channel estimation and decoding of pilot symbol assisted turbo codes over flat-fading channels," *IEEE Journal on Selected Areas in Communications*, vol. 19, pp. 1697–1705, Sep. 2001.
- [77] D. Samarzija and N. Mandayam, "Pilot assisted estimation of MIMO fading channel response and achievable data rates," *IEEE Transactions on Signal Processing*, vol. 51, pp. 2882–2890, Nov. 2003.
- [78] Q. Sun, D. C. Cox, H. C. Huang and A. Lozano, "Estimation of continuous flat fading MIMO channels," *IEEE Transactions on Wireless Communications*, vol. 1, pp. 549–553, Oct. 2002.

- [79] X. Deng, A. M. Haimovich and J. Garcia-Frias, "Decision directed iterative channel estimation for MIMO systems," *Proc. of ICC 2003*, pp. 2326–2329, May 2003.
- [80] X. Zhu and R. D. Murch, "Performance analysis of maximum likelihood detection in a MIMO antenna system," *IEEE Transactions on Communications*, vol. 50, pp. 187–191, Feb. 2002
- [81] N. Prasad and M. K. Varanasi, "Decision feedback detection using modulation constraints for MIMO Rayleigh fading channels," *IEEE International Symposium on Information Theory*, pp. 331, Jul. 2002.
- [82] D. A. Gore, R. W. Heath and A. J. Paulraj, "Transmit selection in spatial multiplexing systems," *IEEE Communications Letters*, vol. 6, pp. 491–493, Nov. 2002.
- [83] D. W. Waters and J. R. Barry, "Noise-predictive decision feedback detection for multiple-input multiple-output channels," *IEEE Transactions on Signal Processing*, vol. 53, pp. 1852–1859, May. 2005.
- [84] K. Liu and A. M. Sayeed, "Improved layered space-time processing in multiple antenna systems," *Proc. 39th Annual Allerton Conference*, Oct. 2001.
- [85] T. Lv, H. Li, and J. Chen, "Joint estimation of symbol timing and carrier frequency offset of OFDM signals over fast time-varying multipath channels," *IEEE Transactions on Signal Processing*, vol. 53, pp. 4526–4535, Dec. 2005.
- [86] I. Barhumi, G. Leus, and M. Moonen, "Optimal training design for MIMO OFDM systems in mobile wireless channels," *IEEE Transactions on Signal Processing*, vol. 51, pp. 1615–1624, Jun. 2003.
- [87] M. C. Jeruchim, P. Balaban and K. S. Shanmugan, *Simulation of communication systems*. New York: Plenum, 1992.
- [88] Y. Li, N. Seshadri, and S. Ariyavisitakul, "Channel estimation for OFDM systems with transmit diversity in mobile wireless channels," *IEEE Journal on Selected Areas Communications*, vol. 17, pp. 461–471, Mar. 1999.
- [89] Y. Xie and C. N. Georghiades, "Two EM-type channel estimation algorithms for OFDM with transmitter diversity," *IEEE Transactions on Communication*, vol. 51, pp. 106–115, Jan. 2003.
- [90] Y. Xie and C. N. Georghiades, "An EM-based channel estimation algorithm for OFDM with transmitter diversity," in *Proc. of IEEE Globecom'01, San Antonio, TX*, pp. 871–875, Nov. 2002.

- [91] O. Edfors, M. Sandell, J. Beek and S. Wilson, "OFDM channel estimation by singular value decomposition," *IEEE Transactions on Communications*, vol. 46, pp. 931–939, Jul. 1998.
- [92] L. L. Scharf, *Statistical Signal Processing: Detection, Estimation, and Time Series Analysis*. MA: Addison-Wesley, 1991.
- [93] J. Akhtar and D. Gesbert, "A closed-form precoder for spatial multiplexing over correlated MIMO channels," *IEEE Global Telecommunications Conference*, vol. 4, pp. 1847–1851, Dec. 2003.
- [94] D. Gesbert, H. Bolcskei, D. Gore and A. Paulraj, "Outdoor MIMO wireless channels: models and performance prediction," *IEEE Transactions on Communications*, vol. 50, pp. 1926–1934, Dec. 2002.
- [95] Y. Li, "Pilot-symbol-aided channel estimation for OFDM in wireless systems," *IEEE Transactions on Vehicular Technology*, vol. 49, pp. 1207–1215, Jul. 2000.
- [96] S. Colieri, M. Ergen, A. Puri and A. Bahai, "A study of channel estimation in OFDM systems," *Vehicular Technology Conference, 2002. Proceedings*, pp. 894–898, vol. 2, Sep. 2002.
- [97] J. J. van de Beek, O. Edfors, M. Sandell, S. K. Wilson and P. O. Borjesson, "On channel estimation in OFDM systems," *Proc. IEEE 45th Vehicular Technology Conference*, Chicago, IL, pp. 815–819, Jul. 1995.
- [98] B. Vucetic and J. Yuan, *Space-time coding*. Jhon Wiley and Sons, Ltd., 2003.
- [99] J. Wang and B. Daneshrad, "A comparative study of MIMO detection algorithms for wideband spatial multiplexing systems," *IEEE Wireless Communications and Networking Conference*, vol. 1, pp. 408–413, Mar. 2005.
- [100] M. R. Spiegel, *Theory and Problems of Probability and Statistics*. New York, McGraw-Hill, 1992.
- [101] S. M. Kay, *Modern Spectral Estimation*. Englewood Cliffs, NJ: Prentice Hall, 1988.
- [102] P. Xia and G. B. Giannakis, "Design and analysis of transmit-beamforming based on limited-rate feedback," *IEEE Vehicular Technology Conference*, pp. 1653–1657, vol. 3, Sep. 2004.

